

July 17, 2023

Docket No. 52-050

U.S. Nuclear Regulatory Commission
ATTN: Document Control Desk
One White Flint North
11555 Rockville Pike
Rockville, MD 20852-2738

SUBJECT: NuScale Power, LLC Submittal of Topical Report "Methodology for the Determination of the Onset of Density Wave Oscillations (DWO)," TR-131981, Revision 1

REFERENCES: 1. NuScale Power, LLC Submittal of Topical Report "Methodology for the Determination of the Onset of Density Wave Oscillations (DWO)," TR-131981, Revision 0, December 30, 2022 (ML22364A333)

NuScale Power, LLC (NuScale) hereby submits Revision 1 of the "Methodology for the Determination of the Onset of Density Wave Oscillations (DWO)," (TR-131981). The purpose of this submittal is to request that the NRC review and approve the evaluation model that provides a method for identifying the margin to the onset of density wave oscillations in NPM-20 helical coil steam generator tubes. NuScale respectfully requests that the acceptance review be completed in 30 days from the date of transmittal.

Enclosure 1 contains the proprietary version of the report entitled "Methodology for the Determination of the Onset of Density Wave Oscillations (DWO)," TR-131981, Revision 1. NuScale requests that the proprietary version be withheld from public disclosure in accordance with the requirements of 10 CFR § 2.390. The enclosed affidavit (Enclosure 3) supports this request. Enclosure 1 has also been determined to contain Export Controlled Information. This information must be protected from disclosure per the requirements of 10 CFR § 810. Enclosure 2 contains the nonproprietary version of the report.

This letter makes no regulatory commitments and no revisions to any existing regulatory commitments.

If you have any questions, please contact Wren Fowler at 541-452-7183 or at sfowler@nuscalepower.com.

Sincerely,



Mark W. Shaver
Acting Director, Regulatory Affairs
NuScale Power, LLC

Distribution: Michael Dudek, NRC
Getachew Tesfaye, NRC
Bruce Bavol, NRC

Enclosure 1: "Methodology for the Determination of the Onset of Density Wave Oscillations (DWO)," TR-131981, Revision 1, proprietary version
Enclosure 2: "Methodology for the Determination of the Onset of Density Wave Oscillations (DWO)," TR-131981, Revision 1, nonproprietary version
Enclosure 3: Affidavit of Mark W. Shaver AF-142066

Enclosure 1:

“Methodology for the Determination of the Onset of Density Wave Oscillations (DWO),”
TR-131981, Revision 1, proprietary version

Enclosure 2:

“Methodology for the Determination of the Onset of Density Wave Oscillations (DWO),”
TR-131981, Revision 1, nonproprietary version

Licensing Topical Report

Methodology for the Determination of the Onset of Density Wave Oscillations (DWO)

July 2023

Revision 1

Docket: 52-050

NuScale Power, LLC

1100 NE Circle Blvd., Suite 200

Corvallis, Oregon 97330

www.nuscalepower.com

© Copyright 2023 by NuScale Power, LLC

Licensing Topical Report

COPYRIGHT NOTICE

This report has been prepared by NuScale Power, LLC and bears a NuScale Power, LLC, copyright notice. No right to disclose, use, or copy any of the information in this report, other than by the U.S. Nuclear Regulatory Commission (NRC), is authorized without the express, written permission of NuScale Power, LLC.

The NRC is permitted to make the number of copies of the information contained in this report that is necessary for its internal use in connection with generic and plant-specific reviews and approvals, as well as the issuance, denial, amendment, transfer, renewal, modification, suspension, revocation, or violation of a license, permit, order, or regulation subject to the requirements of 10 CFR 2.390 regarding restrictions on public disclosure to the extent such information has been identified as proprietary by NuScale Power, LLC, copyright protection notwithstanding. Regarding nonproprietary versions of these reports, the NRC is permitted to make the number of copies necessary for public viewing in appropriate docket files in public document rooms in Washington, DC, and elsewhere as may be required by NRC regulations. Copies made by the NRC must include this copyright notice and contain the proprietary marking if the original was identified as proprietary.

Licensing Topical Report

Department of Energy Acknowledgement and Disclaimer

This material is based upon work supported by the Department of Energy under Award Number DE-NE0008928.

This report was prepared as an account of work sponsored by an agency of the United States Government. Neither the United States Government nor any agency thereof, nor any of their employees, makes any warranty, express or implied, or assumes any legal liability or responsibility for the accuracy, completeness, or usefulness of any information, apparatus, product, or process disclosed, or represents that its use would not infringe privately owned rights. Reference herein to any specific commercial product, process, or service by trade name, trademark, manufacturer, or otherwise does not necessarily constitute or imply its endorsement, recommendation, or favoring by the United States Government or any agency thereof. The views and opinions of authors expressed herein do not necessarily state or reflect those of the United States Government or any agency thereof.

Table of Contents

Abstract 1

Executive Summary 2

1.0 Introduction 4

1.1 Purpose 4

1.2 SG DWO Stability Evaluation Model Scope 4

1.3 Abbreviations 4

2.0 Background 7

2.1 Regulatory Requirements 8

3.0 NuScale Power Module Description and Operations 9

3.1 NuScale Power Module Steam Generator Operation 9

3.2 Evaluation Model Requirements and Figures of Merit 14

3.3 Description of Density Wave Oscillation Phenomenon 15

4.0 Phenomena Identification and Ranking and Scaling Analysis 16

4.1 Phenomena Identification and Ranking Table Objectives 16

4.2 Phenomena Identification and Ranking Table Phenomena 16

4.3 Discussion of High Ranked Phenomena 19

4.3.1 {{ }}^{2(a),(c)} 19

4.3.2 {{ }}^{2(a),(c)} 19

4.3.3 {{ }}^{2(a),(c)} 19

4.3.4 {{ }}^{2(a),(c)} 20

4.3.5 {{ }}^{2(a),(c)} 20

4.3.6 {{ }}^{2(a),(c)} 20

4.3.7 {{ }}^{2(a),(c)} 21

4.3.8 {{ }}^{2(a),(c)} 21

4.3.9 {{ }}^{2(a),(c)} 21

4.3.10 {{ }}^{2(a),(c)} 22

4.3.11 {{ }}^{2(a),(c)} 22

4.3.12 {{ }}^{2(a),(c)} 22

4.3.13 {{ }}^{2(a),(c)} 23

4.3.14 {{ }}^{2(a),(c)} 23

4.4 Scaling Analysis 23

4.4.1 Analysis of TF-2 Scaling 23

Table of Contents

4.4.2	Scaling Analysis Objectives, Methodology, and Fundamental Requirements	25
4.4.3	Density Wave Oscillation Phenomena and Experiment Objectives	26
4.4.4	NuScale Power Module Helical Coil Steam Generator Stability Phenomena Identification and Ranking Table	26
4.4.5	TF-2 Facility Operating Conditions and Dimensions	26
4.4.6	Scaling Evaluation using the Hierarchical Two-Tier Scaling Method	28
4.4.7	NRELAP5 Models for Scaling Assessments	37
4.4.8	Analysis of scaling distortions	39
4.4.9	Scaling Sensitivity and Distortion Optimization Methodology	44
4.4.10	Transient Distortions	46
4.4.11	Scaling and Distortion Analysis Conclusion	50
5.0	NRELAP5 Code Description	51
5.1	Quality Assurance Requirements	52
5.2	Hydrodynamic Model	53
5.2.1	Field Equations	53
5.2.2	State Relations	55
5.2.3	Flow Regime Maps	56
5.2.4	Momentum Closure Relations	61
5.2.5	Heat Transfer	67
5.3	Heat Structure Models	69
5.4	Trips and Control System Models	71
5.5	Special Solution Techniques	72
5.5.1	Abrupt Area Change	72
5.5.2	Form Loss Model	73
5.6	Numerical Methods	73
5.7	Helical Coil Steam Generator Component	75
6.0	NRELAP5 Helical Coil Steam Generator Model Development	77
6.1	Helical Coil Tube Friction	78
6.1.1	Helical Coil Single-Phase Tube Wall Friction	78
6.1.2	Helical Coil Two-Phase Tube Wall Friction	79
6.2	Helical Coil Tube Heat Transfer	80

Table of Contents

6.2.1	Helical Coil Single-Phase Heat Transfer	80
6.2.2	Helical Coil Two-Phase Subcooled and Saturated Flow Boiling Heat Transfer	81
6.2.3	Primary Side Heat Transfer	83
6.3	Subcooled Boiling	83
6.3.1	Onset of Nucleate Boiling	83
6.3.2	Onset of Significant Void	83
6.3.3	Subcooled Void Fraction and Quality	84
6.4	Transition to Dryout	85
6.4.1	Two Phase to Single Phase Vapor Transition	85
7.0	Evaluation Model Description	86
7.1	General Model Overview	86
7.2	Overview of Density Wave Oscillation Simulation	91
7.2.1	Overview of Boundary Condition Methods to Induce Density Wave Oscillation Onset	91
7.2.2	Overview of Parameters Impactful on Density Wave Oscillation Characteristics	92
7.3	Steady-State NuScale Power Module Model for Input to NuScale Power Module Density Wave Oscillation Analysis	93
7.3.1	Boundary Conditions for NuScale Power Module Density Wave Oscillation Analysis	93
7.3.2	Steady-State NuScale Power Module Model	94
7.4	Specific Methods for Density Wave Oscillation Simulation	95
7.4.1	Specific Methods to Induce Density Wave Oscillation Onset	95
7.4.2	Determination of Density Wave Oscillation Stability Boundaries	97
7.4.3	Determination of Density Wave Oscillation Flow Period	99
7.4.4	Application of Specific Methods to Induce Density Wave Oscillation Onset	100
7.4.5	Steam Generator Separation	101
7.5	NuScale Power Module Density Wave Oscillation Analysis Model Requirements	101
7.5.1	Hydrodynamic Volume and Junction Options	102
7.5.2	Heat Structure Options	103
7.5.3	Time Step and System Options	104

Table of Contents

	7.5.4 Initial Conditions	105
7.6	Model Nodalization - Steam Generator Primary Side	105
	7.6.1 Steam Generator Primary Side: Inlet	105
	7.6.2 Steam Generator Primary Side: Upper Downcomer	106
	7.6.3 Steam Generator Primary Side: Exit	107
	7.6.4 Steam Generator Primary Side: Riser	107
	7.6.5 Steam Generator Primary Side: Riser Holes	108
	7.6.6 Steam Generator Primary Side: Upper Plenum	108
7.7	Model Nodalization - Feedwater and Steam Plenums	109
	7.7.1 Feedwater Source	109
	7.7.2 Feedwater Plenum	110
	7.7.3 Steam Plenum	110
	7.7.4 Steam Exit	111
7.8	Model Nodalization - Helical Coil Steam Generator Tubes	111
	7.8.1 Helical Coil Steam Generator Tube Inlets	111
	7.8.2 Helical Coil Steam Generator Tubes	112
	7.8.3 Helical Coil Steam Generator Tube Exits	117
8.0	NRELAP5 Assessments	118
8.1	Assessment of TF-1 Data	123
	8.1.1 Test Description and Experimental Procedure	123
	8.1.2 Phenomena Addressed	125
	8.1.3 NRELAP5 TF-1 Model	125
	8.1.4 Performance against TF-1 Single Effects Test Data	127
	8.1.5 Performance against TF-1 Density Wave Oscillation Data	141
	8.1.6 Summary and Conclusions from TF-1 Density Wave Oscillation Code-to-Data Comparisons	143
8.2	Assessment of TF-2 Data	144
	8.2.1 TF-2 Test Description and Experimental Procedure	144
	8.2.2 Phenomena Addressed	152
	8.2.3 Important NRELAP5 Modeling Techniques	152
	8.2.4 Performance against TF-2 Single Effects Test Data	155

Table of Contents

8.2.5 Performance against TF-2 Density Wave Oscillation Integral Effects Test Data 177

8.2.6 Summary and Conclusions from TF-2 Code-to-Data Comparisons. 182

8.3 Assessment of POLIMI Data 183

8.3.1 Test Description and Experimental Procedure. 183

8.3.2 Phenomena Addressed 188

8.3.3 NRELAP5 Modeling Techniques 188

8.3.4 POLIMI Code-to-Data Comparisons 189

8.3.5 POLIMI Base Model versus Cases Run with TF-1 Characteristics 190

8.3.6 Summary and Conclusions from POLIMI Data to Code Comparisons. 196

9.0 Assessment of Evaluation Model Adequacy. 198

9.1 Adequacy Demonstration Overview. 198

9.2 Evaluation Models and Correlations (Bottom-Up Assessment) 198

9.2.1 Evaluation of Models and Correlations (Bottom-Up Assessment) 199

9.2.2 Applicability Evaluation. 201

9.2.3 Bottom-Up Summary 250

9.3 Evaluation of Integral Performance (Top Down Evaluation Summary) 256

9.3.1 Review of Code Governing Equations and Numerics 257

9.3.2 Evaluations of Density Wave Oscillation Tests 261

10.0 Uncertainty Evaluation and Margin for the NuScale Power Module with Respect to Density Wave Oscillation. 264

10.1 Sensitivity Analysis Methodology Development. 264

10.2 NRELAP5 Code Uncertainty 267

10.3 Other High Ranked Phenomena Identification and Ranking Table Phenomena Not Considered in the Uncertainty Evaluation 277

10.3.1 {{ }}^{2(a),(c)} 277

10.3.2 {{ }}^{2(a),(c),ECI} 277

10.3.3 {{ }}^{2(a),(c),ECI} 278

10.3.4 {{ }}^{2(a),(c)} 281

10.3.5 {{ }}^{2(a),(c)} 282

10.3.6 {{ }}^{2(a),(c),ECI} 282

10.3.7 {{ }}^{2(a),(c),ECI} 292

Table of Contents

10.3.8	{{	$\}}^{2(a),(c),ECI}$	292
10.3.9	{{	$\}}^{2(a),(c)}$	292
10.4	Methodology for Density Wave Oscillation Analysis			293
10.4.1	{{	$\}}^{2(a),(c)}$	295
11.0	Results/Conclusions			298
12.0	References			300
Appendix A	Evaluation Model Development and Assessment Process and Roadmap to the Density Wave Oscillation Evaluation Model			A-1
Appendix B	Sample Calculation for NuScale Power Module			B-1
B.1	NuScale Power Module Density Wave Oscillation Onset Calculations			B-1
B.2	Density Wave Oscillation Model Nodalization and Development			B-1
	B.2.1	Percent Nominal Power Equilibrium Profile		B-1
	B.2.2	NRELAP5 Model Development		B-5
B.3	Boundary Conditions			B-10
B.4	Inlet Flow Restrictor Loss Coefficient Selection			B-11
B.5	Density Wave Oscillation Number of Channels Comparison			B-13
B.6	Margin Calculation			B-17
B.7	Stability Evaluations at 100 Percent Nominal Power Conditions			B-18
B.8	Stability Evaluations at Off-Nominal 100 Percent Power Conditions			B-25
B.9	Results and Conclusions			B-30

List of Tables

Table 1-1	Abbreviations	4
Table 1-2	Definitions	5
Table 4-1	Importance Rankings	16
Table 4-2	Knowledge Level Rankings	17
Table 4-3	Component Designation for Phenomena Identification and Ranking	17
Table 4-4	Density Wave Oscillation Stability Phenomena Identification and Ranking Table	18
Table 4-5	Nomenclature	24
Table 4-6	Index Notation	25
Table 4-7	NuScale Power Module and TF-2 Steady-State Operating Conditions at 100 Percent Power	27
Table 4-8	NuScale Power Module and TF-2 Helical Coil Steam Generator Design Comparison	27
Table 4-9	NuScale Power Module and TF-2 Helical Coil Steam Generator Row 3 Comparison	27
Table 4-10	Field Equations	33
Table 4-11	NuScale Power Module and TF-2 Initial Conditions at Different Power Levels Used for Scaling Analysis	38
Table 4-12	TF-2 Distortion for Density Wave Oscillation Phenomena Compared with 100 Percent NuScale Power Module Operating Condition	40
Table 4-13	TF-2 Distortion for Density Wave Oscillation Phenomena Compared with 15 Percent NuScale Power Module Operating Condition	42
Table 4-14	Pressure Group Distortion at 100 Percent Power Condition	43
Table 4-15	Pressure Group Distortion at 15 Percent Power Condition	43
Table 4-16	Parameter Bounds for the 15 Percent Power Sensitivity Cases	45
Table 4-17	Parameter Bounds for the 100 Percent Power Sensitivity Cases	45
Table 4-18	Distortions for the Optimal Cases	46
Table 4-19	Transient Group Distortion for TF-2 and NuScale Power Module 100 Percent Power	48
Table 4-20	Transient Group Distortion for TF-2 and NuScale Power Module 15 Percent Power	49
Table 4-21	Nondimensional Resultant Momentum Oscillation and Frequency Comparison Between TF-2 and NuScale Power Module at 100 Percent Power	50
Table 4-22	Nondimensional Resultant Momentum Oscillation and Frequency Comparison Between TF-2 and NuScale Power Module at 15 Percent Power	50

List of Tables

Table 5-1	NRELAP5 Code Modifications (Density Wave Oscillation Specific)	52
Table 7-1	Density Wave Oscillation Stability Phenomena Identification and Ranking Table Versus NuScale Power Module Density Wave Oscillation Model Incorporation	89
Table 7-2	NuScale Power Module Steady-State Operating Parameters for Density Wave Oscillation Analysis	93
Table 8-1	Comparison of Geometrical Parameters for NuScale Power Module and Assessment Tests	119
Table 8-2	NuScale Power Module Thermal-Hydraulic Conditions Compared to Assessment Test Program Conditions	121
Table 8-3	{{ }} ^{2(a),(c),ECI}	142
Table 8-4	Density Wave Oscillation Test Matrix	146
Table 8-5	{{ }} ^{2(a),(c),ECI}	148
Table 8-6	TF-2 Density Wave Oscillation Test NRELAP5 Simulation, Density Wave Oscillation Onset Total Error Summary Results	178
Table 8-7	{{ }} ^{2(a),(c),ECI}	184
Table 9-1	NRELAP5 Models and Correlations Associated with High Ranked Phenomena Along with Relevant Assessment Test Data	200
Table 9-2	TF-1 Void Fraction Comparison	214
Table 9-3	TF-2 Cases Used in Primary-Side Temperature Distribution Assessment . . .	216
Table 9-4	Numerical Evaluation of the Transverse Temperature Profiles	224
Table 9-5	Summary of Bottom-Up Evaluation of NRELAP5 Models and Correlations . .	251
Table 9-6	Applicability Summary for High Ranked Phenomena with Original Knowledge Level 2	254
Table 9-7	Assessment Test Data and Associated High-Ranked PIRT Phenomena	257
Table 9-8	NRELAP5 Limitations and Improvement Needs Related to Density Wave Oscillation	261
Table 9-9	Top-Down Assessment Summary for Integral Effects Test	263
Table 10-1	{{ }} ^{2(a),(c),ECI}	265
Table 10-2	{{ }} ^{2(a),(c)}	273
Table 10-3	{{ }} ^{2(a),(c),ECI}	278
Table 10-4	{{ }} ^{2(a),(c),ECI}	283
Table 10-5	{{ }} ^{2(a),(c),ECI}	288

List of Tables

Table 10-6	{{	}} ^{2(a),(c)}	294
Table A-1	Evaluation Model Development and Assessment Process Steps and Associated Document Sections		A-3
Table B-1	{{	}} ^{2(a),(c)}	B-10
Table B-2	{{	}} ^{2(a),(c)}	B-17
Table B-3	NuScale Power Module 100 Percent Nominal Power Density Wave Oscillation Summary Results and Margin		B-25
Table B-4	NuScale Power Module 100 Percent Nominal Power Off-Nominal Assumed Control Action and Trip Times		B-27
Table B-5	{{	}} ^{2(a),(c)}	B-28
Table B-6	{{	}} ^{2(a),(c)}	B-29
Table B-7	Summary of Margin to Density Wave Oscillation Onset.		B-30

List of Figures

Figure 3-1	NuScale Power Module Cut Away	10
Figure 3-2	Thermal Conversion System	11
Figure 3-3	NuScale Power Module Secondary Side Configuration	12
Figure 3-4	Tube Bundle with the Reactor Pressure Vessel and Riser (Left) and Tube Bundle Only (Right)	13
Figure 4-1	Flow Diagram for the Hierarchical Two-Tier Scaling Analysis	29
Figure 4-2	Helical Coil Steam Generator Breakdown into Hierarchical Levels and Primary Operational Modes	30
Figure 4-3	NuScale Power Module Helical Coil Steam Generator Region Breakdown	31
Figure 4-4	Density Wave Oscillation Onset	37
Figure 5-1	Schematic of Vertical Flow-Regime Map Indicating Transitions	58
Figure 5-2	Schematic of Horizontal Flow Regime Map with Shaded Regions Indicating Transition (Interpolation) Regions	59
Figure 5-3	Schematic of Horizontally Stratified Flow in a Pipe, with Definition of θ	60
Figure 5-4	NRELAP5 Boiling and Condensing Curves	69
Figure 5-5	Physical Meaning of the Courant Number	75
Figure 6-1	Basic Geometry of a Helical Tube	77
Figure 7-1	Example of a NuScale Power Module Density Wave Oscillation Model	87
Figure 7-2	Evaluation Model Input/Output Flow Chart (Simplified)	88
Figure 7-3	General Feedwater Flow-Controlled Boundary Condition Method, Example Illustration	96
Figure 7-4	Bulk Feedwater Flow-Controlled Boundary Condition Method, Example Illustration	97
Figure 7-5	$\{ \{ \} \}^{2(a),(c)}$	99
Figure 7-6	Example Illustrating Density Wave Oscillation Flow Period Behavior Summary	100
Figure 8-1	Tube-to-Coil Diameter Ratio for NuScale Power Module and Assessment Test Programs	120
Figure 8-2	Secondary Side Parameter Ranges for NuScale Power Module and Assessment Tests	122
Figure 8-3	TF-1 Test Section and Instrumentation Configuration	124
Figure 8-4	Relative Heat Flux Versus Position Along the Tube	125
Figure 8-5	NRELAP5 Model of TF-1	126
Figure 8-6	TF-1 Differential Pressure for Coil 1 Adiabatic Tests	129
Figure 8-7	TF-1 Differential Pressure for Coil 2 Adiabatic Tests	130

List of Figures

Figure 8-8	TF-1 Differential Pressure for Coil 3 Adiabatic Tests	131
Figure 8-9	TF-1 Differential Pressure for Coil 1 Diabatic Tests	132
Figure 8-10	TF-1 Differential Pressure for Coil 2 Diabatic Tests	133
Figure 8-11	TF-1 Differential Pressure for Coil 3 Diabatic Tests	134
Figure 8-12	TF-1 Fluid Temperature Comparison for Coil 1	136
Figure 8-13	Fluid Temperature Comparison for Coil 2	137
Figure 8-14	Fluid Temperature Comparison for Coil 3	138
Figure 8-15	Wall Temperature Comparison for Coil 1	139
Figure 8-16	Wall Temperature Comparison for Coil 2	140
Figure 8-17	Wall Temperature Comparison for Coil 3	141
Figure 8-18	TF-1 Density Wave Oscillation Code-to-Data Comparison, Density Wave Oscillation Onset Power	143
Figure 8-19	TF-2 Secondary-side Tube Bundle Configuration in the Primary-Side Flow Annulus	150
Figure 8-20	TF-2 Configuration Piping and Instrumentation Diagram	151
Figure 8-21	TF-2 NRELAP5 Adiabatic and Diabatic Test Nodalization Diagram	153
Figure 8-22	TF-2 Density Wave Oscillation Test NRELAP5 Model Nodalization Diagram - Only Row 3 Active	154
Figure 8-23	TF-2 Adiabatic Tests, Primary-side Differential Pressure Comparison	157
Figure 8-24	TF-2 Diabatic Tests, Primary-Side Differential Pressure Comparison	158
Figure 8-25	TF-2 Diabatic Tests, Primary-Side Temperature Comparison	159
Figure 8-26	{{ }} ^{2(a),(c),ECI}	161
Figure 8-27	{{ }} ^{2(a),(c),ECI}	162
Figure 8-28	{{ }} ^{2(a),(c),ECI}	163
Figure 8-29	{{ }} ^{2(a),(c),ECI}	164
Figure 8-30	{{ }} ^{2(a),(c),ECI}	165

List of Figures

Figure 8-31	{{		
		}} ^{2(a),(c),ECI}	166
Figure 8-32	{{		
		}} ^{2(a),(c),ECI}	167
Figure 8-33	{{		
		}} ^{2(a),(c),ECI}	168
Figure 8-34	{{		
		}} ^{2(a),(c),ECI}	169
Figure 8-35	{{		
		}} ^{2(a),(c),ECI}	170
Figure 8-36	{{		
		}} ^{2(a),(c),ECI}	171
Figure 8-37	{{		
		}} ^{2(a),(c),ECI}	173
Figure 8-38	{{		
		}} ^{2(a),(c),ECI}	174
Figure 8-39	{{		
		}} ^{2(a),(c),ECI}	175
Figure 8-40	{{		
		}} ^{2(a),(c),ECI}	176
Figure 8-41	{{		
		}} ^{2(a),(c),ECI}	177
Figure 8-42	Predicted Versus Measured Feedwater Flowrate at Density Wave Oscillation Onset for the Least-Stable Tube.		180
Figure 8-43	Predicted Versus Measured Average Density Wave Oscillation Flow Period for the Least-Stable Tube.		181
Figure 8-44	Predicted Versus Measured Average Density Wave Oscillation Amplitude for the Least-Stable Tube.		182
Figure 8-45	Overview of POLIMI Parallel Helical Coil Steam Generator Configuration ...		186
Figure 8-46	Schematic of POLIMI Test with Instrumentation Locations		187
Figure 8-47	POLIMI Parallel Helical Coil Steam Generator Facility NRELAP5 Model Nodalization Diagram.		189

List of Figures

Figure 8-48	POLIMI Test 46 Code to Data Differential Pressure Along the Tube Compared to NRELAP5	191
Figure 8-49	POLIMI NRELAP5 Helical Coil Steam Generator Tube Pressure Drop Ratio Versus Pressure (Base Model and Model with TF-1 Characteristics)	192
Figure 8-50	POLIMI NRELAP5 Density Wave Oscillation Onset Power Ratio Versus Pressure (Base Model and Model with TF-1 Coil Characteristics)	193
Figure 8-51	POLIMI NRELAP5 Helical Coil Steam Generator Tube Pressure Drop Ratio Versus Tube A Inlet Loss Coefficient	194
Figure 8-52	POLIMI NRELAP5 Density Wave Oscillation Onset Power Ratio Versus Tube A Inlet Loss Coefficient	195
Figure 8-53	POLIMI NRELAP5 Code-to-Data Comparison, Tube A Axial Wall Temperature	196
Figure 9-1	{{ }} ^{2(a),(c)}	205
Figure 9-2	{{ }} ^{2(a),(c)}	205
Figure 9-3	{{ }} ^{2(a),(c)}	206
Figure 9-4	{{ }} ^{2(a),(c)}	206
Figure 9-5	{{ }} ^{2(a),(c)}	207
Figure 9-6	{{ }} ^{2(a),(c)}	207
Figure 9-7	{{ }} ^{2(a),(c)}	208
Figure 9-8	{{ }} ^{2(a),(c)}	208
Figure 9-9	{{ }} ^{2(a),(c)}	209
Figure 9-10	{{ }} ^{2(a),(c)}	209
Figure 9-11	{{ }} ^{2(a),(c)}	210
Figure 9-12	{{ }} ^{2(a),(c)}	210
Figure 9-13	{{ }} ^{2(a),(c)}	211
Figure 9-14	{{ }} ^{2(a),(c)}	211
Figure 9-15	{{ }} ^{2(a),(c)}	212
Figure 9-16	{{ }} ^{2(a),(c)}	218
Figure 9-17	{{ }} ^{2(a),(c)}	220
Figure 9-18	{{ }} ^{2(a),(c)}	222
Figure 9-19	{{ }} ^{2(a),(c)}	223

List of Figures

Figure 9-20	{{	$\}}^{2(a),(c)}$	225
Figure 9-21	{{	$\}}^{2(a),(c)}$	228
Figure 9-22	{{	$\}}^{2(a),(c)}$	229
Figure 9-23	{{	$\}}^{2(a),(c)}$	230
Figure 9-24	{{	$\}}^{2(a),(c)}$	231
Figure 9-25	{{	$\}}^{2(a),(c)}$	232
Figure 9-26	{{	$\}}^{2(a),(c)}$	233
Figure 9-27	{{	$\}}^{2(a),(c)}$	234
Figure 9-28	{{	$\}}^{2(a),(c)}$	235
Figure 9-29	{{	$\}}^{2(a),(c)}$	236
Figure 9-30	{{	$\}}^{2(a),(c)}$	237
Figure 9-31	Numerical Diffusion Evaluation in Helical Coil Steam Generator Tube Single-Phase Liquid Region		239
Figure 9-32	Single-Phase Liquid Temperature Oscillation Numerical Damping Evaluation.		240
Figure 9-33	Single-Phase Liquid Temperature Oscillation Numerical Damping Evaluation.		243
Figure 9-34	Two-Phase Void Fraction Oscillation Numerical Damping Evaluation		244
Figure 9-35	NuScale Power Module Feedwater Plenum (Top) and Steam Plenum (Bottom)		248
Figure 9-36	Physical Meaning of the Courant Number		260
Figure 10-1	{{	$\}}^{2(a),(c),ECI}$	279
Figure 10-2	{{	$\}}^{2(a),(c),ECI}$	280
Figure 10-3	{{	$\}}^{2(a),(c),ECI}$	281
Figure 10-4	{{	$\}}^{2(a),(c),ECI}$	284
Figure 10-5	{{	$\}}^{2(a),(c),ECI}$	286
Figure 10-6	{{	$\}}^{2(a),(c),ECI}$	287
Figure 10-7	{{	$\}}^{2(a),(c),ECI}$	289

List of Figures

Figure 10-8	{{	}} ^{2(a),(c),ECI}	290
Figure 10-9	{{	}} ^{2(a),(c),ECI}	291
Figure 10-10	{{	}} ^{2(a),(c)}	297
Figure A-1		Evaluation Model Development and Assessment Process	A-2
Figure B-1		100 Percent Nominal Power, Equilibrium Quality Versus Helical Coil Steam Generator Tube Length	B-2
Figure B-2		100 Percent Nominal Power, Equilibrium Quality Versus Helical Coil Steam Generator Tube Length, Detailed View	B-3
Figure B-3		Density Wave Oscillation Model 1, For Evaluations from 70 Percent to 100 Percent Nominal Power	B-4
Figure B-4		Representation of the Primary Side of the NRELAP5 Density Wave Oscillation Model	B-8
Figure B-5		Representation of the Secondary Side of the NRELAP5 Density Wave Oscillation Model	B-9
Figure B-6	{{	}} ^{2(a),(c)}	B-12
Figure B-7	{{	}} ^{2(a),(c)}	B-13
Figure B-8	{{	}} ^{2(a),(c)}	B-15
Figure B-9	{{	}} ^{2(a),(c)}	B-16
Figure B-10	{{	}} ^{2(a),(c)}	B-21
Figure B-11	{{	}} ^{2(a),(c)}	B-22
Figure B-12	{{	}} ^{2(a),(c)}	B-23
Figure B-13	{{	}} ^{2(a),(c)}	B-24

Abstract

NuScale Power, LLC (NuScale) is requesting Nuclear Regulatory Commission (NRC) review and approval to use the Density Wave Oscillation (DWO) Evaluation Model (EM) described herein for analyses of the onset of DWO in the NuScale Power Module (NPM-20) in the US460 design during normal and off-normal operating conditions at nominal reactor power levels between 20 percent and 100 percent. Use of this EM outside of these limitations requires justification.

The DWO evaluation model uses the proprietary NRELAP5 system analysis code. The NRELAP5 code includes models and correlations for heat transfer and pressure drop for the NPM-20 helical coil steam generator (SG). Extensive NRELAP5 validation was performed to ensure the DWO evaluation model is applicable for important phenomena and processes. The validation suite includes separate effects test (SET) and integral effects test (IET) data developed specifically for the NPM-20 application.

This EM addresses identification of the onset of potential DWOs within the SG tubes for evaluating a preferred operating domain. This EM is not used to verify safety-related functions of structures, systems, and components (SSC).

Although not required because this method is not used to verify safety-related functions of SSC, this DWO evaluation method follows the guidance provided in “Transient and Accident Analysis Methods,” Regulatory Guide (RG) 1.203. Key aspects of RG 1.203 that are addressed include:

- development of the DWO phenomena identification and ranking table (PIRT)
- assessment of separate effects and integral effects DWO tests
- quantification of code uncertainty based on comparisons to test data
- EM development
- EM adequacy assessment using bottom-up assessment of NRELAP5 models and correlations, and top-down assessment of NRELAP5 models for mass, momentum, and energy conservation, and numerical solution techniques
- integral effects test facility scaling

Uncertainty quantification and margin evaluation applies to the NRELAP5 analysis of DWO onset for the NPM-20.

For illustrative purposes to aid the reader's understanding of the context of the application of this DWO evaluation method sample calculations of the implemented EM using NRELAP5 are provided. Sample calculations for the NPM-20 demonstrate that DWO onset does not occur in the NPM-20 steam generator at nominal or off-nominal steady-state operation at 100 percent power if the inlet flow restrictor (IFR) loss coefficient is $\{ \{ \} \}^{2(a),(c)}$. Example calculations illustrate that a $\{ \{ \} \}^{2(a),(c)}$ exists at 100 percent power.

Executive Summary

NuScale Power, LLC (NuScale) is requesting Nuclear Regulatory Commission (NRC) review and approval to use the Density Wave Oscillation (DWO) Evaluation Model (EM) described in this topical report for analyses of DWO onset prediction during nominal and off-nominal operating conditions at reactor power levels between 20 percent and 100 percent. Although not required because this EM is not used to verify safety-related functions of systems, structures, and components (SSC), this DWO evaluation model is consistent with the guidance provided in “Transient and Accident Analysis Methods,” Regulatory Guide (RG) 1.203 (Reference 12.1), because it contains industry best practices for EM development. This topical report is not intended to provide final design values or results; rather, it contains sample calculations using the EM for illustrative purposes to aid the reader's understanding of the context of the application of the DWO evaluation model.

NuScale developed a small modular reactor (SMR) design that supports operation of multiple NuScale Power Modules (NPM-20s) at a specific site. Each NPM-20 is an advanced, light-water, integrated pressurized water reactor (PWR) using natural circulation for the primary coolant flow. Within each NPM-20 there are two independent helical coil steam generators (SG) in the upper outer annulus of the primary reactor pressure vessel (RPV). Each SG consists of a large number of helical tubes connected in parallel to common feedwater (FW) plenums at the bottom and common steam plenums at the top. Each SG tube has an inlet flow restrictor (IFR) that is sized to provide secondary-side hydraulic resistance within the single-phase region to enhance secondary flow stability.

Systems that utilize convective boiling flow, such as the NPM-20 steam generators can be found in a variety of industrial applications, including boiling water reactors, steam boilers, heat exchangers, and condensers. Such systems offer the advantage of high heat transfer rates at moderate temperature differences. A drawback is that these systems are susceptible to thermally-induced two-phase DWO that require additional engineering design to address. For the NuScale Power Module (NPM-20) steam generators, secondary-side fluid boiling within the tubes creates conditions potentially prone to parallel tube DWO. Hydraulic sizing of the tube IFR is important to ensuring acceptable flow stability.

This EM is used to identify the onset of potential DWO within the SG tubes for evaluating a preferred operating domain. The qualification of applicable portions of the reactor coolant system (RCS) integral RPV and SG given the occurrence of DWO is outside the scope of this topical report. This EM is not used to verify safety-related functions of SSC.

This DWO evaluation model uses the NuScale-proprietary NRELAP5 computer code as the computational tool. This software was derived from the Idaho National Laboratory (INL) RELAP5-3D[®] computer code. It includes the necessary models for characterization of the NPM-20 hydrodynamics, heat transfer between structures and fluids, modeling of fuel, reactor kinetics models, and control systems. The NRELAP5 code includes models and correlations for heat transfer and pressure drop for the NPM-20 helical coil SG.

Validation and verification of the DWO evaluation model was conducted following the principles and guidance in the Evaluation Model Development and Assessment Process (EMDAP) of RG 1.203. A phenomena identification and ranking table (PIRT) that identifies the important

phenomena and processes impacting DWO was developed. Seventeen phenomena were identified as important to DWO, which were considered in the DWO evaluation model. Six of these important phenomena have a low knowledge level (level = 2) and require assessment against test data.

Extensive NRELAP5 code assessment was performed to ensure applicability of the DWO evaluation model for the important PIRT phenomena over the range of conditions encountered in the NPM-20. The validation tests included separate effects test (SET) and integral effects test (IET) performed at the Società Informazioni Esperienze Termoidrauliche S.p.A. (SIET) TF-1 facility in 2013 and at SIET TF-2 in 2015, as well as DWO tests performed at the SIET TF-2 facility in 2022. Additional validation was conducted using an external database obtained from Polytechnic University of Milan (POLIMI). For TF-1 and TF-2 testing, predicted-to-measured values of DWO onset are in reasonable-to-excellent agreement. For POLIMI, which has longer tubes and a tighter helix than the NPM-20 steam generator, NRELAP5 predictions of DWO onset are conservative.

The EM adequacy for analysis of DWO onset for the NPM-20 is demonstrated through bottom-up and top-down evaluations performed with NRELAP5 for high-ranking PIRT phenomena and through NRELAP5 validation against relevant test data. For the bottom-up assessment, adequacy of the models and correlations in NRELAP5 are examined by considering their pedigree, applicability, and fidelity to appropriate fundamental or SET data, and scalability to the DWO onset conditions. Integral or top-down performance is assessed by evaluating the mathematical models for mass, momentum, and energy conservation; numerical solution techniques employed; and integral effects test predictions of TF-2 where integral system response is present. The conclusion drawn from the bottom-up and top-down assessments is that the EM is adequate for the purpose of predicting DWO onset for the NPM-20.

An uncertainty analysis uses TF-1 and TF-2 test data. Using a 95 percent confidence interval, the NRELAP5 uncertainty in predicting helical coil SG tube pressure drop and heat transfer is calculated. When highly conservative biasing parameter uncertainty is applied to TF-2 NRELAP5 models, NRELAP5 uncertainty for predicting DWO onset is calculated to be $\{\{ \} \}^{2(a),(c)}$. This uncertainty is then applied to the NPM-20 steam generator DWO onset analysis calculations.

Sample calculations are provided to demonstrate application of the EM in an NPM-20 steam generator model. These sample calculations demonstrate that appropriate NRELAP5 modeling can be used to predict DWO onset. The sample calculations provide context for the reader's understanding of the application of the DWO evaluation model. The sample calculations demonstrate that the IFR loss coefficient (K_{inlet}) and expected operating conditions can be used to prevent onset of DWO at nominal and off-nominal operating conditions at 100 percent nominal power. This methodology application also illustrates how to determine margin to DWO onset, apply code uncertainty, and account for the effect of deviations from nominal conditions in DWO onset predictions. The results of the sample calculations show that margin to DWO onset is possible at nominal and off-nominal 100 percent power conditions.

1.0 Introduction

1.1 Purpose

This evaluation model (EM) addresses identification of the onset of potential density wave oscillations (DWO) within the steam generator (SG) tubes in the NuScale Power Module (NPM-20) design for evaluating a preferred operating domain. This EM is not used to verify safety-related functions of structures, systems, and components (SSC).

1.2 SG DWO Stability Evaluation Model Scope

The scope of this EM is limited to the NPM-20 steam generator and nominal reactor power levels between 20 percent and 100 percent. Use of this EM for components other than the SG or outside of the nominal 20 percent to 100 percent power range requires further justification.

This method is not used to verify safety-related functions of SSC; therefore, Regulatory Guide (RG) 1.203 is not required. However, this EM is consistent with the guidance in “Transient and Accident Analysis Methods,” RG 1.203 (Reference 12.1) because it contains industry best practices for thermal-hydraulic (T-H) EM development. As such, this report describes the NPM-20 steam generator design and operation, phenomena identification and ranking table (PIRT), and NRELAP5 input model, correlations, and applicability to DWO onset analysis. This report also summarizes NRELAP5 assessments against separate effects test (SET) and integral effects test (IET) data and presents an uncertainty analysis and DWO onset margin methodology.

Qualification of NPM-20 structural components, such as the integral reactor pressure vessel (RPV) and SG, given the occurrence of DWO are outside of the scope of this report.

1.3 Abbreviations

Table 1-1 Abbreviations

Term	Definition
1-D	one-dimensional
ASME	American Society of Mechanical Engineers
BC	boundary condition
CHF	critical heat flux
DF	distortion factor
DOE	Department of Energy
DWO	density wave oscillation
EM	evaluation model
EMDAP	evaluation model development and assessment process
ESDU	Engineering Science Data Unit
FoM	figures of merit
FW	feedwater
GDC	general design criterion
GDF	general design framework

Table 1-1 Abbreviations (Continued)

Term	Definition
H2TS	Hierarchical Two-Tier Scaling
HC	helical coil
HCSG	helical coil steam generator
IC	initial condition
IET	integral effects test
IFR	Inlet flow restrictor
INL	Idaho National Laboratory
LOCA	loss of coolant accident
NPM-20	NuScale Power Module
NRC	Nuclear Regulatory Commission
NVG	net vapor generation
ONB	onset of nucleate boiling
OSV	onset of significant void
PIRT	phenomena identification and ranking table
POLIMI	Polytechnic University of Milan
PWR	pressurized water reactor
RCS	reactor coolant system
RG	regulatory guide
RPV	reactor pressure vessel
SG	steam generator
SET	separate effects test
SIET	Società Informazioni Esperienze Termoidrauliche S.p.A.
SSC	systems, structures, and components
TF-1	test facility at SIET
TF-2	test facility at SIET
T-H	thermal-hydraulic
US	United States

Table 1-2 Definitions

Term	Definition
excellent agreement	One of the acceptance criteria defined in RG 1.203. "Excellent" agreement applies when the code exhibits no deficiencies in modeling a given behavior. Major and minor phenomena and trends are correctly predicted. The calculated results are judged to agree closely with the data. The calculation, with few exceptions, lies within the specified or inferred uncertainty bands of the data. The code may be used with confidence in similar applications.
figure of merit	A parameter selected to characterize and quantify acceptance of results
insufficient agreement	One of the acceptance criteria defined in RG 1.203. "Insufficient" agreement applies when the code exhibits major deficiencies. The code provides an unacceptable prediction of the test data because major trends are not predicted correctly. Most calculated values lie outside the specified or inferred uncertainty bands of the data. Selected code models and facility model nodding need to be reviewed and modified before the code can be used with confidence in similar applications.

Table 1-2 Definitions

Term	Definition
minimal agreement	One of the acceptance criteria defined in RG 1.203. "Minimal" agreement applies when the code exhibits significant deficiencies. Overall, the code provides a prediction that is only conditionally acceptable. Some major trends or phenomena are not predicted correctly and some calculated values lie considerably outside the specified or inferred uncertainty bands of the data. Incorrect conclusions about trends and phenomena may be reached if the code were to be used in similar applications and an appropriate warning needs to be issued to users. Selected code models and facility model nodding need to be reviewed, modified, and assessed before the code can be used with confidence in similar applications.
reasonable agreement	One of the acceptance criteria defined in RG 1.203. "Reasonable" agreement applies when the code exhibits minor deficiencies. Overall, the code provides an acceptable prediction. Major trends and phenomena are correctly predicted. Differences between calculation and data are greater than deemed necessary for excellent agreement. The calculation frequently lies outside but near the specified or inferred uncertainty bands of the data. However, the correct conclusions about trends and phenomena would be reached if the code was used in similar applications.
standard deviation	Standard deviation provides the estimate of how closely individual data points cluster around the average values
standard error	Standard error is a measure of how individual values vary from the true values
standard error in mean	Standard error in mean provides the estimate of how individual mean values vary from the true values
uncertainty	General definition of data uncertainty is standard deviation of the data divided by the square root of number of data points

2.0 Background

The nuclear steam supply system of the NPM-20 uses natural circulation for core heat removal. The nuclear core serves as the heat source for the system, while the helical coil SG tubes inside the RPV serve as an elevated heat sink. During steady-state conditions, the difference in density and elevation between subcooled liquid water in the core and in the SG tubes creates the buoyancy force that drives primary-side flow. In the secondary side, feedwater (FW) is pumped into a FW plenum, from which it enters the SG tubes. Inside the SG tubes, water is transformed into superheated steam via boiling and convection. This dry, superheated steam exits the SG tubes into a steam plenum before being directed to a turbine.

The NPM-20 utilizes a helical coil SG (HCSG) in the upper outer annulus of the primary pressure vessel. The NPM-20 has two independent SGs. The inlet of each SG tube connects to one of four FW plenums at the bottom of the tube bundle and ends at one of four steam plenums at the top of the bundle. A large number of SG tubes are connected in parallel from each of the four common inlet headers. The HCSG tubes have a low inclination angle but traverse a large vertical height and therefore have behavior of both horizontal and vertical tubes in parallel. Unlike more common once-through SGs, the secondary side of the NPM-20 steam generator is inside the SG tubes, and the primary side is on the exterior of the SG tubes. The liquid in each SG tube undergoes a phase change on the inside of the SG tube as it travels upward through the SG secondary side, then it exits as superheated steam under normal operating conditions. A more detailed design explanation is given in Section 3.1.

Helical coil SG tube bundles are capable of high thermal performance due to their large surface area per unit height and can accommodate more thermal expansions and flow induced vibration than straight SG tube bundles. Due to the curved shape of the coil, a centrifugal force acts upon the flowing fluid within the SG tube. In two-phase flow, this centrifugal force keeps the SG tube wall wet up to very high qualities, shifting the location at which dry-out occurs toward the vapor region, reducing the extension of the post dry-out two-phase flow region. Because the SG tube wall is kept wet for more boiling length, the heat transfer capability increases compared to a vertical straight SG tube, especially in the high-quality region of the channel. The HCSG tube promotes mixing of the fluid, thus increasing the heat transfer capability and pressure drop.

Systems based on convective boiling flow are found in a wide variety of industrial applications, such as boiling water reactors, boilers, heat exchangers, and condensers. Such systems take advantage of the high heat transfer rates that a boiling fluid can reach at moderate temperature differences. However, those systems are susceptible to thermally-induced two-phase flow instabilities. The major concern with a SG located inside an RPV is the fact that boiling takes place inside the SG tubes, a condition potentially prone to parallel-channel flow instability. This concern, though common to once-through designs, could be significant in the NPM-20 due to the HCSG design with a very high ratio of SG tube length to SG tube diameter and high pressure drop.

Oscillations in SG tube flow, pressure, and SG tube wall temperature can cause control problems and thermal fatigue, which can potentially reduce the lifespan of an SG. For the

NPM-20 helical coil SG, excessive secondary-side flow oscillations can potentially exceed American Society of Mechanical Engineers (ASME) fatigue limits at the FW plenum tube-to-tubesheet weld (i.e., at the SG tube inlet), causing unacceptable cavitation and accelerated wear during oscillations. Thus, SG flow instabilities should be prevented or reduced to acceptable levels.

Secondary-side instabilities in the NPM-20 steam generator can be mitigated by design components, such as an inlet flow restrictor (IFR), and by controlling operational parameters such as steam outlet pressure and superheat. The methodology herein provides the basis for performing calculations to determine stable operating domains and characteristics of the NPM-20 steam generator in order to prevent or reduce DWO instabilities to acceptable levels.

2.1 Regulatory Requirements

The EM for DWO onset in the NPM-20 does not have any regulatory requirements other than addressing the portion of the combined operating license item 3.9-14 from the US600 design regarding onset prediction.

3.0 NuScale Power Module Description and Operations

3.1 NuScale Power Module Steam Generator Operation

The NPM-20, shown in Figure 3-1 is the fundamental building block of NuScale's small modular reactor (SMR) based power plant. It consists of a 250 MW thermal reactor core housed with other primary system components in an integral RPV surrounded by a steel containment vessel, which is partially immersed in a large pool of water that serves as the ultimate heat sink.

The primary reactor coolant path is upward through the reactor core. Heated water flows upward through the hot riser tube due to buoyancy forces and is turned downward at the pressurizer baffle plate. It then flows over the shell side of the SG, where it is cooled by conduction and convection of heat to the secondary coolant and continues to flow downward until its direction is again reversed at the lower RPV head and turned upward back into the core. Coolant circulation is maintained entirely by natural buoyancy forces of the lower-density heated water exiting the core and the higher-density cooled water exiting the SG annulus.

The NuScale design uses the Rankine thermal conversion cycle (Figure 3-2) to produce electricity. In the secondary circuit of each NPM-20, FW is pumped into four total FW plenums, two per SG, where the FW is heated by the primary-side coolant and boiled to produce superheated steam. As shown in Figure 3-3, two main steam lines from each NPM-20 combine into a single line and route the steam to a dedicated turbine generator system that generates electricity. Low pressure steam exiting the turbine is condensed and recirculated through three FW heater stages to the FW plenums.

The NPM-20 has two independent HCSGs in the upper outer annulus of the primary RPV. Each SG tube is connected to one of four FW plenums at the bottom of the tube bundle and terminates at one of four steam plenums at the top of the bundle as shown in Figure 3-3. A large number of SG tubes are connected in parallel from each of the four common inlet plenums as shown in Figure 3-4. The HCSG tubes have a low inclination angle but steeper transition sections at the inlet and outlet and therefore have behavior of both horizontal and vertical tubes in parallel. Unlike more common once-through SGs, the secondary-side of the NPM-20 steam generator is inside the HCSG tubes, and the primary-side is on the exterior of the HCSG tubes. Each SG tube or set of SG tubes undergo phase change of the fluid on the inside of the SG tube as it travels upward through the SG secondary side, where it exits as superheated steam under normal operating conditions.

Systems based on convective boiling flow such as the NPM-20 steam generator are found in a wide variety of industrial applications, such as boiling water reactors, boilers, heat exchangers, and condensers. Such systems take advantage of the high heat transfer rates that a boiling fluid can reach at moderate temperature differences. However, these systems are susceptible to thermally-induced two-phase DWO instabilities. The concern for the NPM-20 steam generator is the fact that boiling takes place inside of the SG tubes, a condition potentially prone to parallel-channel DWO. This concern is common to once-through SG designs.

Oscillations in SG tube flow and SG tube wall temperature resulting from DWO can cause thermal fatigue, which can impact SG lifespan. These instabilities can be mitigated both by design features, such as a SG tube IFR, and by controlling operational parameters, such as steam outlet pressure and steam superheat.

Figure 3-1 NuScale Power Module Cut Away

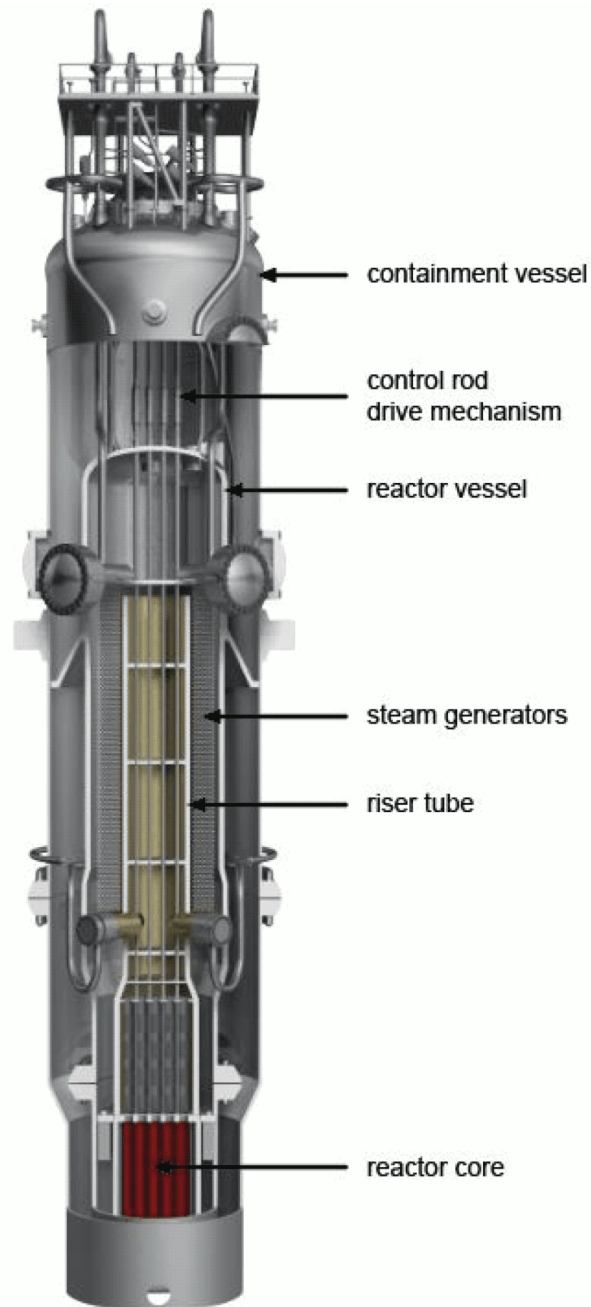
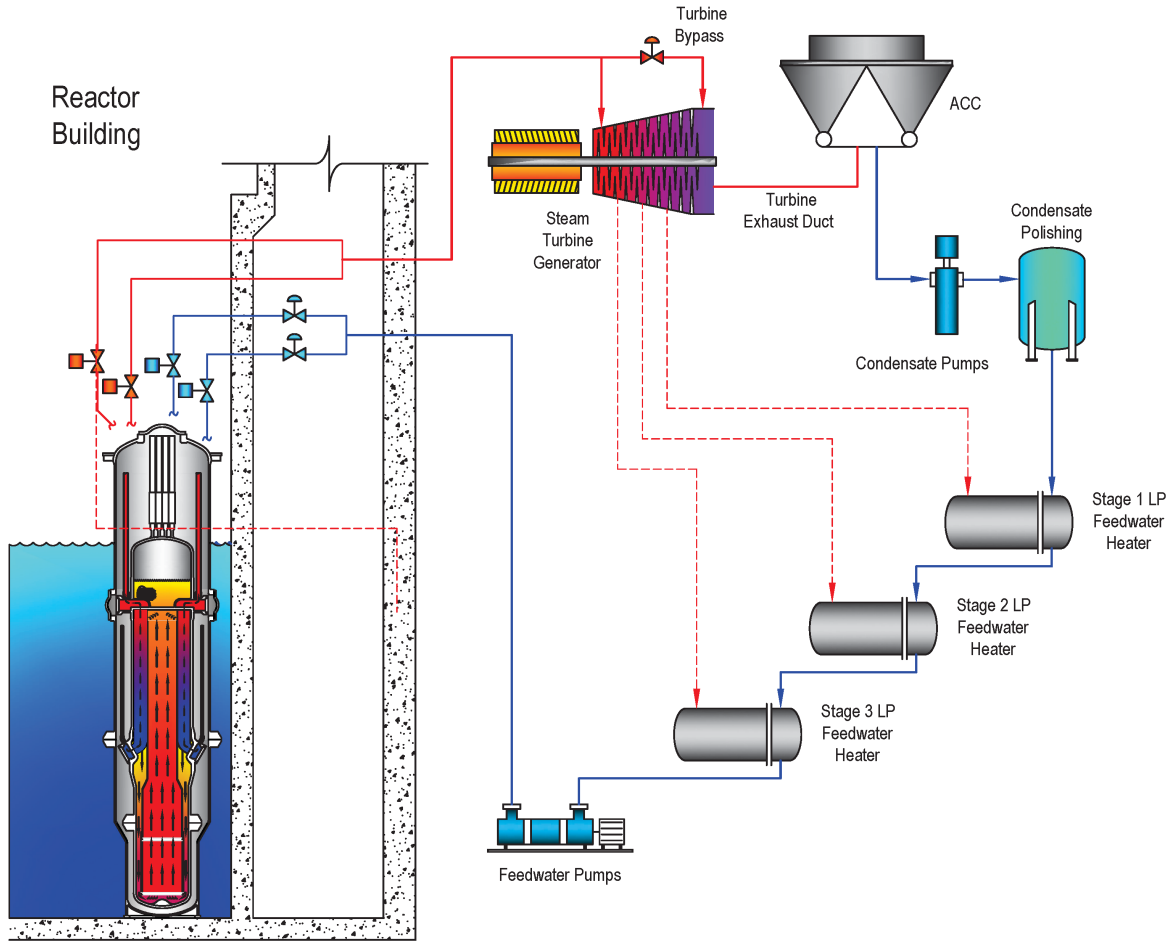


Figure 3-2 Thermal Conversion System



© NuScale Power, LLC

Figure 3-3 NuScale Power Module Secondary Side Configuration

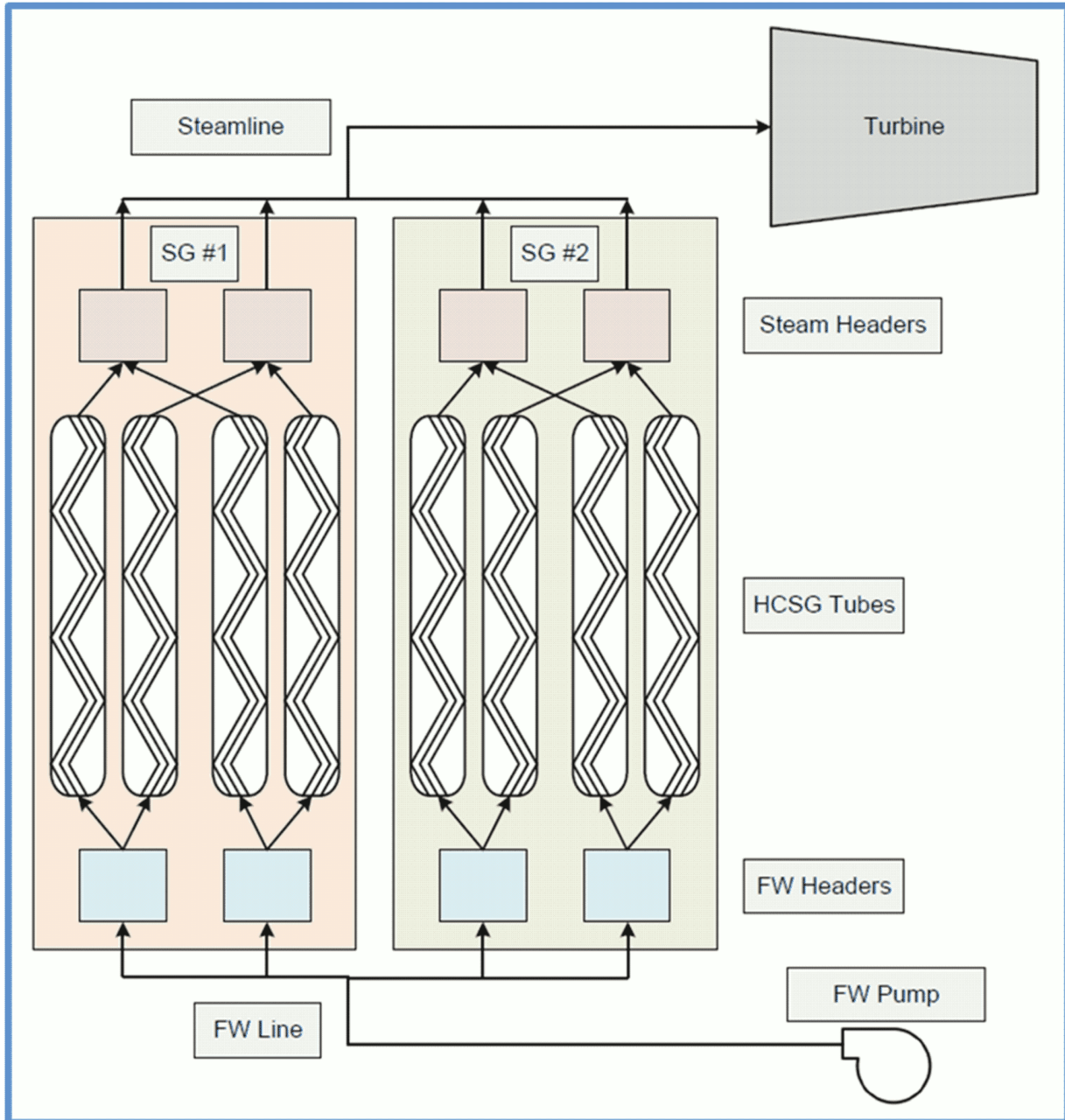


Figure 3-4 Tube Bundle with the Reactor Pressure Vessel and Riser (Left) and Tube Bundle Only (Right)



3.2 Evaluation Model Requirements and Figures of Merit

This EM provides a validated method for calculating the margin to the onset of density wave oscillations in the NPM-20 steam generator tubes that use an IFR.

In order to evaluate SG stability with respect to DWO onset, the following figure of merit (FoM) is selected:

1. DWO onset

Two supplemental FoMs are used:

1. DWO flow change amplitude
2. DWO flow rate frequency

Because the three FoMs are inextricably linked to the DWO phenomena, the use of DWO flow change amplitude and DWO flow rate frequency must be considered in order to accurately predict onset of DWO related to instabilities in the NPM-20 helical coil SG. For this DWO onset EM, reasonable-to-excellent agreement is needed for prediction of DWO onset (FoM 1) because DWO onset prediction is the purpose of the DWO evaluation model. Minimal agreement is needed for flow change amplitude and flow rate frequency (FoMs 2 and 3) because these FoMs can have higher uncertainty and still support the accurate prediction of DWO onset and ensure that the DWO onset is attributable to the correct phenomena.

The calculation of margin is performed using realistic operating parameters that are used by non-safety-related secondary-side control systems for monitoring and control of power production.

This report provides a description of the NuScale DWO evaluation model. The following steps are used to develop the EM.

- determining the requirements for the EM
- developing an assessment base consistent with the determined requirements
- developing the EM
- assessing the adequacy of the EM

Appendix A provides a description of how various sections of this report align to these four principles of the EM development and assessment process (EMDAP).

This EM utilizes the NRELAP5 code, which was developed from the Idaho National Laboratory (INL) RELAP5-3D[®] computer code. This report discusses the code and modeling requirements needed to address the phenomenon of the NPM-20 steam generator design and prediction of DWO onset.

3.3 Description of Density Wave Oscillation Phenomenon

A DWO occurs in parallel-flow channels (e.g., HCSG tubes) due to feedback effects between flow, density, void fraction, and pressure drop. In a two-phase system, density decreases as fluid is heated along the channel. Pressure drop increases in the two-phase region compared to the single-phase region. As flow perturbations are induced at the inlet, the channel axial void fraction distribution changes. There is a time delay between the propagated void fraction change and the flow perturbation. At specific flow oscillations, the pressure drop at the exit becomes completely out of phase with the inlet perturbation. Because the propagated void fraction change is referred to as a density wave, this 180-degree phase difference causes flow oscillations known as DWO.

During NPM-20 startup, shutdown, and high power operation, dynamic instability such as DWO is of primary concern. Onset of DWO in a single tube depends on the tube pressure drop, inlet subcooling, power distribution, flow rate, and IFR pressure drop. For parallel tube configurations, experiments show that self-sustaining DWO can occur. The FW flow enters the HCSG tubes and is heated via primary-to-secondary heat transfer. Within the SG tubes and after the single-phase liquid region, boiling occurs and voiding continues to increase until eventually superheated steam is produced at the exit. This heated channel arrangement is subject to DWO.

4.0 Phenomena Identification and Ranking and Scaling Analysis

NuScale developed a PIRT for DWO in the NPM-20 steam generator. Reference 12.1 outlines the EMDAP, which is summarized in Appendix A. Developing the PIRT is the first step of the EMDAP process because it provides critical input to the development of the EM, assessment bases, and methodology of its application. This EM utilizes the process as needed to facilitate the PIRT development in a tractable manner.

4.1 Phenomena Identification and Ranking Table Objectives

The objectives of the PIRT are to

- establish FoM.
- identify phenomena affecting FoM.
- rank phenomena applicable to the appropriate FoM.
- identify the knowledge base associated with the phenomena, and to provide a recommendation for closing the knowledge gap, as applicable.
- determine the high-importance/low knowledge level phenomena to focus the development of the analytical model and to determine additional testing requirements and design improvements.

Traditionally, the PIRT development uses a simplified nine-step process described in Reference 12.2. Those nine steps were followed on an as-needed basis in the development of the NPM-20 density wave oscillation PIRT. The PIRT supports scaling of SET and prototypical testing, and design and operation of test facilities. The PIRT identifies the most important T-H phenomena for DWO.

4.2 Phenomena Identification and Ranking Table Phenomena

Each phenomenon identified in the PIRT was assigned an importance ranking and knowledge level ranking. Table 4-1 and Table 4-2 describe the importance rankings and the knowledge level rankings considered by the PIRT panel.

Phenomena are evaluated and ranked on component bases. For the NPM-20 helical coil SG, the necessary components are the FW line, the FW plenum, the HCSG tube internal fluid, the HCSG tube wall metal, the HCSG tube external fluid (i.e., primary side liquid), the steam plenum, and the steam line. These components are grouped as shown in Table 4-3.

Table 4-1 Importance Rankings

Importance Ranking	Definition
High (H)	Significant influence on FoM
Medium (M)	Moderate influence on FoM
Low (L)	Small influence on FoM
Inactive (I)	Phenomenon not present or negligible

Table 4-2 Knowledge Level Rankings

Knowledge Level	Definition
4	Well-known and low uncertainty
3	Known and low uncertainty
2	Partially known and moderate uncertainty
1	Very limited knowledge or uncertainty cannot be characterized

Table 4-3 Component Designation for Phenomena Identification and Ranking

Component	Description	Identification
Tube inside	HCSG inside evaluated for T-H phenomena	1
Tube geometry	HCSG tube wall thickness, roughness, geometry	2
Tube outside	Primary side T-H condition for heat transfer and boundary conditions	3
FW line and FW plenum	FW line, FW plenum, and other components upstream of HCSG	4
Steam line and steam plenum	Steam line, steam plenum, and other components downstream of HCSG	5

The DWO stability PIRT (Table 4-4) is organized as follows.

- The first column lists the components identified for the system.
- The second column lists the phenomena likely to occur relevant to that component.
- The FoM columns are split where:
 - 1 refers to DWO onset.
 - 2 refers to DWO flow change amplitude.
 - 3 refers to DWO temperature change amplitude.
 - 4 refers to DWO frequency.

The four FoM are important to quantifying tube inlet fluid temperature oscillations that can cause stress cycles.

- The seventh column identifies the importance ranking.
- The eighth column identifies the knowledge level ranking (where 4 indicates the highest knowledge level).

The DWO stability PIRT (Table 4-4) lists a total of 26 phenomena or processes for the NPM-20 helical coil SG related to the following FoM: DWO onset, DWO flow amplitude, DWO temperature amplitude, and DWO frequency. No phenomena or processes are ranked with a knowledge level of one. Seventeen are importance ranked H, and a subset of six are importance ranked H with a knowledge level of two. The subset of six H-2 ranked phenomena are emphasized in bold font in Table 4-4, and are discussed in Section 4.3.

Table 4-4 Density Wave Oscillation Stability Phenomena Identification and Ranking Table

{{

}}2(a),(c)

4.3 Discussion of High Ranked Phenomena

This section provides a summary of the high (H) ranked phenomena, bases for phenomena importance ranking, and knowledge level.

4.3.1 {{ }}^{2(a),(c)}
{{

4.3.2 {{ }}^{2(a),(c)}
{{ }}^{2(a),(c)}

4.3.3 {{ }}^{2(a),(c)}
{{

}}^{2(a),(c)}

	{{			
		}}2(a),(c)		
4.3.4	{{		}}2(a),(c)	
	{{			
				}}2(a),(c)
4.3.5	{{		}}2(a),(c)	
	{{			
				}}2(a),(c)
4.3.6	{{		}}2(a),(c)	
	{{			
				}}2(a),(c)

4.3.10 {{ }}^{2(a),(c)}

{{

}}^{2(a),(c)}

4.3.11 {{ }}^{2(a),(c)}

{{

}}^{2(a),(c)}

4.3.12 {{ }}^{2(a),(c)}

{{

}}^{2(a),(c)}

Table 4-5 Nomenclature

Variable	Definition
A	Area (m^2)
D	Diameter (m)
e	Specific energy (J/kg) - includes enthalpy, kinetic, and potential energies
\bar{e}	Specific energy (J/kg) without pressure and density definition
g	Gravitational pull (m/s^2)
h	Specific enthalpy (J/kg)
H	Axial coil pitch
j	Quantity flux
k	Thermal conductivity ($\frac{W}{mK}$)
L	Length (m)
F	Forces in momentum equation, separated as friction, gravity, shear, and form loss
f_g	Variable associated with transition from liquid to vapor.
m	Mass (kg) - equivalent to ρV
P	Pressure (Pa)
q	Heat flux ($J/m^2 s$)
Q	Heat transfer (J/s)
v	Velocity (m/s)
V	Volume (m^3)
ψ	Density of some quantity X (X/m^3)
χ	Steam quality
z	Elevation of the center of mass (m)
α	Void fraction or volume fraction
ϕ	The SG tube angle from horizontal - a subscript is used if the angle is different from average SG tube angle
Γ	Water mass conversion rate from liquid to vapor per volume ($kg/m^3 s$)
λ	latent heat of vaporization
ρ	Density (kg/m^3)
t	Time (s)
τ	Characteristic time (s)
T	Temperature (K)
W	Work done by fluid (J)
ω	Characteristic frequency (s^{-1})

Table 4-6 Index Notation

Index Part	Definition
B	Buoyancy.
u, c, s, v, h	Indexes used in the steam generator region to indicate (u) the unheated liquid region, (c) the subcooled liquid region, (s) the two-phase saturated region, (v) the single-phase vapor region, and (h) steam header region
f, g	Indexes used to indicate (f) liquid and (g) gas or vapor
h	Heated length when applied to a L variable
$he1, hex, hen$	Steam header (h) at exit to steam generator tubes (e) for tube 1, tubes 2 through n-1 (x), and tube n
i, o	Inlet or outlet to a region as determined by the standard operational direction of flow
out, in	The outer diameter or inner diameter of a tube
m	Term used to indicate the property is part of the momentum analysis
Or	The orifice to a region
w	Index used to indicate the property is the wall
F	Frictional pressure loss
G	Gravitational head
I	Interfacial shear pressure loss
L	Pressure loss due to other loss terms such as orifice
sat	Saturated
sub	Subcooled
T	Variable associated with the combined steam generator tubes
$T1$	Variable associated with a single steam generator tube
0	Initial condition value
-	The bar above a property indicates that it is not pressure dependent
\sim	The tilde on a property indicates that the property is the value of the surrounding body
\cdot	Indication term is a flow rate

4.4.2 Scaling Analysis Objectives, Methodology, and Fundamental Requirements

The main objective of the scaling analysis is to evaluate the distortion resulting from physical dimensions and operating conditions of a scaled test facility capable of simulating the important flow and heat transfer behavior of the NPM-20 secondary side under steady-state and DWO conditions. Distortions are evaluated with specific objectives for each operational mode of interest identified below.

- Thermal hydraulic processes important to the DWO phenomena are identified.
- The similarity criteria that should be preserved or distortions between the test facility and the full-scale prototype are calculated.

- The priorities for preserving the similarity criteria for testing are established, or reducing distortions for testing are determined.
- Specifications for the test facility modifications are established, if required.
- Biases due to scaling distortions are identified.

To assure that the scaling objectives are met in an organized and clear traceable manner, a general design framework (GDF) was established. The model for this framework includes features drawn from Reference 12.4.

4.4.3 Density Wave Oscillation Phenomena and Experiment Objectives

The first task outlined by the GDF is to specify the experimental objectives. The experimental objectives define the types of tests that are performed to address specific design or certification needs. These objectives determine the general modes of operation that should be simulated in the test facility. There are practical limits concerning what can be studied in a single facility. The TF-2 test facility primarily focuses on evaluating steady-state operation and DWO onset criteria with operational margin.

The objectives of DWO testing at TF-2 are to obtain qualified data to benchmark computer codes and models that are used to evaluate the NPM-20 secondary side. These objectives include: measurements of steady-state T-H conditions on the secondary side and characterization of DWO phenomena.

4.4.4 NuScale Power Module Helical Coil Steam Generator Stability Phenomena Identification and Ranking Table

The second task outlined by the GDF is the development of a PIRT. PIRT information is presented in Section 4.1 through Section 4.3.

The DWO phenomena identification and rankings are provided in Table 4-3. The PIRT table results are presented in Table 4-4.

4.4.5 TF-2 Facility Operating Conditions and Dimensions

This section presents preliminary TF-2 facility operating conditions and physical dimensions and compares them to the corresponding preliminary values for the full-scale NPM-20.

4.4.5.1 Secondary-Side Steady-State Operating Conditions

This section provides the physical dimensions and operating conditions for the NPM-20 and TF-2 facility. For the NPM-20, operating conditions at 100 percent power are provided. For TF-2, test facility technical specifications and maximum allowable operation range from the existing data are provided. For evaluating distortions, discrete NPM-20 operating conditions are compared with corresponding TF-2 conditions. The TF-2 facility underwent a power upgrade to

better cover NPM-20 conditions. The TF-2 maximum power is 8.5 MW thermal. Due to the power limitations of TF-2, different modeling schemes are used for 15 percent power and 100 percent power simulations. Table 4-7 shows nominal conditions for NPM-20 and TF-2 to allow variations in the boundary conditions to reduce distortions.

Table 4-7 NuScale Power Module and TF-2 Steady-State Operating Conditions at 100 Percent Power*

Parameter (range)	NPM-20	TF-2	Units
Core power/tube (maximum)	181.2	33.73 (all rows) 163.46 (row 3 only)	kW
Primary pressure	2000 (137.9)	1450 (100)	psia (bar)
Secondary side SG temperature change	357.1 (453.74)	243 (408)	degrees F (K)
Secondary side FW pressure	545.7 (37.63)	507.63 (35)	psia (bar)
Secondary side steam plenum pressure	500 (34.48)	482.98 (33.3)	psia (bar)
Secondary side inlet temperature	200 (366.4)	200 (366.4)	degrees F (K)
Secondary side FW flow/tube	0.0705	0.05	kg/sec
Inlet loss coefficient	{{ }} ^{2(a),(c),ECI}	{{ }} ^{2(a),(c),ECI}	N/A

* Note: The best available information used for scaling analysis

Table 4-8 NuScale Power Module and TF-2 Helical Coil Steam Generator Design Comparison

Parameter	NPM-20	TF-2	Units
Tube material	Alloy 690	AISI 304L	N/A
Number of tubes	1380	252	N/A
Tube outside diameter	15.88	16.07	mm
Tube inside diameter	13.34	13.17	mm
Tube length (active)	22.4 to 25.9	25.01	m
Tube thickness	1.27	1.45	mm
Single tube inside flow area	139.66	136.24	mm ²
Helical coil radius	{{ }} ^{2(a),(c),ECI}	{{ }} ^{2(a),(c),ECI}	m

Table 4-9 NuScale Power Module and TF-2 Helical Coil Steam Generator Row 3 Comparison

Parameter	NPM-20	TF-2	Units
	Column 3	Row 3	
Coil radius	{{ }} ^{2(a),(c),ECI}	{{ }} ^{2(a),(c),ECI}	m
Active length	24.91	25.01	m
Number of tubes per column	52	52	N/A
Inclination angle	13.69	13.978	degrees
Single tube, interior fluid volume	0.0035	0.0036	m ³
Inside heat transfer area	1.044	1.1079	m ²
Tube material	Alloy 690	AISI 304L	N/A

Table 4-8 shows TF-2 and NPM-20 geometry parameter comparison. Tube inner diameter and length are very close, which enhances in-tube T-H scaling. The SG tube thickness is 15 percent larger for TF-2, which increases the primary-to-secondary heat transfer resistance somewhat, but the tube metal is not the dominant resistance to heat transfer. Heat flux can be increased with an increased primary hot leg temperature (T_{hot}).

Table 4-9 provides a geometry comparison specifically for Row 3. As shown in Table 4-9, the TF-2 Row 3 geometrical parameters closely match the NPM-20 Column 3 parameters.

4.4.6 Scaling Evaluation using the Hierarchical Two-Tier Scaling Method

The next step in the GDF method requires scaling analyses for each of the hierarchical levels (e.g., systems and subsystems) and their modes of operation, as defined in Section 4.4.5. This section describes the Hierarchical Two-Tier Scaling (H2TS) method. This method has been used to develop the similarity criteria necessary to scale NuScale Integral System Test Facility for loss of coolant accident (LOCA) transients. The H2TS method was developed by the NRC and is fully described in Reference 12.4. It was expanded upon in Reference 12.5, Reference 12.6, and Reference 12.7.

Figure 4-1 presents the four basic elements of the H2TS analysis method. The first element consists of subdividing the plant into a hierarchy of systems. Each system is subdivided into interacting subsystems, which are further subdivided into interacting modules, which are further subdivided into interacting constituents (materials), which are further subdivided into interacting phases (liquid, vapor, or solid). Each phase can be characterized by one or more geometrical configurations, and each geometrical configuration can be described by three field equations (e.g., mass, energy, and momentum conservation equations). Each field equation can incorporate several processes.

Figure 4-1 Flow Diagram for the Hierarchical Two-Tier Scaling Analysis

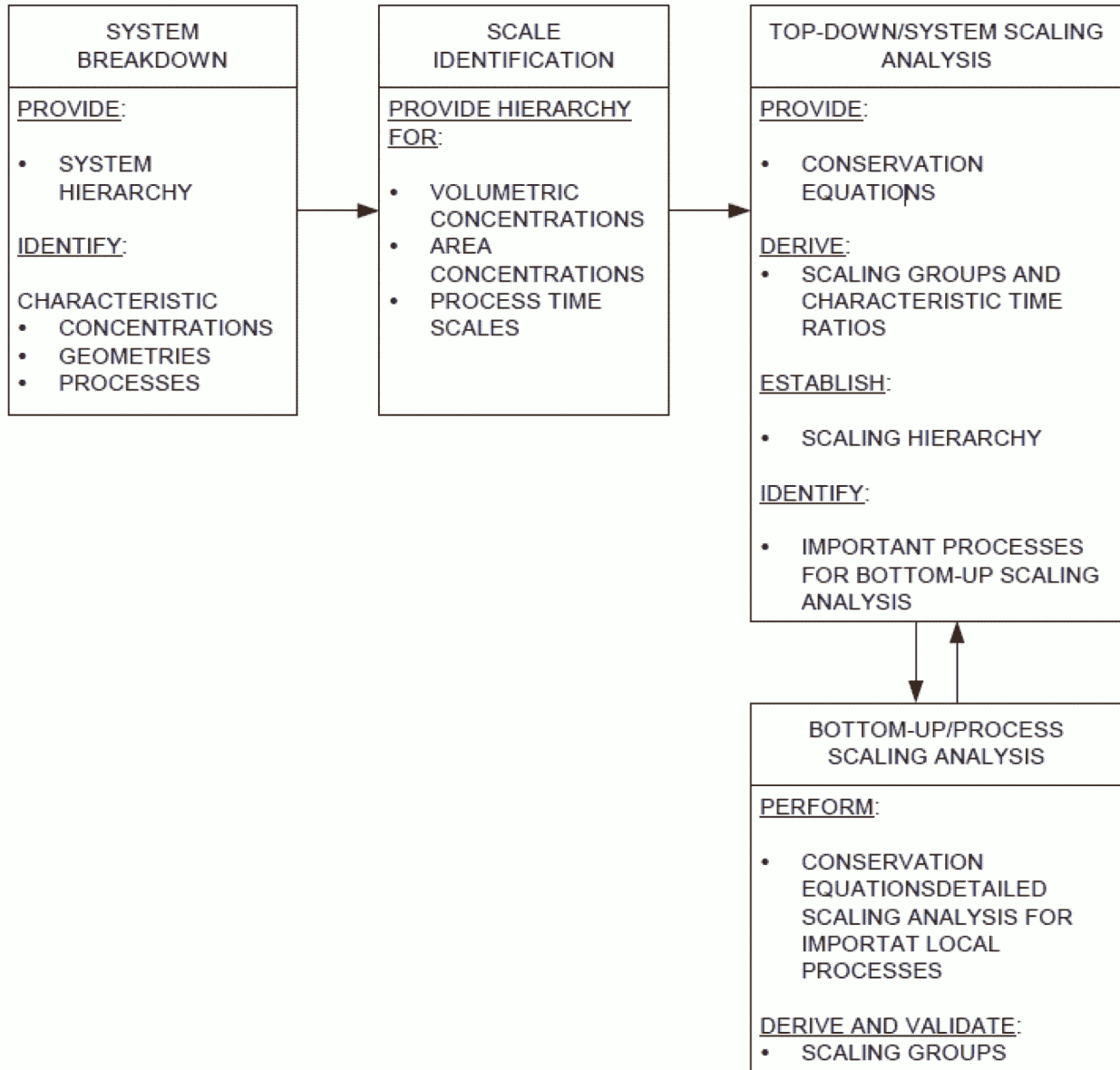


Figure 4-2 Helical Coil Steam Generator Breakdown into Hierarchical Levels and Primary Operational Modes

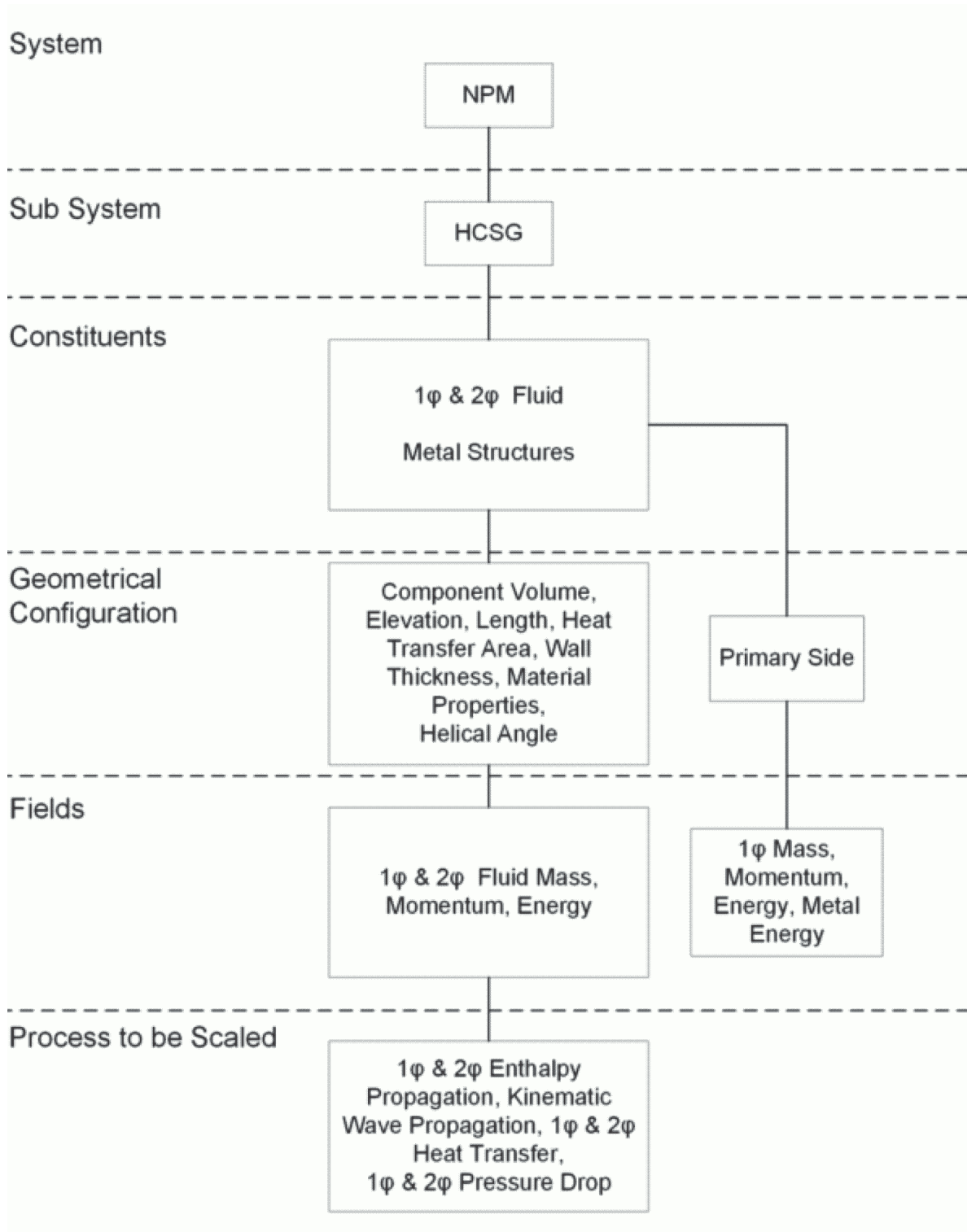
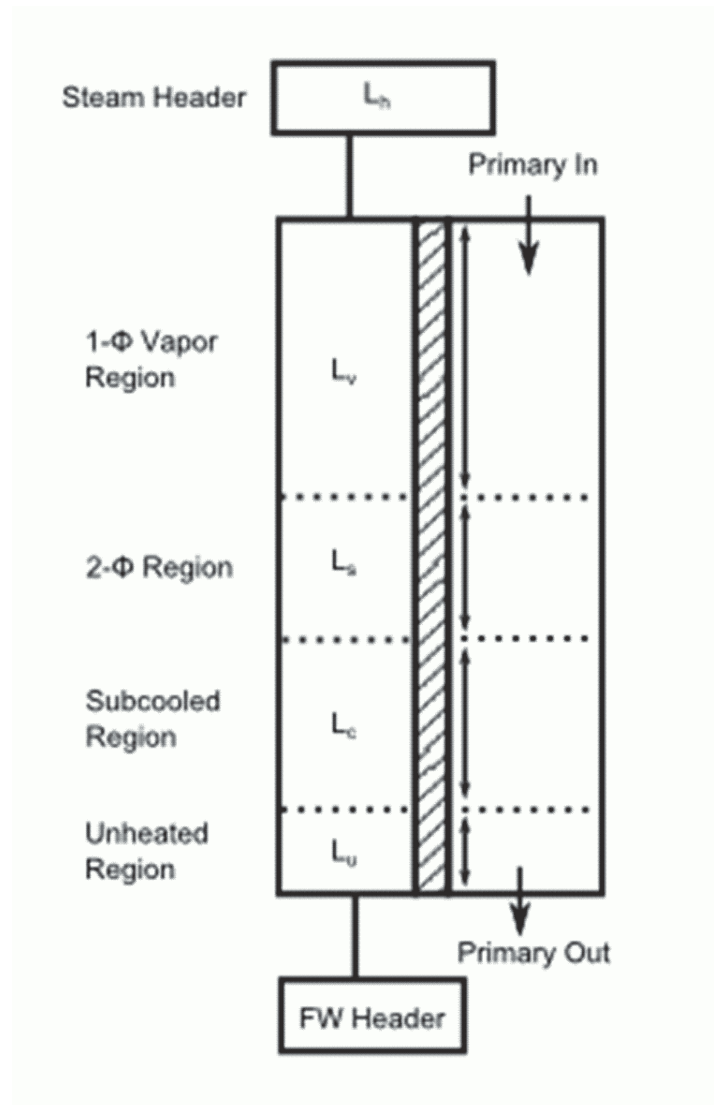


Figure 4-2 presents the breakdown of the NPM-20 into hierarchical levels and high-level processes to be scaled. It provides a roadmap used to structure the subsequent scaling analyses. The RCS and the HCSG tubes are the focus of this scaling study.

4.4.6.1 Scaling Analysis Methodology

The basic objective of the H2TS scaling method is to develop a set of characteristic time ratios for the physical processes that play a significant role in the system response. For DWO phenomena, different physics or terms in the system equations are dominant in different regions of the HCSG tube. Thus, the HCSG tube region is divided into regions where different terms are dominant.

Figure 4-3 NuScale Power Module Helical Coil Steam Generator Region Breakdown



As shown in Figure 4-3, the HCSG secondary side is divided into five regions: four regions for the HCSG tube and a fifth steam header region where the HCSG tubes merge. The FW header provides a boundary condition. An orifice at the inlet to the HCSG region plays an important role in stabilizing DWO behavior and is included in the model as part of an unheated entrance section of the SG tube. In order to induce DWO, the orifice is modeled as a valve that slowly opens over the simulation. Note that the TF-2 experiment includes an unheated section of pipe beyond the heated orifice, while the NPM-20 does not include an unheated section of pipe after the orifice. This configuration is followed by the heated single-phase liquid region, the two-phase mixture region, and the single-phase vapor region. Lengths of the heated regions depend on initial and boundary conditions. The length of the subcooled region is established by OSV if void information is available. When insufficient void information is available but heat transfer data are available, the length of the single-phase region can be estimated by the amount of heat addition required for the water to reach saturation conditions. Because systems typically exhibit some subcooled boiling, the use of void fraction data is the preferable method to calculate the boundary of the subcooled and two-phase regions. The boundary between the two-phase region and the single-phase vapor region is determined by the energy required to heat the liquid entering the HCSG to saturated conditions and convert it to steam.

4.4.6.2 Fluid Field Equations

As part of the two-tiered hierarchical scaling analysis, after the system is divided into relevant systems, subsystems, modules, constituents, phases, and geometrical configurations, the relevant field equations for a particular geometrical configuration are scaled. Table 4-10 shows the basic field equations, which are the mass continuity equation, the energy equation, and the momentum equation.

Table 4-10 Field Equations

Field	Field Equation
Mass	$\frac{dm}{dt} - \dot{m}_i + \dot{m}_o = \nabla \Gamma, \dot{m} = \rho Av, m = \rho V = (\text{i.e. for two phase } (\rho \alpha V))$
Energy	$\frac{d(m\bar{e})}{dt} - \dot{m}_i e_i + \dot{m}_o e_o = Q - W$
	$e = h + \frac{1}{2}v^2 + gz = u + \frac{P}{\rho} + \frac{1}{2}v^2 + gz, \bar{e} = u + \frac{1}{2}v^2 + gz$
Momentum	$\frac{d(mv)}{dt} - \dot{m}_i v_i + \dot{m}_o v_o = -\Delta PA + F_G + F_I + F_L + F_F$
	or
	$\frac{d(L\rho v)}{dt} - \rho_i v_i^2 + \rho_o v_o^2 = -\Delta P + \frac{F_G}{A} + \frac{F_I}{A} + \frac{F_L}{A} + \frac{F_F}{A}$
	F_G (Gravitational Force), F_I (Interfacial Force)
	F_L (Form Loss), F_F (Frictional Force)

The typical definition of ΔP (i.e., the downstream pressure minus the upstream pressure) leads to a negative ΔP value for pressure-driven flow. In order to obtain positive Π group values, the definition is reversed (upstream pressure minus downstream pressure).

In the heated region, the enthalpy and internal energy terms are much larger than the kinetic and potential energy terms.

At an operating pressure of 2000 psia, the enthalpy of vaporization is $\{ \}^{2(a),(c)}$, and the change in internal energy is $\{ \}^{2(a),(c)}$. At 100 percent power, the exit velocity of the HCSG tubes is about $\{ \}^{2(a),(c)}$, which equates to a kinetic energy of $\{ \}^{2(a),(c)}$. The difference in elevation across the HCSG tube (h) is about $\{ \}^{2(a),(c)}$. The change in potential energy across the HCSG tubes is about $\{ \}^{2(a),(c)}$ (gh). Thus, enthalpy and internal energy are over three orders of magnitude larger than kinetic and potential energy in the heated region; the kinetic and potential energy are ignored in this region. The variable W represents the work due to pressure loss terms. Neglecting the kinetic energy and potential energy terms leads to the following simplified energy equation, which is used in the heated region of the HCSG tube.

$$\frac{d(mu)}{dt} - \dot{m}_i h_i + \dot{m}_o h_o = Q - W \tag{Equation 4-1}$$

As noted previously, the SG tube is divided into four regions, with the steam header comprising the fifth region. The field equations are evaluated in each of these regions. These regions are an unheated region, a subcooled liquid region, a two-phase vapor generation region, a single-phase vapor region, and the steam header region. The subscripts i and o are used to indicate boundary terms at the inlet and outlet of the HCSG tube region. A subscript is used with the field equations to identify variables associated with each region: u for the unheated region, c for the subcooled region, s for the saturated two-phase region, v for the single-phase vapor region, and h for the steam header region. Thus, for example, v_{so} indicates the velocity at the outlet of the two-phase region. The boundary between the subcooled liquid region and the two-phase region is determined by OSV when void data are available. Since OSV can occur when the bulk temperature is below saturation conditions, the two-phase region may contain some liquid that is not yet at saturation conditions.

For the single-phase liquid and single-phase vapor regions, the vapor generation term Γ and the interfacial friction force term F_I are zero. This condition is also true in the two-phase region when considered as a mixture because the liquid and vapor equations each have an equal and opposite vapor generation. The interfacial friction and buoyancy terms also have equal and opposite forces between liquid and vapor, which cancel when liquid and vapor equations are summed.

4.4.6.3 Evaluation of Scaling Analysis Equations

The scaling analysis calculations are based on NRELAP5 models of the NPM-20 and the TF-2 facility. Calculations are summed over cells within the models, and many of the calculations are summed only over the cells in a particular region. For example, the length of the subcooled region is determined by the location of OSV, which is defined as void of 0.5 percent. The location typically includes only a fraction of a cell.

Once the cells have been defined for a region, calculations for quantities defined over the region are evaluated by summing the quantities over the cells in the region. The summation symbol is implied for the region calculations. At the edges of a region, when only a fraction of a cell is included in the region, linear interpolation is used to partition the calculated value between the adjacent regions.

As an example, in the subcooled region the gravitational Π group is defined in Equation 4-2.

$$\Pi_{cG} = \frac{\rho_{c0} g L_{c0}}{S_m} \sin(\phi_c) \quad \text{Equation 4-2}$$

4.4.6.4 Calculating Temporal Scales and Frequencies

The two-tiered hierarchical scaling methodology directs calculating temporal scales associated with processes in order to group processes into those of the same order of magnitude. This is done when examining a control volume in order to determine the relative importance.

The temporal scale characterizes a process that occurs across a boundary into a control volume. The formula for calculating the temporal scale is shown in Equation 4-3.

$$\tau = \frac{V\psi}{Aj} \quad \text{Equation 4-3}$$

The variable V is the control volume being analyzed, and A is the area of the boundary across which a transfer process occurs. ψ is the quantity density (i.e., quantity per volume), and j is the quantity flux (i.e., transfer of quantity per area) associated with the field equation being analyzed. For example, the quantity may be mass and the density is then mass density. The flux represents mass flux across a boundary or possibly a mass conversion process such as condensation. In a case like condensation, where the rate may be expressed as a volumetric rate, Aj would need to be replaced by $V\psi'$, where $V\psi'$ represents the transfer rate per volume.

It is also common for quantities to be specified on a per mass basis (γ). The temporal scale for mass transfer in the volume, which is used commonly in development of the non-dimensional Π groups, is shown in Equation 4-4.

$$\tau = \frac{m}{\dot{m}} \quad \text{Equation 4-4}$$

A non-dimensional Π group is defined for each term in the field equations. Given the time scale associated with a Π group, the Π groups are decomposed into the product of the temporal scale and a specific frequency of the process ω as shown in Equation 4-5.

$$\Pi = \tau\omega \quad \text{Equation 4-5}$$

4.4.6.5 The Phase Change Number and Subcooling Number

The standard parameters used to characterize DWO stability are the phase change (or Zuber) number and the subcooling number, which are defined in Equation 4-6 and Equation 4-7.

$$N_{pch.eq} = \frac{Q}{\dot{m} h_{fg}} \frac{\rho_f - \rho_g}{\rho_g} \quad \text{Equation 4-6}$$

$$N_{sub} = \frac{\Delta h_i}{\Delta h_{fg}} \frac{\rho_f - \rho_g}{\rho_g} \quad \text{Equation 4-7}$$

These equations are useful for comparing results to the literature. While these parameters are useful for generating a stability map for individual systems, it is well known that the stability results do not directly translate to other systems. However, different systems are expected to show similar stability map trends relative to these parameters.

4.4.6.6 Selecting the Time Point for Performing Scaling Analysis

The scaling analysis is used to characterize conditions at the onset of DWO. For both the NPM-20 and TF-2 models, the K_{inlet} for the SG tubes is set high enough that the model is initially in a stable state that exhibits no DWO instability. In order to induce DWO in the NRELAP5 model, the K_{inlet} is reduced by slowly opening the valve. As the orifice resistance goes below a critical threshold, DWO onset is observed.

Non-dimensional numbers are also used to evaluate the onset of DWO. Because DWO typically shows the flow and velocity oscillation, HCSG outlet velocity is chosen as a parameter to indicate the onset of DWO. For non-dimensionalization, an inlet liquid velocity that is fixed from the boundary condition is used as a non-dimensional parameter. The ratio of the HCSG tube outlet vapor velocity to the HCSG tube inlet liquid velocity is selected to identify the onset of DWO because it provides a good indication of the onset of DWO. This ratio is defined as Π_v and is related to the Zuber number and phase change number that are commonly used to characterize the onset of DWO.

Below is an example plot of Π_v for the TF-2 facility at 15 percent power. From Figure 4-4 it is apparent that DWO onset occurs at about $\{ \{ \}^{2(a),(c)}$. This time is used as the time point for performing the non-dimensionalization. While $\{ \{ \}^{2(a),(c)}$ shows that oscillations begin at a later time, each case can only have one point where the non-dimensionalization time starts. The onset of DWO can be seen in the ratio of the HCSG tube outlet velocity to the fixed HCSG tube inlet velocity during DWO onset and full-cycle DWO.

Figure 4-4 Density Wave Oscillation Onset

{{

}}2(a),(c)

4.4.7 NRELAP5 Models for Scaling Assessments

The NPM-20 cases are selected to cover 100 percent power and 15 percent power. A power level of 100 percent is important because the plant is expected to operate at this level most often. A 15 percent power condition represents the low power condition where the full set of TF-2 rows are operational. Table 4-11 lists the steady-state parameters expected for the NPM-20 and TF-2 secondary side at selected power levels.

4.4.8 Analysis of scaling distortions

Nondimensional Π groups are derived for the system governing equations to allow comparison of the TF-2 test facility results with the NPM-20 simulation results. The Π groups help establish the relative importance of different terms in the governing equations. The Π group development allows separation of relevant from irrelevant DWO phenomena.

A comparison of the TF-2 and NPM-20 Π groups determines if the scale model geometry, boundary, or initial conditions introduce significant scaling distortions. The effect of distortion in the model for a specific process can be quantified as shown in Equation 4-8.

$$DF = \frac{[\Pi_i]_P - [\Pi_i]_m}{[\Pi_i]_P} \quad \text{Equation 4-8}$$

Index m indicates the reduced scale model (TF-2 experimental model) that is used for validation purposes, and P is full-scale prototype (NPM-20). The distortion factor (DF) represents the fractional difference in the amount of conserved property transferred through the evolution of a specific process in the prototype to the amount of property conserved through the same process in the model during the respective residence time. The degree to which a specific transfer process impacts a particular transient is determined by comparing the maximum characteristic time ratio for each of the transfer processes that arise during the transient.

A global distortion factor is defined that combines the individual distortion factors, weighted by the relative magnitude of the Π groups in order to give proper weighting to the distortion factors. The global distortion factor is calculated for each of the executed simulations.

Results are summarized in Table 4-12 and Table 4-13 that tabulate values of the Π groups with the distortion from Equation 4-8. {{

}}2(a),(c)

The scaling analysis gives rise to several Π groups. The Π groups are defined for each of the SG tube regions (unheated, subcooled, two-phase, single-phase vapor, and steam header), with Π groups calculated for both the primary and secondary side. A Π group is defined for each term of each field equation used to characterize the behavior in a region.

Not all of the Π groups are important for characterizing DWO behavior. The Π groups that provide similar information are not included; for example, several

single-phase vapor Π groups and steam header Π groups provide the similar flow information. Therefore, only one set of Π groups are used.

There are Π groups calculated for the primary side flow across the SG tubes. While these Π groups provide some information about the source of heat transfer to the secondary side, the overall heat transfer to each region is of primary importance. Heat transfer is already characterized by the secondary side heat transfer Π groups. Thus, the primary side Π groups tend to provide repetitive information.

In order to determine which of the SG secondary side Π groups are important, it is useful to look at the Π group values. Note that the Π group terms for the momentum equation in each of the regions is scaled by the total pressure drop across the tubes rather than by a pressure drop across the region. Scaling by total pressure drop across the tubes is done in order to allow Π groups in different regions to be compared directly in order to determine the relative importance of each momentum Π group over the tube region. Similarly, the energy equation in each region is scaled relative to the energy needed to convert the liquid entering the region from saturated liquid to saturated vapor. Thus, the energy Π groups in each region can be compared for relative importance. Based on the values of Π groups, only the dominant Π groups are presented in the scaling analysis.

Table 4-12 TF-2 Distortion for Density Wave Oscillation Phenomena Compared with 100 Percent NuScale Power Module Operating Condition

{{

}}^{2(a),(c)}

Table 4-13 TF-2 Distortion for Density Wave Oscillation Phenomena Compared with 15 Percent NuScale Power Module Operating Condition (Continued)

{{

}}^{2(a),(c)}

Table 4-14 provides the comparison between pressure drop II groups for similar regions in the NPM-20 and at TF-2 at 100 percent power levels. Note that the overall region lengths are comparable between NPM-20 and TF-2. Table 4-15 provides the comparison of pressure drop II groups for similar regions in the NPM-20 and at TF-2.

Table 4-14 Pressure Group Distortion at 100 Percent Power Condition

{{

}}^{2(a),(c)}

Table 4-15 Pressure Group Distortion at 15 Percent Power Condition

{{

}}^{2(a),(c)}

 {{

$$\}}^{2(a),(c)}$$

4.4.9 Scaling Sensitivity and Distortion Optimization Methodology

The baseline boundary conditions for the TF-2 tests are selected to align with boundary conditions in the NPM-20 at equivalent power. Ideally, the TF-2 tests for the given power levels would have zero distortion relative to the NPM-20 at equivalent power. Due to differences between the TF-2 facility and the NPM-20 steam generator, some distortion is expected. However, it is desirable for this distortion to be as small as possible. Minimizing distortion is accomplished via optimization; the objective of optimization is to identify adjusted TF-2 boundary conditions at which to run the system in order to have the smallest distortion. However, given that separate distortion factors are calculated for each Π group, the Π groups are combined into a single system-wide distortion factor that can be minimized in order to determine whether a change in boundary conditions leads to a smaller overall distortion.

The list of Π groups included to calculate the global distortion is:

{{ $\}}^{2(a),(c)}$

Global distortions are calculated from a set of sensitivity cases to identify conditions that lead to minimal distortions.

There are several parameters that can be varied in the experiments that have an impact on the Π groups and the associated distortions. The following five parameters are likely to have an impact.

- {{

}}2(a),(c)

For each parameter, a lower and an upper sensitivity bound is selected around the baseline parameter value. A sensitivity analysis is performed on each of the parameters individually. A summary of the results are provided in Table 4-16, Table 4-17, and Table 4-18.

Table 4-16 Parameter Bounds for the 15 Percent Power Sensitivity Cases

{{

}}2(a),(c)

Table 4-17 Parameter Bounds for the 100 Percent Power Sensitivity Cases

{{

}}2(a),(c)

Table 4-18 Distortions for the Optimal Cases

{{

}}2(a),(c)

4.4.10 Transient Distortions

For the current scaling analysis, the momentum equation is non-dimensionalized over the whole tube. The same base momentum equation (Equation 4-9) is used with the terms calculated for the whole SG tube rather than region-specific terms used in the steady state analysis.

{{

Equation 4-9

}}2(a),(c)

The non-dimensionalization of the whole SG tube is similar to the non-dimensionalization of the different regions of the SG tube. The same scaling factor $1/\Delta P_{T1}$ is used for whole SG tube scaling. However, the left-hand momentum terms are divided into three Π groups. The nondimensionalized equation after applying the scaling factor is shown in Equation 4-10.

{{

Equation 4-10

}}2(a),(c)

Π Groups Π_P , Π_g , Π_F , and Π_O are a natural extension of the associated Π groups from each of the SG tube regions; they are the sum of the associated Π groups over a SG tube region. The Π group definitions for each of the terms is shown in Equation 4-11 through Equation 4-17.

{	{	Equation 4-11
	}}2(a),(c)	
{	{	Equation 4-12
	}}2(a),(c)	
{	{	Equation 4-13
	}}2(a),(c)	
{	{	Equation 4-14
	}}2(a),(c)	
{	{	Equation 4-15
	}}2(a),(c)	
{	{	Equation 4-16
	}}2(a),(c)	
{	{	Equation 4-17
	}}2(a),(c)	

The variables m and v are whole-tube quantities defined in Equation 4-18 and Equation 4-19, respectively. Subscript i is an index associated with NRELAP5 cells in the SG tube region; subscript 0 indicates the value evaluated at the time selected for nondimensionalization. For the transient analysis, the DWO onset point is used as the time for nondimensionalization.

$$m = \sum m_i, \quad m^+ = \frac{m}{m_0} \tag{Equation 4-18}$$

$$v = \frac{\sum m_i v_i}{\sum m_i}, \quad v^+ = \frac{v}{v_0} \tag{Equation 4-19}$$

The non-dimensional time is defined in Equation 4-20.

$$t^+ = \frac{t}{\tau} \tag{Equation 4-20}$$

The variable τ is defined as m/\dot{m} . It represents the time required to transport liquid through the SG tube or the time required to replace the fluid in the SG tube. In order to examine the frequency of oscillation or time period, the non-dimensionalized

momentum term is expanded as shown in Equation 4-21. Plots of this term represent the change in momentum with time scaled by the pressure force applied across the SG tubes.

{{

Equation 4-21

}}^{2(a),(c)}

For comparing non-dimensionalized transient scaling factors and evaluating distortions, NPM-20 and TF-2 NRELAP5 cases are run beyond DWO onset and are allowed to reach the limit cycle. The DWO onset and transient parameters are used to evaluate the transient II groups.

Transient Response for TF-2

{{

}}^{2(a),(c)}

Transient II groups for 100 percent and 15 percent power for NPM-20 and TF-2 are shown in Table 4-19 and Table 4-20 below.

Table 4-19 Transient II Group Distortion for TF-2 and NuScale Power Module 100 Percent Power

{{

}}^{2(a),(c)}

Table 4-20 Transient Π Group Distortion for TF-2 and NuScale Power Module 15 Percent Power

{{

}}2(a),(c)

{{

}}2(a),(c)

Table 4-21 and Table 4-22 show the DWO amplitude (or resultant delta oscillation) and frequency distortions between NPM-20 and TF-2 for 100 percent and 15 percent power.

{{

}}2(a),(c)

Table 4-21 Nondimensional Resultant Momentum Oscillation and Frequency Comparison Between TF-2 and NuScale Power Module at 100 Percent Power

{{

}}2(a),(c)

Table 4-22 Nondimensional Resultant Momentum Oscillation and Frequency Comparison Between TF-2 and NuScale Power Module at 15 Percent Power

{{

}}2(a),(c)

4.4.11 Scaling and Distortion Analysis Conclusion

Scaling analysis on TF-2 is performed using the H2TS method to identify the important Π groups providing a comparison of phenomena important to DWO onset between NPM-20 and TF-2 in non-dimensional space. Scaling optimization is also performed to reduce the distortions by optimizing the test conditions at TF-2. Transient scaling analysis evaluates relative distortions by comparing oscillation magnitude and frequency in non-dimensional space. The purpose of TF-2 is not to provide a direct simulation of NPM-20 conditions but rather to generate applicable validation test data. Testing at TF-2 provides an adequately-scaled prototypic test facility for providing validation data for DWO onset in the NPM-20 over a range of power conditions.

5.0 NRELAP5 Code Description

The NuScale DWO evaluation model is based on the NRELAP5 system T-H code. The NRELAP5 code includes models for characterization of hydrodynamics, heat transfer between structure and fluids, modeling of fuel, reactor kinetics models, and control systems. NRELAP5 uses a two-fluid, non-equilibrium, non-homogeneous model to simulate system T-H responses.

This section provides a general overview of the code structure, models, and correlations. This section also addresses specific code models and improvements implemented to address unique design features and phenomena for the NPM-20. The adequacy of code models and correlations essential for modeling the high-ranked PIRT phenomena is discussed in Section 4.0. The full details of the models and correlations that makeup NRELAP5 can be found in the NRELAP5 Theory Manual (Reference 12.8).

RELAP5-3D[®], version 4.1.3, is the baseline development platform for the NRELAP5 code. RELAP5-3D[®] was procured and underwent commercial grade dedication, which was performed by NuScale to establish the baseline NRELAP5 code. Subsequently, features were added and changes were made to NRELAP5 to address the unique aspects of the NPM-20 design and licensing methodology. Those aspects of NRELAP5 that are new or revised specifically for the NPM-20 application include:

- helical coil SG heat transfer and pressure drop models
- core critical heat flux (CHF) models
- wall condensation models
- critical flow models
- interfacial drag models for large-diameter pipes
- core CHF limit stop

The HCSG heat transfer and pressure drop models are of particular importance to prediction of DWO onset and are detailed in Section 6.0. Code modifications of importance to prediction of DWO onset are listed and described in Table 5-1.

The RELAP5 series of codes were developed at the INL under sponsorship of the Department of Energy (DOE), the NRC, members of the International Code Assessment and Applications Program, members of the Code Applications and Maintenance Program, and members of the International RELAP5 Users Group. Specific applications of the code have included simulations of transients in light water reactor systems, such as loss of coolant accidents, anticipated transients without scram, and anticipated operational occurrences, such as loss of FW, loss of offsite power, station blackout, and turbine trip.

The RELAP5 code, including the RELAP5-3D[®] version that was used as the development platform for NRELAP5, has an extensive record of usage and acceptable performance for nuclear safety analysis. RELAP5-3D[®] is the latest version of the RELAP5 code that has been under continuous development since 1975, first under NRC

sponsorship and then with additional DOE sponsorship beginning in the early 1980s. While NRC sponsorship ended in 1997, the DOE continued sponsorship of RELAP5-3D[®] to meet its own reactor safety assessment needs. The RELAP5 code was chosen by DOE as the T-H analysis tool because of its widespread acceptance.

Table 5-1 NRELAP5 Code Modifications (Density Wave Oscillation Specific)

{{

}}2(a),(c)

5.1 Quality Assurance Requirements

The NRELAP5 code is developed following the requirements of the NuScale Quality Assurance Program Description (Reference 12.9). The NuScale corporate Software Configuration Management Plan provides a framework for NRELAP5 configuration management and change control in conformance with the requirements outlined in the NuScale Software Program Plan. The NuScale Quality Assurance Program Description complies with the requirements of 10 CFR 50, Appendix B, “Quality Assurance Criteria for Nuclear Power Plants and Fuel Reprocessing Plants” (Reference 12.10) and ASME NQA-1-2008 and NQA-1a-2009 Addenda, “Quality Assurance Program Requirements for Nuclear Facility Applications” (Reference 12.11).

5.2 Hydrodynamic Model

The NRELAP5 hydrodynamic model is a transient, two-fluid model for flow of a two-phase vapor-gas-liquid mixture that can contain non-condensable components in the vapor-gas phase as well as a soluble component (i.e., boron) in the liquid phase. The two-fluid equations of motion that are used as the basis for the NRELAP5 hydrodynamic model are formulated in terms of volume and time-averaged parameters of the flow. Phenomena that depend upon transverse gradients, such as friction and heat transfer, are formulated in terms of the bulk properties using empirical transfer coefficient formulations. In situations where transverse gradients cannot be represented within the framework of empirical transfer coefficients, such as subcooled boiling, additional models specifically developed for the particular situation are employed. The system model is solved numerically using a semi-implicit, finite-difference technique.

5.2.1 Field Equations

The NRELAP5 T-H model solves eight field equations for eight primary dependent variables. The primary dependent variables are pressure, phase-specific internal energies, vapor or gas volume fraction, phasic velocities, non-condensable quality, and boron density. For the one-dimensional equations, the independent variables are time and distance. Non-condensable quality is defined as the ratio of the non-condensable gas mass to the total vapor or gas phase mass.

The secondary dependent variables used in the equations are phasic densities, phasic temperatures, saturation temperature, and non-condensable mass fraction in the non-condensable gas phase for the i_{th} non-condensable species.

The basic field equations for the two-fluid, non-equilibrium model consist of two phasic continuity equations, two phasic momentum equations, and two phasic energy equations. The equations are time-averaged and one-dimensional. The phasic continuity equations are shown in Equation 5-1 and Equation 5-2.

$$\frac{\partial}{\partial t}(\alpha_g \rho_g) + \frac{1}{A} \frac{\partial}{\partial x}(\alpha_g \rho_g v_g A) = \Gamma_g \quad \text{Equation 5-1}$$

$$\frac{\partial}{\partial t}(\alpha_f \rho_f) + \frac{1}{A} \frac{\partial}{\partial x}(\alpha_f \rho_f v_f A) = \Gamma_f \quad \text{Equation 5-2}$$

Continuity consideration yields the interfacial condition of Equation 5-3.

$$\Gamma_f = -\Gamma_g \quad \text{Equation 5-3}$$

The interfacial mass transfer model assumes that total mass transfer can be partitioned into mass transfer at the vapor to liquid interface in the bulk fluid (Γ_{ig}) and mass transfer at the vapor to liquid interface in the thermal boundary layer near the walls (Γ_w) as defined by Equation 5-4.

$$\Gamma_g = \Gamma_{ig} + \Gamma_w \quad \text{Equation 5-4}$$

The phasic momentum equations are in the form of Equation 5-5 and Equation 5-6.

$$\begin{aligned} \alpha_g \rho_g A \frac{\partial v_g}{\partial t} + \frac{1}{2} \alpha_g \rho_g A \frac{\partial v_g^2}{\partial x} = & -\alpha_g A \frac{\partial P}{\partial x} + \alpha_g \rho_g B_x A - (\alpha_g \rho_g A) F W G \cdot v_g \\ & + \Gamma_g A (v_{gI} - v_g) - (\alpha_g \rho_g A) F I G \cdot (v_g - v_f) \\ & - C \alpha_g \alpha_f \rho_m A \left[\frac{\partial (v_g - v_f)}{\partial t} + v_f \frac{\partial v_g}{\partial x} - v_g \frac{\partial v_f}{\partial x} \right] \end{aligned} \quad \text{Equation 5-5}$$

$$\begin{aligned} \alpha_f \rho_f A \frac{\partial v_f}{\partial t} + \frac{1}{2} \alpha_f \rho_f A \frac{\partial v_f^2}{\partial x} = & -\alpha_f A \frac{\partial P}{\partial x} + \alpha_f \rho_f B_x A - (\alpha_f \rho_f A) F W F \cdot v_f \\ & - \Gamma_g A (v_{fI} - v_f) - (\alpha_f \rho_f A) F I F \cdot (v_f - v_g) \\ & - C \alpha_f \alpha_g \rho_m A \left[\frac{\partial (v_f - v_g)}{\partial t} + v_g \frac{\partial v_f}{\partial x} - v_f \frac{\partial v_g}{\partial x} \right]. \end{aligned} \quad \text{Equation 5-6}$$

The force terms on the right sides of Equation 5-5 and Equation 5-6 are, respectively, the pressure gradient, the body force (i.e., gravity and pump head), wall friction, momentum transfer due to interface mass transfer, interface frictional drag, and force due to virtual mass. The terms *FWG* and *FWF* are part of the wall frictional drag, which are linear in velocity and are products of the friction coefficient, the frictional reference area per unit volume, and the magnitude of the fluid bulk velocity. The coefficients *FIG* and *FIF* are part of the interface frictional drag; two different models (drift flux and drag coefficient) are used for the interface frictional drag, depending on the flow regime.

Conservation of momentum at the interface requires that the force terms associated with interface mass and momentum exchange sum to zero as shown by Equation 5-7.

$$\begin{aligned} \Gamma_g A v_{gI} - (\alpha_g \rho_g A) F I G \cdot (v_g - v_f) - C \alpha_g \alpha_f \rho_m A \left[\frac{\partial (v_g - v_f)}{\partial t} \right] \\ - \Gamma_g A v_{fI} - (\alpha_f \rho_f A) F I F \cdot (v_f - v_g) - C \alpha_f \alpha_g \rho_m A \left[\frac{\partial (v_f - v_g)}{\partial t} \right] = 0 \end{aligned} \quad \text{Equation 5-7}$$

The phasic thermal energy equations are defined by the following Equation 5-8 and Equation 5-9.

$$\begin{aligned} \frac{\partial}{\partial t} (\alpha_g \rho_g U_g) + \frac{1}{A} \frac{\partial}{\partial x} (\alpha_g \rho_g U_g v_g A) = & -P \frac{\partial \alpha_g}{\partial t} - \frac{P}{A} \frac{\partial}{\partial x} \alpha_g v_g A \\ & + Q_{wg} + Q_{ig} + \Gamma_{ig} h_g^* + \Gamma_w h_g' + DISS_g \end{aligned} \quad \text{Equation 5-8}$$

$$\begin{aligned} \frac{\partial}{\partial t}(\alpha_f \rho_f U_f) + \frac{1}{A} \frac{\partial}{\partial x}(\alpha_f \rho_f U_f \mathcal{V}_f A) = & -P \frac{\partial \alpha_f}{\partial t} - \frac{P}{A} \frac{\partial}{\partial x}(\alpha_f \mathcal{V}_f A) \\ & + Q_{wf} + Q_{if} - \Gamma_{ig} h_f^* - \Gamma_w h_f' + DISS_f. \end{aligned} \quad \text{Equation 5-9}$$

In the phasic energy equations, Q_{wg} and Q_{wf} are the phasic wall heat transfer rates per unit volume. These phasic wall heat transfer rates satisfy Equation 5-10 where Q is the total wall heat transfer rate to the fluid per unit volume.

$$Q = Q_{wg} + Q_{wf} \quad \text{Equation 5-10}$$

The vapor generation (or condensation) consists of two parts: vapor generation that results from energy exchange in the bulk fluid (Γ_{ig}), and energy exchange in the thermal boundary layer near the wall (Γ_w) (Equation 5-4). Each of the vapor generation (or condensation) processes involves interface heat transfer effects. The interface heat transfer terms (Q_{ig} and Q_{if}) appearing in Equation 5-8 and Equation 5-9 include heat transfer from the fluid states to the interface due to interface energy exchange in the bulk and in the thermal boundary layer near the wall. The vapor generation (or condensation) rates are established from energy balance considerations at the interface.

The phasic energy dissipation terms, $DISS_g$ and $DISS_f$, are the sums of wall friction, pump, and turbine effects. The dissipation effects due to interface mass transfer, interface friction, and virtual mass are neglected.

5.2.2 State Relations

The six-equation model uses five independent state variables with an additional equation for the non-condensable gas component. The independent state variables are P , α_g , U_g , U_f , and X_n . The remaining thermodynamic fluid variables (temperatures, densities, partial pressures, qualities, etc.) are expressed as functions of these five independent state variables (Equation 5-11). In addition to these variables, several state derivatives are needed for some of the linearizations used in the numerical scheme.

$$\left(\frac{\partial \rho_g}{\partial P}\right)_{U_g, X_n}, \left(\frac{\partial \rho_g}{\partial U_g}\right)_{P, X_n}, \left(\frac{\partial \rho_g}{\partial X_n}\right)_{P, U_g}, \left(\frac{\partial \rho_f}{\partial P}\right)_{U_f}, \left(\frac{\partial \rho_f}{\partial U_f}\right)_P \quad \text{Equation 5-11}$$

The interphase mass and heat transfer models use an implicit (linearized) evaluation of the temperature potentials $T_I - T_f$ and $T_I - T_g$. The quantity T_I is the temperature that exists at the phase interface. The implicit (linearized) evaluation of the

temperature potentials in the numerical scheme requires the derivatives of the phasic and interface temperatures defined by Equation 5-12.

$$\begin{aligned} & \left(\frac{\partial T_g}{\partial P} \right)_{U_g, X_n}, \left(\frac{\partial T_g}{\partial U_g} \right)_{P, X_n}, \left(\frac{\partial T_g}{\partial X_n} \right)_{P, U_g}, \left(\frac{\partial T_f}{\partial P} \right)_{U_f}, \\ & \left(\frac{\partial T_f}{\partial U_f} \right)_P, \left(\frac{\partial T^s}{\partial P} \right)_{U_g, X_n}, \left(\frac{\partial T^s}{\partial U_g} \right)_{P, X_n}, \left(\frac{\partial T^s}{\partial X_n} \right)_{P, U_g} \end{aligned} \quad \text{Equation 5-12}$$

5.2.2.1 Water Property Tables

The set of basic properties for light water is used for the calculations. Implementation is activated by the user. These thermodynamic tables tabulate saturation properties as a function of temperature, saturation properties as a function of pressure, and single-phase properties as a function of pressure and temperature. The tables are based on the 1995 Steam Tables from the International Association for the Properties of Water and Steam and are known as IAPWS-95. The temperature and pressure range covered in the property table is 273.16 K (32.018 degrees F) to 5000 K (8540.33 degrees F) and 611.6 Pa (0.0887 psia) to 100 MPa (14,504 psia). The properties and derivatives in the tables are saturation pressure, saturation temperature, specific volume (v), specific internal energy, specific entropy, and three derivatives: the isobaric thermal expansion coefficient (β), the isothermal compressibility (κ), and the specific heat at constant pressure (C_p).

Liquid properties are obtained from the thermodynamic tables, given P and U_f . The desired density and temperature derivatives can then be obtained from the derivatives of κ_f , β_f , and C_{pf} . In the case of the vapor being subcooled or the liquid being superheated (i.e., metastable states), the calculation of v , T , κ , β , and C_p incorporates a constant pressure extrapolation from the saturation state for the temperature and specific volume.

5.2.3 Flow Regime Maps

The one-dimensional nature of the field equations for the two-fluid model used in NRELAP5 precludes direct simulation of effects that depend upon transverse gradients of physical parameters, such as velocity or energy. Consequently, such effects must be accounted for through algebraic terms added to the conservation equations.

The mapping for flow conditions to a specific flow regime is required to provide closure to the two-fluid equations. The selected flow regime determines the constitutive relationships that are applied for interphase friction, the coefficient of virtual mass, wall friction, wall heat transfer, and interphase heat and mass transfer.

The flow regime maps are based on the work of Taitel and Dukler (Reference 12.12 and Reference 12.13) and Ishii (Reference 12.14, Reference 12.15, and Reference 12.16). Taitel and Dukler have simplified flow regime classifications and developed semi-empirical relations to describe flow regime transitions. However, some of their transition criteria are complex, and further simplification have been carried out in order to efficiently apply these criteria in NRELAP5.

The flow regime maps for the volumes and junctions are identical but used differently as a result of the finite difference scheme and staggered mesh used in the numerical scheme. The volume map is based on volume quantities. It is used for interphase heat and mass transfer, wall friction, and wall heat transfer. The junction map is based on junction quantities and is used to calculate the interfacial friction coefficient.

Three flow-regime maps in both volumes and junctions for two-phase flow are used in the NRELAP5 code: a horizontal map for flow in pipes; a vertical map for flow in pipes, annuli, and bundles; and a high mixing map for flow through pumps.

Wall heat transfer depends on the volume flow regime maps in a less direct way. Generally, void fraction and mass flux are used to incorporate the effects of the flow regime. Since the wall heat transfer is calculated before the hydrodynamics, the flow information is taken from the previous time step.

5.2.3.1 Vertical Volume Flow Regime Map

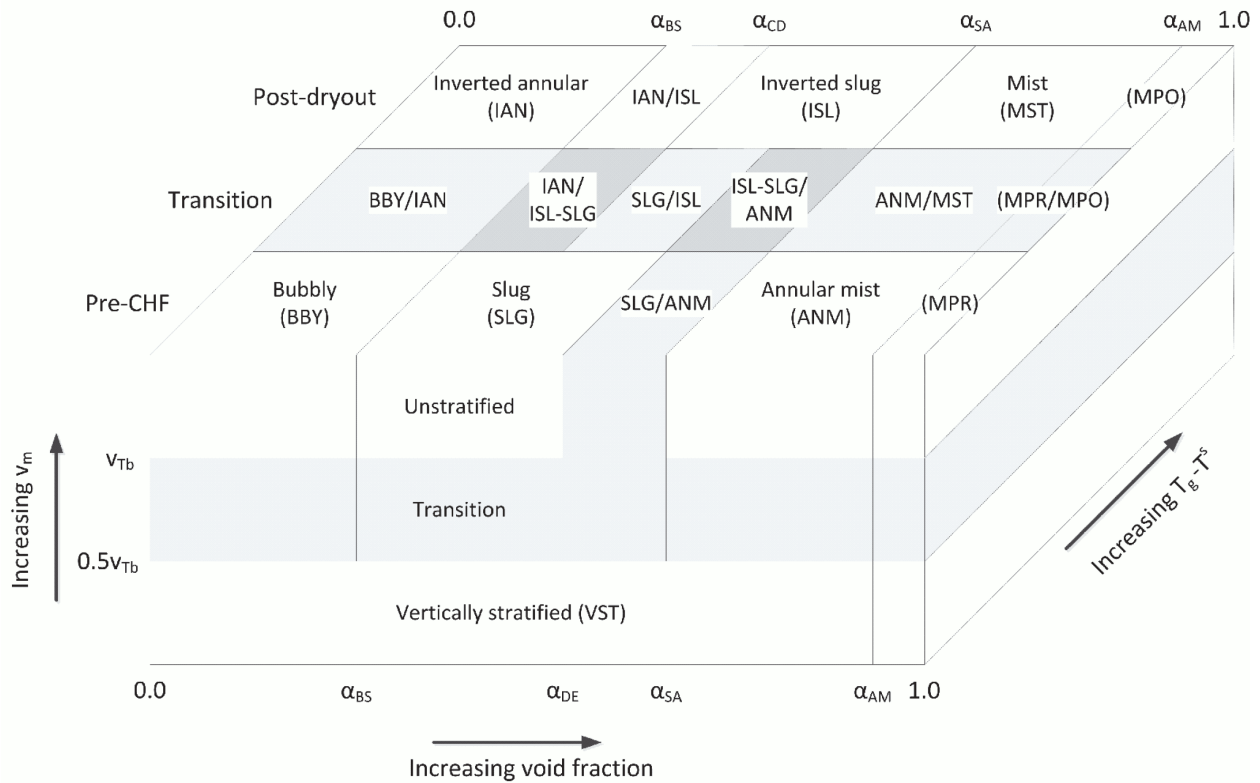
The vertical volume flow regime map is for upflow, downflow, and counter-current flow in volumes whose inclination (vertical) angle ϕ is such that $60 < |\phi| \leq 90$ degrees. An interpolation region between vertical and horizontal flow regimes is used for volumes whose absolute value of the inclination angle is between 30 degrees and 60 degrees.

This map is modeled as nine regimes:

- four regimes for pre-CHF heat transfer - bubbly, slug, annular-mist, and dispersed (droplet or mist)
- four regimes for post-CHF heat transfer - inverted annular, inverted slug, mist, and dispersed (droplet or mist)
- one regime for vertical stratification

Figure 5-1 shows a schematic of the vertical flow regime map as coded in NRELAP5. The schematic is three-dimensional to illustrate flow-regime transitions as functions of void fraction α_g , average mixture velocity v_m , and boiling.

Figure 5-1 Schematic of Vertical Flow-Regime Map Indicating Transitions

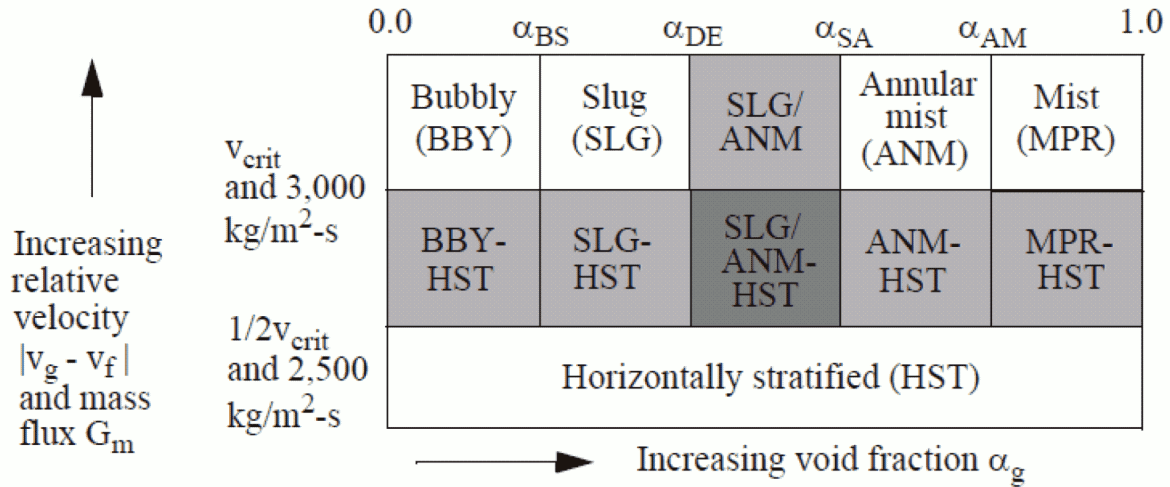


5.2.3.2 Horizontal Flow Regime Map

The horizontal volume flow regime map is for volumes whose inclination angle ϕ is such that $0 < |\phi| \leq 30$ degrees. The inclination angles for NPM-20 and the three acceptance tests are less than 30 degrees (Table 8-1); therefore, horizontal flow regimes are applicable to the helical coils.

A schematic of the horizontal volume flow regime map as coded in NRELAP5 is illustrated in Figure 5-2. Transition regions used in the code are indicated with shaded areas. Such transitions are included in the map to preclude discontinuities when going from one correlation to another. Details of the interpolating functions employed between correlations are given in the sections that describe the various correlations in Reference 12.8.

Figure 5-2 Schematic of Horizontal Flow Regime Map with Shaded Regions Indicating Transition (Interpolation) Regions



The bubble-slug transition void fraction is calculated using Equation 5-13.

$$\alpha_{BS} = \begin{cases} 0.25 & G_m \leq 2000 \text{ kg/m}^2\text{s} \\ 0.25 + 0.00025(G_m - 2000) & 2000 < G_m < 3000 \text{ kg/m}^2\text{s} \\ 0.50 & G_m \geq 3000 \text{ kg/m}^2\text{s} \end{cases} \quad \text{Equation 5-13}$$

The mixture mass flux is calculated using Equation 5-14.

$$G_m = \alpha_g \rho_g |v_g| + \alpha_f \rho_f |v_f| \quad \text{Equation 5-14}$$

The transition region between slug flow and annular mist flow is defined by $\alpha_{DE} = 0.75$ and $\alpha_{SA} = 0.80$. The annular mist to dispersed transition criterion is $\alpha_{AM} = 0.80$.

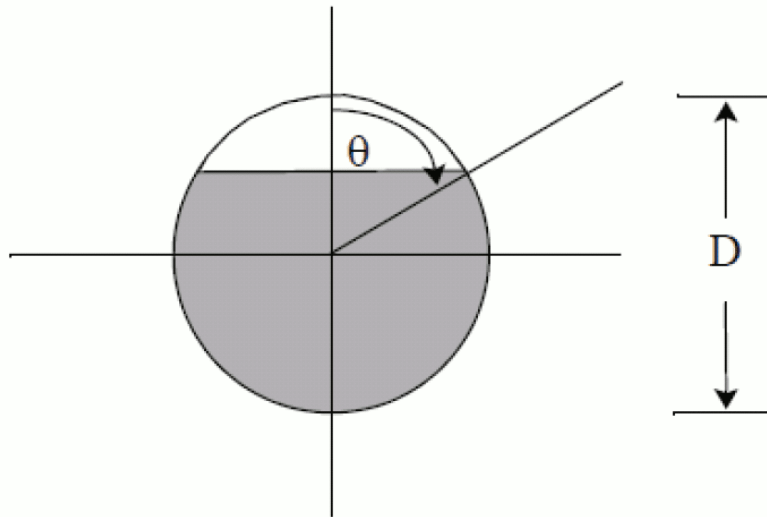
The criterion defining the horizontally-stratified regime is based on the one developed by Taitel and Dukler (Reference 12.13). According to Taitel and Dukler, the flow field is horizontally stratified if the vapor/gas velocity satisfies the condition as described in Equation 5-15 and Equation 5-16.

$$|v_g| < v_{crit} \quad \text{Equation 5-15}$$

$$v_{crit} = \frac{1}{2} \left[\frac{(\rho_f - \rho_g) g \alpha_g A}{\rho_g D \sin \theta} \right]^{1/2} (1 - \cos \theta) \quad \text{Equation 5-16}$$

The variable θ is the angle from vertical of the stratified liquid level, defined in Figure 5-3.

Figure 5-3 Schematic of Horizontally Stratified Flow in a Pipe, with Definition of θ



The algebraic relationship between vapor fraction α_g and angle θ is described in Equation 5-17.

$$\pi \alpha_g = \theta - \cos \theta \sin \theta \quad \text{Equation 5-17}$$

The flow is horizontally stratified if the phasic relative velocity and the mass flux satisfies the condition in Equation 5-18.

$$|v_g - v_f| < v_{crit} \quad \text{and} \quad G_m < 3000 \text{ kg/m}^2\text{s} \quad \text{Equation 5-18}$$

If the conditions in Equation 5-18 are met, the flow field undergoes a transition to the horizontally stratified flow regime. If the conditions are not met, then the flow field transitions to the bubble, slug, annular mist, or mist pre-CHF flow regime.

The lower transition limit of the interpolation region for $|v_g - v_f|$ is $\left(\frac{1}{2}\right)v_{crit}$ and for G_m is $2500 \text{ kg/m}^2\text{s}$.

5.2.3.3 Junction Flow Regime Maps

The junction map is based on both junction and volume quantities. It is used for the interphase drag and shear, as well as for the coefficient of virtual mass. The flow regime maps used for junctions are the same as those used for the volumes and are based on the work of Taitel and Dukler (Reference 12.12 and Reference 12.13), Ishii (Reference 12.16), and Tandon, et. al. (Reference 12.17)

As with the volumes, three junction flow regime maps are used:

- horizontal map for flow in pipes
- vertical map for flow in pipes/bundles
- high mixing map for flow in pumps

The vertical flow regime map is for junctions whose junction inclination (vertical) angle ϕ_j is $60 < |\phi_j| \leq 90$ degrees. The horizontal flow regime map is for junctions whose junction inclination angle ϕ_j is $0 < |\phi_j| \leq 30$ degrees. An interpolation region between vertical and horizontal flow regimes is used for junctions whose junction inclination angle ϕ_j is $30 < |\phi_j| \leq 60$ degrees. This interpolation region is used to smoothly change between vertical and horizontal flow regimes.

Junction quantities used in the map decisions are junction phasic velocities, donored (based on phasic velocities) phasic densities, and donored (based on superficial mixture velocity) surface tension.

The junction void fraction (α_{gj}^*) is calculated from either of the volume void fractions of the neighboring volumes, $\alpha_{g,k}$ or $\alpha_{g,L}$, using a donor direction based on the mixture superficial velocity j_m .

5.2.4 Momentum Closure Relations

NRELAP5 uses two different models for the phasic interfacial friction force computation, the drift flux method, and the drag coefficient method. The choice of which model to use depends upon the flow regime. The methods are described in Section 5.2.4.1 and Section 5.2.4.2.

5.2.4.1 Drift Flux Model

The drift flux approach is used only in the bubbly and slug-flow regimes for vertical flow. The drift flux model specifies the distribution coefficient and the vapor/gas drift velocity. These two quantities must be converted into a constitutive relation for the interfacial frictional force per unit volume.

Such a relation can be found by assuming that the interfacial friction force per unit volume is given by Equation 5-19.

$$F_i = C_i |v_R| v_R = \alpha_f \alpha_g (\rho_f - \rho_g) g \quad \text{Equation 5-19}$$

The interfacial frictional force per unit volume is balanced by the buoyancy force per unit volume, where C_i is an unknown coefficient and v_R is the relative velocity between the phases. Within the context of the drift flux model, the relative velocity between the phases is not the difference between the phasic velocities but is a weighted difference between the phase velocities given by Equation 5-20.

$$v_R = C_1 v_g - C_0 v_f \quad \text{Equation 5-20}$$

Variable C_0 is calculated using the drift flux correlations, and C_1 is calculated using Equation 5-21.

$$C_1 = \frac{1 - \alpha_g C_0}{1 - \alpha_g} \quad \text{Equation 5-21}$$

Substituting these relations into Equation 5-19 calculates the interfacial friction force per unit volume in terms of the phasic velocities, as shown in Equation 5-22.

$$F_i = C_i |C_1 v_g - C_0 v_f| (C_1 v_g - C_0 v_f) \quad \text{Equation 5-22}$$

Here, the coefficient C_i is yet undetermined. The drift flux model also specifies that the relative velocity (v_R) is the ratio of the vapor/gas drift velocity and the liquid volume fraction and is calculated using Equation 5-23.

$$v_R = \frac{v_{gj}}{\alpha_f} \quad \text{Equation 5-23}$$

The vapor/gas drift velocity (v_{gj}) is calculated using the drift flux correlations. Substituting this value of the relative velocity into Equation 5-19 allows the coefficient C_i to be determined from Equation 5-24.

$$C_i = \frac{\alpha_g \alpha_f^3 (\rho_f - \rho_g) g}{v_{gj}^2} \quad \text{Equation 5-24}$$

5.2.4.2 Drag Coefficient Model

The drag coefficient approach is used in flow regimes other than vertical bubbly and slug-flow. The model uses correlations for drag coefficients and for the computation of the interfacial area density.

The constitutive relation for the frictional force on a body moving relative to a fluid is shown in Equation 5-25.

$$F = \frac{1}{2} \rho v^2 C_D A \quad \text{Equation 5-25}$$

where,

F = drag force

ρ = fluid density

v = velocity of body relative to the fluid

C_D = drag coefficient

A = projected area of the body

Expressing the frictional force for a group of bodies moving relative to a fluid (e.g., bubbles moving through liquid or droplets moving through vapor/gas) in terms of the frictional force for each body leads to the constitutive relation of Equation 5-26 for the interfacial frictional force per unit volume.

$$F_i = \frac{1}{8} \rho_c |v_g - v_f| (v_g - v_f) C_D S_F a_{gf} = C_i |v_g - v_f| (v_g - v_f) \quad \text{Equation 5-26}$$

where,

F_i = interfacial friction force per unit volume

$$C_i = \frac{1}{8} \rho_c C_D S_F a_{gf}$$

ρ_c = density of continuous phase

a_{gf} = interfacial area per unit volume

S_F = shape factor

The additional factor of 1/4 comes from the conversion of the projected area of spherical particles (i.e., πr^2) into the interfacial area (i.e., $4\pi r^2$), and the shape factor is included to account for non-spherical particles. The drag coefficient model for the global interfacial friction coefficient is reduced to the specification of the continuous density, drag coefficient, interfacial area density, and shape factor for the flow regimes. Once these quantities have been computed, the interfacial friction force per unit volume (F_i) is calculated using Equation 5-20, from which the global interfacial friction coefficient is calculated.

5.2.4.3 Wall Friction

The wall friction is determined based on the volume flow regime map. The wall friction force terms include only wall shear effects. Losses due to abrupt area change are calculated using mechanistic form-loss models. Other losses due to elbows or complicated flow passage geometry are modeled using energy-loss coefficients that must be input by the user.

The semi-implicit scheme, one-dimensional, finite difference equations for the sum momentum equation and the difference momentum equation contain the terms of Equation 5-27, which represent the phasic wall frictional pressure drop.

$$FWG_j^n \cdot (v_g)_j^{n+1} \Delta x_j \Delta t \text{ and } FWF_j^n \cdot (v_f)_j^{n+1} \Delta x_j \Delta t \quad \text{Equation 5-27}$$

These terms represent the pressure loss due to wall shear from cell center to cell center of the cell volumes adjoining the particular junction that the momentum equation is considering. The wall drag or friction depends not only on the phase of the fluid, but also on the flow regime characteristics.

The wall friction model is based on a two-phase multiplier approach in which the two-phase multiplier is calculated from the heat transfer and fluid flow service (HTFS) modified Baroczy correlation. The individual phasic wall friction components are calculated by apportioning the two-phase friction between the phases using a technique derived from the Lockhart-Martinelli model (Reference 12.18). The model is based on the assumption that the frictional pressure drop may be calculated using a quasi-steady form of the momentum equation, as used by Chisholm. This wall friction partitioning model is used with the drag coefficient method of the interphase friction model.

The Lockhart-Martinelli model calculates the overall two-phase friction pressure drop in terms of the liquid-alone and vapor/gas-alone wall friction pressure drop as shown in Equation 5-28.

$$\left(\frac{dP}{dx}\right)_{2\phi} = \phi_f^2 \left(\frac{dP}{dx}\right)_f = \phi_g^2 \left(\frac{dP}{dx}\right)_g \quad \text{Equation 5-28}$$

Here ϕ_f and ϕ_g are the liquid-alone and vapor/gas-alone two-phase Darcy-Weisbach friction multipliers, respectively. The phasic wall friction pressure gradients are expressed by Equation 5-29 for the liquid and vapor/gas alone.

$$\left(\frac{dP}{dx}\right)_f = \frac{\lambda'_f Re_f M_f^2}{2D\rho_f A^2} \quad \text{and} \quad \left(\frac{dP}{dx}\right)_g = \frac{\lambda'_g Re_g M_g^2}{2D\rho_g A^2} \quad \text{Equation 5-29}$$

Here the prime indicates the liquid and vapor/gas-alone Darcy-Weisbach friction factors, respectively, calculated at the respective Reynolds numbers shown in Equation 5-30.

$$Re'_f = \frac{M_f D}{\mu_f A} \quad \text{and} \quad Re'_g = \frac{M_g D}{\mu_g A} \quad \text{Equation 5-30}$$

The liquid and vapor/gas mass flow rates, respectively, are defined by Equation 5-31.

$$M_f = \alpha_f \rho_f v_f A \quad \text{and} \quad \alpha_g \rho_g v_g A \quad \text{Equation 5-31}$$

The overall two-phase friction pressure gradient is calculated using two-phase friction multiplier correlations. The multipliers are interrelated using Equation 5-23 and Equation 5-24 and the Lockhart-Martinelli ratio defined by Equation 5-32.

$$\chi^2 = \frac{\left(\frac{dP}{dx}\right)_f}{\left(\frac{dP}{dx}\right)_g} = \frac{\phi_g^2}{\phi_f^2} \quad \text{Equation 5-32}$$

The HTFS correlation is used to calculate the two-phase friction multipliers. This correlation is chosen because it is correlated to empirical data over broad ranges of phasic volume fractions, phasic flow rates, and phasic flow regimes. The correlation is also shown to give good agreement with empirical data.

The HTFS correlation for the two-phase friction multiplier is expressed with Equation 5-33.

$$\phi_f^2 = 1 + \frac{C}{\chi} + \frac{1}{\chi^2} \quad \text{and} \quad \phi_g^2 = \chi^2 + C\chi + 1 \quad \text{Equation 5-33}$$

Variable C is the correlation coefficient and χ is the Lockhart-Martinelli ratio given by Equation 5-32. If the HTFS correlation is combined with the wall friction formulations by combining Equation 5-28, Equation 5-29, Equation 5-31,

Equation 5-32, and Equation 5-33, then the combined two-friction pressure drop is expressed by Equation 5-34.

$$\begin{aligned} \left(\frac{dP}{dx}\right)_{2\phi} &= \phi_f^2 \left(\frac{dP}{dx}\right)_f = \phi_g^2 \left(\frac{dP}{dx}\right)_g = \frac{1}{2D} (\{\lambda'_f \rho_f (\alpha_f v_f)^2\} \\ &+ C[\lambda'_f \rho_f (\alpha_f v_f)^2 \lambda'_g \rho_g (\alpha_g v_g)^2]^{1/2} + \lambda'_g \rho_g (\alpha_g v_g)^2) \end{aligned} \quad \text{Equation 5-34}$$

The phasic wall friction coefficients are defined by Equation 5-35 and Equation 5-36.

$$FWF(\alpha_f \rho_f v_f)A = \tau_f p_f = \alpha_f \left(\frac{dP}{dx}\right) \bigg|_{2\phi} \left(\frac{Z^2}{\alpha_g + \alpha_f Z^2}\right)^A \quad \text{Equation 5-35}$$

$$FWG(\alpha_g \rho_g v_g)A = \tau_g p_g = \alpha_g \left(\frac{dP}{dx}\right) \bigg|_{2\phi} \left(\frac{1}{\alpha_g + \alpha_f Z^2}\right)^A \quad \text{Equation 5-36}$$

Here Z is defined by Equation 5-37.

$$Z^2 = \frac{\lambda_f (Re_f) \rho_f v_f^2 \frac{\alpha_{fw}}{\alpha_f}}{\lambda_g (Re_g) \rho_g v_g^2 \frac{\alpha_{gw}}{\alpha_g}} \quad \text{Equation 5-37}$$

Taking the sum of these two equations gives the overall quasi-static, two-phase wall friction pressure gradient, as shown by Equation 5-38.

$$FWF(\alpha_f \rho_f v_f)A + FWG(\alpha_g \rho_g v_g)A = \left(\frac{dP}{dx}\right) \bigg|_{2\phi} A \quad \text{Equation 5-38}$$

The phasic friction factors used in the wall friction model are computed from correlations for laminar and turbulent flows with interpolation in the transition regime. The friction factor model is simply an interpolation scheme linking the laminar, laminar-turbulent transition, and turbulent flow regimes. The laminar friction factor is calculated by Equation 5-39.

$$\lambda_L = \frac{64}{Re \phi_S} \quad \text{for } 0 \leq Re \leq 2200 \quad \text{Equation 5-39}$$

Here ϕ_S is a user-input shape factor for non-circular flow channels (ϕ_S is 1.0 for circular channels).

The friction factor in the transition region between laminar and turbulent flows is computed by reciprocal interpolation with Equation 5-40.

$$\lambda_{L,T} = \left(3.75 - \frac{8,250}{Re}\right)(\lambda_{T,3000} - \lambda_{L,2200}) + \lambda_{L,2200} \quad \text{Equation 5-40}$$

for $2200 < Re < 3000$

Here $\lambda_{L,2200}$ is the laminar factor at a Reynolds number of 2200, $\lambda_{T,3000}$ is the turbulent friction factor at a Reynolds number of 3000, and the interpolation factor is between zero and one.

The turbulent friction factor is given by the Zigrang-Sylvester approximation (Reference 12.19) to the Colebrook-White correlation (Reference 12.20) with Equation 5-41, where ε is the surface roughness.

$$\left(\frac{1}{\sqrt{\lambda_T}} = -2 \log_{10} \left\{ \frac{\varepsilon}{3.7D} + \frac{2.51}{Re} \left[1.14 - 2 \log_{10} \left(\frac{\varepsilon}{D} + \frac{21.25}{Re^{0.9}} \right) \right] \right\} \right) \quad \text{Equation 5-41}$$

for $Re \geq 3000$

5.2.5 Heat Transfer

The liquid and vapor/gas energy solutions include the wall heat flux to liquid or vapor/gas. During boiling, the saturation temperature based on the total pressure is the reference temperature, and during condensation the saturation temperature based on the partial pressure is the reference temperature. The general expression for the total wall heat flux is defined by Equation 5-42.

$$\begin{aligned} \ddot{q}_{total} = & h_{wgg}(T_w - T_g) + h_{wgspt}(T_w - T_{spt}) + h_{wgspp}(T_w - T_{spp}) \\ & + h_{wff}(T_w - T_f) + h_{wfspt}(T_w - T_{spt}) \end{aligned} \quad \text{Equation 5-42}$$

where,

h_{wgg} = heat transfer coefficient to vapor/gas, with the vapor/gas temperature as the reference temperature (W/m² K)

h_{wgspt} = heat transfer coefficient to vapor/gas, with the saturation temperature based on the total pressure as the reference temperature (W/m² K)

h_{wgspp} = heat transfer coefficient to vapor/gas, with the saturation temperature based on the vapor partial pressure as the reference temperature (W/m² K)

h_{wff} = heat transfer coefficient to liquid, with the liquid temperature as the reference temperature (W/m² K)

h_{wfspt} = heat transfer coefficient to liquid, with the saturation temperature based on the total pressure as the reference temperature (W/m² K)

T_w = wall surface temperature (K)

T_g = vapor/gas temperature (K)

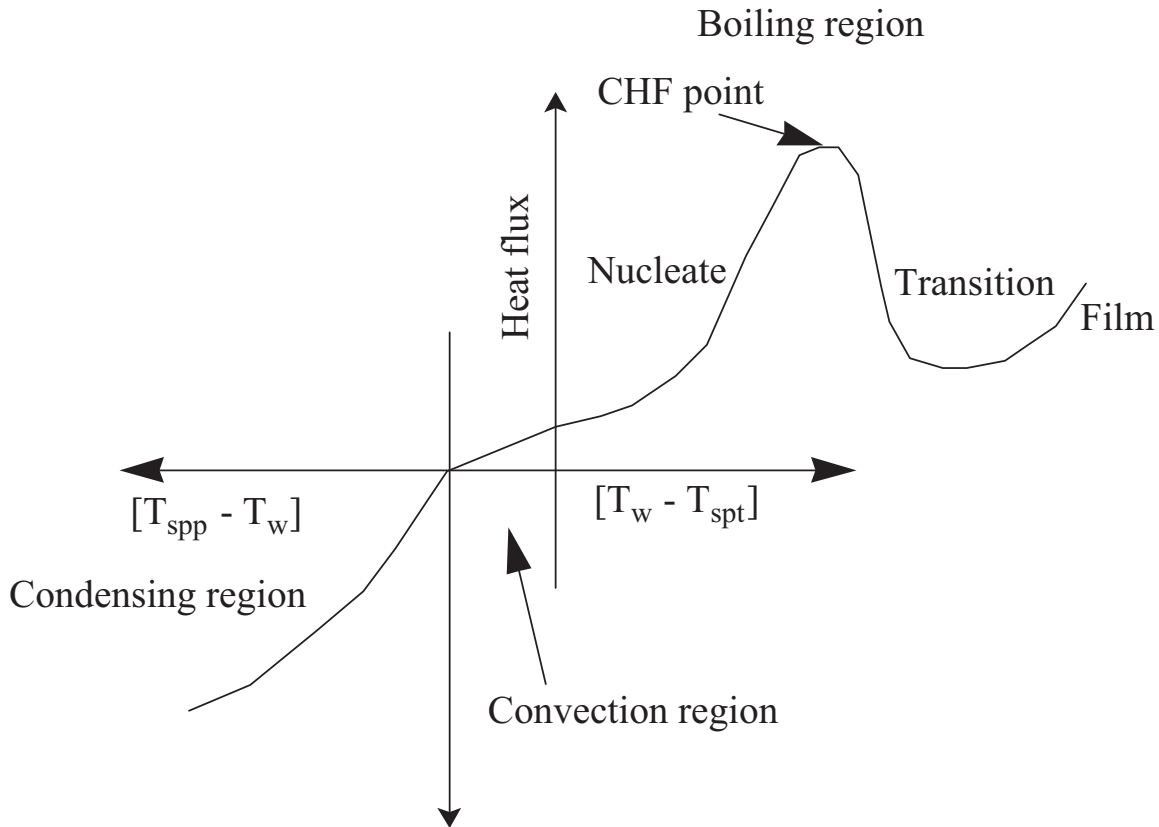
T_f = liquid temperature (K)

T_{spt} = saturation temperature based on the total pressure (K)

T_{spp} = saturation temperature based on the partial pressure of vapor in the bulk (K)

A boiling curve is used in NRELAP5 to govern the selection of the wall heat transfer correlations when the wall surface temperature is above the saturation temperature (superheated relative to the saturation temperature based on total pressure). When a hydraulic volume is voided and the adjacent surface temperature is subcooled, vapor condensation on the surface is predicted. If non-condensable gases are present, the phenomena are more complex because condensation is based on the partial pressure of vapors present in the region. When the wall temperature is less than the saturation temperature based on total pressure, but greater than the saturation temperature based on vapor partial pressure, a convection condition exists. Figure 5-4 illustrates these three regions of the curve.

Figure 5-4 NRELAP5 Boiling and Condensing Curves



The boiling curve uses the Chen boiling correlation (Reference 12.21) up to the CHF point.

5.3 Heat Structure Models

Heat structures provided in NRELAP5 permit calculation of the heat transfer across solid boundaries of hydrodynamic volumes. Modeling capabilities of heat structures are general and include fuel pins or plates with nuclear or electrical heating, heat transfer across SG tubes, and heat transfer from pipe and vessel walls. Temperatures and heat transfer rates are computed from the one-dimensional form of the transient heat conduction equation.

Heat structures are represented using rectangular, cylindrical, or spherical geometry. Surface multipliers are used to convert the unit surface of the one-dimensional calculation to the actual surface of the heat structure. Temperature-dependent and space-dependent thermal conductivities and volumetric heat capacities are provided in tabular or functional form either from built-in or user-supplied data.

Finite differences are used to advance the heat conduction solutions. Each mesh interval may contain different mesh spacing, a different material, or both. The spatial dependence of the internal heat source, if any, may vary over each mesh interval. The

time-dependence of the heat source can be obtained from reactor kinetics, one of several tables of power versus time, or a control system variable. Boundary conditions include symmetry or insulated conditions; a heat transfer correlation package; and tables of surface temperature versus time; heat flux versus time; heat transfer coefficient versus time; and heat transfer coefficient versus surface temperature.

The heat transfer correlation package can be used for heat structure surfaces connected to hydrodynamic volumes. The heat transfer correlation package contains correlations for convective, nucleate boiling, transition boiling, and film boiling heat transfer from the wall to the fluid, and it contains reverse heat transfer from the fluid to the wall including correlations for condensation. The heat conduction model also includes a gap conduction model and a radiation enclosure model.

The integral form of the heat conduction equation is defined by Equation 5-43.

$$\iiint_V \rho C_p(T, \bar{x}) \frac{\partial T}{\partial t}(\bar{x}, t) dV = \iint_S k(T, \bar{x}) \bar{\nabla} T(\bar{x}, t) \cdot d\bar{s} + \iiint_V S(\bar{x}, t) dV \quad \text{Equation 5-43}$$

where,

$k(T, \bar{x})$ = thermal conductivity

s = surface

S = internal volumetric heat source

t = time

T = temperature

V = volume

x = space coordinates

ρC_p = volumetric heat capacity

The boundary conditions applied to the exterior surface have the form of Equation 5-44.

$$A(T)T(t) + B(T)\frac{\partial T(t)}{\partial n} = D(T, t) \quad \text{Equation 5-44}$$

The n denotes the unit normal vector away from the boundary surface. Thus, the desired boundary condition is that the heat transferred out of the surface equals a heat transfer coefficient (h) times the difference between the surface temperature (T) and the sink temperature (T_{sk}) as shown by Equation 5-45.

$$-k \frac{\partial T}{\partial n} = h(T - T_{sk}) \quad \text{Equation 5-45}$$

Then, the correspondence between Equation 5-45 and Equation 5-44 yields Equation 5-46.

$$A = h, B = k, \text{ and } D = T_{sk} \quad \text{Equation 5-46}$$

One-dimensional heat conduction in rectangular, cylindrical, and spherical geometry can be used to represent the heat structures in the components in NRELAP5. The equations governing one-dimensional heat conduction are defined by Equation 5-47, Equation 5-48, and Equation 5-49.

$$\rho C_p \frac{\partial T}{\partial t} = \frac{\partial}{\partial x} \left(k \frac{\partial T}{\partial x} \right) + S \text{ for rectangular geometry} \quad \text{Equation 5-47}$$

$$\rho C_p \frac{\partial T}{\partial t} = \frac{1}{r} \left[\frac{\partial}{\partial r} \left(r k \frac{\partial T}{\partial r} \right) \right] + S \text{ for cylindrical geometry} \quad \text{Equation 5-48}$$

$$\rho C_p \frac{\partial T}{\partial t} = \frac{1}{r^2} \left[\frac{\partial}{\partial r} \left(r^2 k \frac{\partial T}{\partial r} \right) \right] + S \text{ for spherical geometry} \quad \text{Equation 5-49}$$

Heat may flow across the external heat structure boundaries to either the environment or to the working fluid. For heat structure surfaces connected to hydrodynamic volumes containing the working fluid, a heat transfer package is provided containing correlations for heat transfer from wall-to-liquid and reverse heat transfer from liquid-to-wall. Any number of heat structures may be connected to each hydrodynamic volume, or heat transfer coefficient versus surface temperature can be used to simulate the boundary conditions.

The heat conduction equation can be solved by various numerical techniques. NRELAP5 uses the Crank-Nicolson method (Reference 12.22) for solving this equation.

5.4 Trips and Control System Models

The control system provides the capability to evaluate simultaneous algebraic and ordinary differential equations. The capability is primarily intended to simulate control systems typically used in hydrodynamic systems, but it can also model other phenomena described by algebraic and ordinary differential equations. Another use is to define auxiliary output quantities, such as differential pressures, so they can be printed in major and minor edits for plotting.

The control system consists of several types of control components. Each component defines a control variable as a specific function of time-advanced quantities. The time-advanced quantities include hydrodynamic volume, junction, pump, valve, heat structure, reactor kinetics, trip quantities, and the control variables themselves (including the control variable being defined). This approach permits control variables to be developed from components that perform simple, basic operations.

The trip system consists of the evaluation of logical statements. Each trip statement is a simple logical statement that has a true or false result and an associated variable. Two types of trip statements are provided; variable and logical trips.

5.5 Special Solution Techniques

Special process models are used in NRELAP5 to simulate special processes, which are sufficiently complex that they must be modeled using empirical models.

Special process models include choked flow, entrainment/pull through model, thermal stratification model, counter-current flooding, form-loss model, and abrupt area change. Choked flow, stratification, and counter-current flooding are not important to DWO.

5.5.1 Abrupt Area Change

The general reactor system contains piping networks with many sudden area changes and orifices. To apply the NRELAP5 hydrodynamic model to such systems, analytical models for these components are included in the code. The basic hydrodynamic model is formulated for slowly varying (continuous) flow area variations; therefore, special models are not required for this case.

The abrupt area change model, is based on the Borda-Carnot formulation (Reference 12.23) for a sudden (i.e., sharp, blunt) enlargement and standard pipe flow relations, including the vena-contracta effect for a sudden (i.e., sharp, blunt) contraction or sharp-edge orifice or both. This type of change is referred to as the full abrupt area change model. It does not include the case where an enlargement, contraction, or orifice is rounded or beveled.

Quasi-steady continuity and momentum balances are employed at points of an abrupt area change. The numerical implementation of these balances is such that hydrodynamic losses are independent of upstream and downstream nodalization. In effect, the quasi-steady balances are employed as jump conditions that couple fluid components having abrupt changes in a cross-sectional area. This coupling process is achieved without change to the basic numerical time-advancement schemes.

The basic assumption used for the transient calculation of two-phase flow in flow passages with points of abrupt area change is that the transient flow process can be approximated as a quasi-steady flow process that is instantaneously satisfied by the upstream and downstream conditions (i.e., transient inertia, mass, and energy storage are neglected at abrupt area changes). However, the upstream and downstream flows are treated as fully transient flows.

The volume of fluid and associated mass, energy, and inertia at points of abrupt area change is generally small compared with the volume of upstream and downstream fluid components. The transient mass, energy, and inertia effects are approximated by lumping them into upstream and downstream flow volumes. Finally, the quasi-steady approach is consistent with modeling of other important phenomena in transient codes (i.e., heat transfer, pumps, and valves).

Activation of the full abrupt area change model in NRELAP5 results in the code internally calculating the form and interfacial losses across a junction. Utilization of the partial area change model allows the user to specify the form loss while allowing the code to internally calculate the interfacial loss. Activation of the smooth area change model allows the user to specify the form loss with no internal calculation of the interfacial losses.

More detailed discussion concerning this model can be found in the NRELAP5 theory manual (Reference 12.8).

5.5.2 Form Loss Model

The form loss model in NRELAP5 allows specifying a user-defined form loss coefficient to calculate the friction pressure drop for complicated geometry.

The form loss coefficient in NRELAP5 calculates the pressure drop term HLOSSG (for vapor) and HLOSSF (for liquid) in the phasic momentum equation (Equation 5-50).

$$HLOSSG = \frac{1}{2}(K_g + K_{in})|V_{g,j}| \quad \text{Equation 5-50}$$

$$HLOSSF = \frac{1}{2}(K_f + K_{in})|V_{f,j}|$$

Variable K_{in} is the user-specified loss coefficient. This is either the forward loss K_F or reverse loss K_R depending on the phasic velocity direction. The code-calculated abrupt area loss terms K_g and K_f are discussed in Section 5.5.1.

In many cases, the form loss coefficient is specified as a function of the Reynolds number. The user-specified form loss for Reynolds number dependency can be expressed using Equation 5-51.

$$K_R = A_F + B_F Re^{-C_F} \quad \text{Equation 5-51}$$

$$K_R = A_R + B_R Re^{-C_R}$$

Variables A_F , A_R , B_F , B_R , C_F , and C_R , are user-defined constants, and Re is the Reynolds number based on the mixture fluid properties.

5.6 Numerical Methods

NRELAP5 solves the one-dimensional two-fluid model equations. The local instantaneous equations are developed for each phase. These equations are then

averaged over time and cross-sectional area to generate governing equations that are solved numerically.

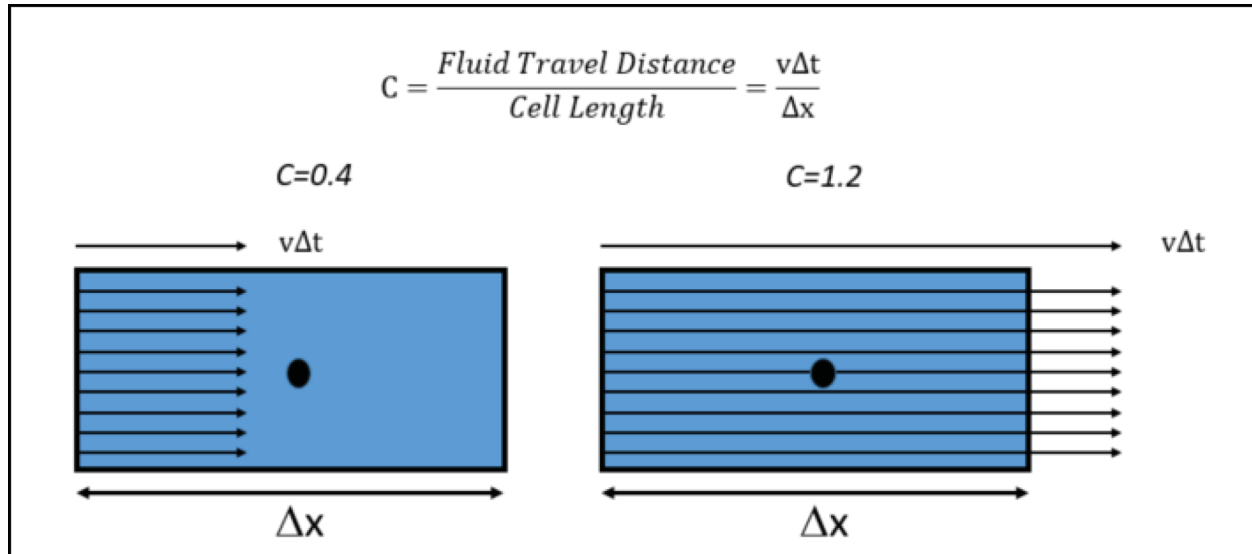
The difference equations implement mass and energy conservation by equating accumulation to the rate of mass or energy inflow and outflow through the cell boundaries, minus the rate of mass or energy out through the cell boundaries, plus source terms such as heat input. This approach necessitates defining mass and energy volume average properties and requiring knowledge of velocities at the volume boundaries. The velocities at the cell edges are defined through the use of momentum control volumes centered on the mass and energy cell boundaries. This approach results in a numerical scheme having a staggered spatial mesh with the momentum control volumes extending from the mass and energy cell centers to the neighboring mass and energy cell centers. The scalar properties of the flow (pressure, specific internal energies, and void fraction) are defined at mass and energy cell boundaries.

The governing equations are discretized in time and space and are solved numerically using a semi-implicit finite-difference technique. A nearly-implicit finite-difference technique, which allows violation of the material Courant limit, is also available. However, the DWO evaluation model and the supporting assessment calculations use only the semi-implicit numerical scheme. The semi-implicit numerical solution scheme is based on replacing the system of differential equations with a system of finite difference equations partially implicit in time.

NRELAP5's semi-implicit solution scheme behaves like a classic explicit scheme and introduces numerical diffusion, which acts to damp inlet perturbations. The amount of numerical diffusion can vary considerably as it is dependent on the number of nodes used and the Courant number, C , which is the time-step size normalized to the transport time through a volume per Equation 5-52.

$$C = v\Delta t/\Delta x \quad \text{Equation 5-52}$$

Variable v is the velocity (m/s), Δt is the time step (s), and Δx is the node length (m). The physical meaning of C , illustrated in Figure 5-5, is the distance a fluid particle travels in a time step ($v\Delta t$), divided by the node length (Δx). It is desirable to keep the distance traveled less than the node length (i.e., $C=0.4$, as seen on the left). If the distance traveled exceeds the node length (i.e., $C=1.2$, as seen on the right), information may not be correctly propagated from node to node.

Figure 5-5 Physical Meaning of the Courant Number

For the NRELAP5 semi-implicit scheme, the range of allowable Courant number values is $0 < C < 1$. In an NRELAP5 simulation, if the velocity in a node (i.e., either liquid velocity or gas velocity) would cause $C > 1$, the time-step is automatically reduced such that $C < 1$. Note that in NRELAP5, nodes use the same time-step. Often, NRELAP5 models with uniform nodalizations have their time-step controlled by the node with the highest velocity, so more course nodalization in high velocity regions is sometimes used to keep the time-step from becoming very small, impacting the overall solution time.

When generating a solution of finite difference equations, there is a possibility that the solution may not converge. This could be the result of an ill-posed problem, inappropriate time-step size selection, inadequate spatial nodalization, or an instability. Sensitivity studies have proven useful to assure convergence and stability of the NRELAP5 solutions.

Adherence to the known modeling limitations and requirements of RELAP5, discussed in Section 9.0, assist in assuring that the governing equations are well-posed. Requirements for nodalization and time-step sensitivity studies assure converged solutions. Solutions are examined to identify unstable or unphysical behavior. {{

}}2(a),(c)

5.7 Helical Coil Steam Generator Component

A new hydrodynamic component and heat transfer package is added to NRELAP5 to model flow and heat transfer inside an HCSG. This model is developed based on helical coil geometry-specific heat transfer and wall friction correlations. The need for improved

models is based on inadequate agreement with pressure drop and heat transfer performance with the baseline RELAP5-3D[®] code results against prototypic HCSG testing performed at SIET. Improvements and adequacy of the implemented models in NRELAP5 are demonstrated through prototypic assessments of the NPM-20 helical coil SG using SIET test data (Section 8.1 and Section 8.2). These tests assessed heat transfer and pressure drop on both the secondary side (within SG tubes) and primary side (external to SG tubes) of the HCSG.

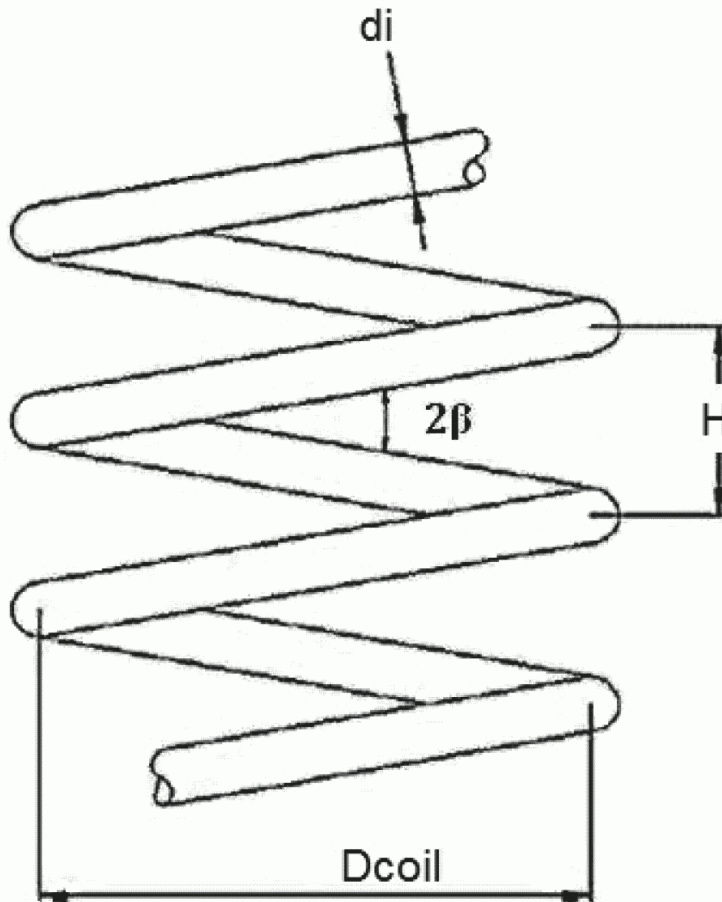
A wide range of pressure drop and heat transfer correlations were investigated for analyzing the inside of the helical coils. A down-selection of these investigated models is performed for implementation into the NRELAP5 code based on the applicability of the models to the NPM-20 helical coil SG. These models are described in Section 6.0.

6.0 NRELAP5 Helical Coil Steam Generator Model Development

Models developed specifically for the NPM-20 helical coil SG are described in this section. Additional details of the model development and supporting data can be found in Reference 12.8.

Figure 6-1 shows a schematic of a helical coil as a visual reference for the parameters used in helical coil heat transfer and pressure drop correlations found in open literature. The pipe has an inner diameter d_i . The coil diameter is represented by D_{coil} (measured between the centers of the pipes). The distance between two adjacent turns, called axial pitch, is H . The ratio of pipe diameter to coil diameter (d_i/D_{coil}) is called curvature ratio. The ratio of pitch to developed length of one turn (H/D_{coil}) is termed torsion. Consider the projection of the coil on a plane passing through the axis of the coil. The angle that projection of one turn of the coil makes with a plane perpendicular to the axis is called the tube inclination angle, β (degrees). Consider any cross-section of the pipe created by a plane passing through the coil axis. The side of the pipe wall nearest to the coil axis is termed the inner side of the coil, and the farthest side is termed the outer side of the coil.

Figure 6-1 Basic Geometry of a Helical Tube



Similar to the Reynolds number for flow in pipes, the Dean number is used to characterize the flow in a helical pipe. The predominant parameter governing the physics of flow within helical tubes is the Dean number (De), as described in Equation 6-1.

$$De = Re \sqrt{\frac{d_i}{D_{coil}}} \quad \text{Equation 6-1}$$

The Dean number couples inertial and centrifugal effects.

6.1 Helical Coil Tube Friction

6.1.1 Helical Coil Single-Phase Tube Wall Friction

{

}^{2(a),(c)}

{

Equation 6-2

Equation 6-3

}^{2(a),(c)}

{

Equation 6-4

$\}}^{2(a),(c)}$

6.1.2 Helical Coil Two-Phase Tube Wall Friction

{

Equation 6-5

Equation 6-6

Equation 6-7

Equation 6-8

$\}}^{2(a),(c)}$

{{

Equation 6-9

}}^{2(a),(c)}

6.2 Helical Coil Tube Heat Transfer

A new heat transfer package is added to NRELAP5 and differs from that of the standard NRELAP5 pipe geometry in the single-phase heat transfer and two-phase flow boiling heat transfer. A new geometry type represents the inside of the helical tubes.

{{

}}^{2(a),(c)}

6.2.1 Helical Coil Single-Phase Heat Transfer

{{

Equation 6-10

Equation 6-11

}}^{2(a),(c)}

{

Equation 6-12

}^{2(a),(c)}

6.2.2 Helical Coil Two-Phase Subcooled and Saturated Flow Boiling Heat Transfer

The saturated flow boiling heat transfer correlation is used for both subcooled and saturated flow boiling conditions. This correlation is similar to the treatment of a standard pipe component, though the heat transfer coefficient is slightly different for helical tubes.

{

Equation 6-13

Equation 6-14

}^{2(a),(c)}

{

Equation 6-15

Equation 6-16

$\}}^{2(a),(c)}$

{

Equation 6-17

Equation 6-18

$\}}^{2(a),(c)}$

6.2.3 Primary Side Heat Transfer

During normal NPM-20 operation, the primary-side is expected to be in single-phase liquid conditions throughout the entire operating range. {{

Equation 6-19

Equation 6-20

}}^{2(a),(c)}

6.3 Subcooled Boiling

6.3.1 Onset of Nucleate Boiling

{{

}}^{2(a),(c)}

6.3.2 Onset of Significant Void

Onset of Significant Void signifies the transition from the single-phase liquid region to the two-phase region. OSV is sometimes called the point of Net Vapor Generation (NVG) or the bubble departure point in the external literature (Reference 12.37).

In NRELAP5, OSV is calculated using the Saha-Zuber model (Reference 12.33). The Saha-Zuber model uses the Peclet number to determine if the heat flux at OSV is related to the Nusselt Number (low flow, thermally-controlled bubble growth) or the Stanton number (high flow, hydrodynamically-controlled bubble growth). The correlation for the liquid enthalpy at OSV is shown in Equation 6-21.

$$h_{cr} = \begin{cases} h_{f,sat} - \frac{St' C_{pf}}{0.0055 - 0.0009 \cdot F(p)}, & Pe > 70,000 \\ h_{f,sat} - \frac{Nu' C_{pf}}{455}, & Pe \leq 70,000 \end{cases} \quad \text{Equation 6-21}$$

$$Nu' = \frac{q_f'' d_i}{k_f} \quad St' = \frac{Nu'}{Pe}$$

$$Pe = RePr = \frac{G d_i C_{pf}}{k_f}$$

q_f'' = wall heat flux to the liquid

G = mass flux (mass flow rate / tube area)

k_f = liquid thermal conductivity

C_{pf} = liquid heat capacity at constant pressure

The value of $F(p)$ in the denominator of the Stanton number criterion is a function of pressure defined using Equation 6-22.

$$F(p) = \frac{1.0782}{1.015 + e^{\frac{\left(\frac{p}{6.894757 \times 10^3}\right) - 140.75}{28}}} \quad \text{Equation 6-22}$$

When the local enthalpy exceeds h_{OSV} , a fraction of the wall heat flux goes to vapor generation and the remainder goes to heating the liquid. This partitioning of the heat flux continues until the liquid reaches the saturation temperature, then the heat flux goes into vapor generation. This heat partitioning fraction (called Mul in Reference 12.34, Eq. 4.7-11) is calculated in NRELAP5 using a model developed by Lahey (Reference 12.35).

6.3.3 Subcooled Void Fraction and Quality

The quality (x) in the subcooled flow region can be estimated according to Levy in Reference 12.36. Equation 6-23 holds for straight channel flow.

$$x = x_{th} - x_{th@NVG} \exp\left(\frac{x_{th}}{x_{th@NVG}} - 1\right) \quad \text{Equation 6-23}$$

Variable x_{th} is the thermodynamic equilibrium quality, and $x_{th@NVG}$ is the thermodynamic equilibrium quality at the point of net vapor generation.

6.4 Transition to Dryout

The helical coil component is exclusively used to model a SG. {{

}}2(a),(c)

6.4.1 Two Phase to Single Phase Vapor Transition

In NRELAP5, the transition from nucleate boiling heat transfer and single-phase vapor heat transfer to single-phase vapor is accomplished by an interpolation between the two-phase and single-phase vapor heat transfer starting at a void fraction of 0.995 and continuing until a void fraction of 0.9999, where heat transfer to pure vapor begins. This transition is the natural occurrence of the onset of dryout.

7.0 Evaluation Model Description

This section provides a detailed description of the NPM-20 DWO evaluation model.

The nodalization and modeling options selected for each NPM-20 component are discussed along with the rationale for each choice. Justifications are provided for the boundary conditions (BCs) and initial conditions (ICs) selected for the model. A description of how DWO is analyzed and interpreted is included.

This analysis follows the recommended best practices for the preparation of a RELAP5-3D[®] input (per Reference 12.34) that are applicable to the NRELAP5 DWO model as well as NuScale-specific DWO best practices per Reference 12.8. The NPM-20 DWO evaluation model is consistent with conclusions from density wave oscillation SET assessments, density wave oscillation IET assessments, and related engineering analysis (e.g., nodalization studies) as detailed in Section 8.0.

Appendix B contains results of sample calculations of DWO onset analysis of the NPM-20.

7.1 General Model Overview

The NRELAP5 model for analyzing DWO within the NPM-20 steam generator is developed through a process that reviews different NPM-20 operating conditions, the key phenomena described in the NPM-20 PIRT (Section 4.2), and the numerical behavior of NRELAP5.

The model describes the key components of the NPM-20 that pertain to identification of DWO onset as follows:

- the SG primary-side
 - Upper downcomer
 - Other adjacent regions, if desired
- the SG secondary-side
 - the FW and steam plenums
 - the HCSG tubes

An example of a general nodalization for these components is shown in Figure 7-1, which presents the schematic for a model with {{

}}^{2(a),(c)} (Section 7.5

through Section 7.8).

Note that the specifics of model nodalization, including the number of boiling channels needed, depend on the BC method applied (Section 7.4 and Section 7.8).

Figure 7-2 shows an example flow chart of the EM content, inputs to the EM, and outputs from the EM.

Table 7-1 provides a cross-walk between the NPM-20 steam generator T-H stability PIRT and the model described herein, for which details are described in the following sections.

Figure 7-1 Example of a NuScale Power Module Density Wave Oscillation Model

{{

}}^{2(a),(c)}

Figure 7-2 Evaluation Model Input/Output Flow Chart (Simplified)

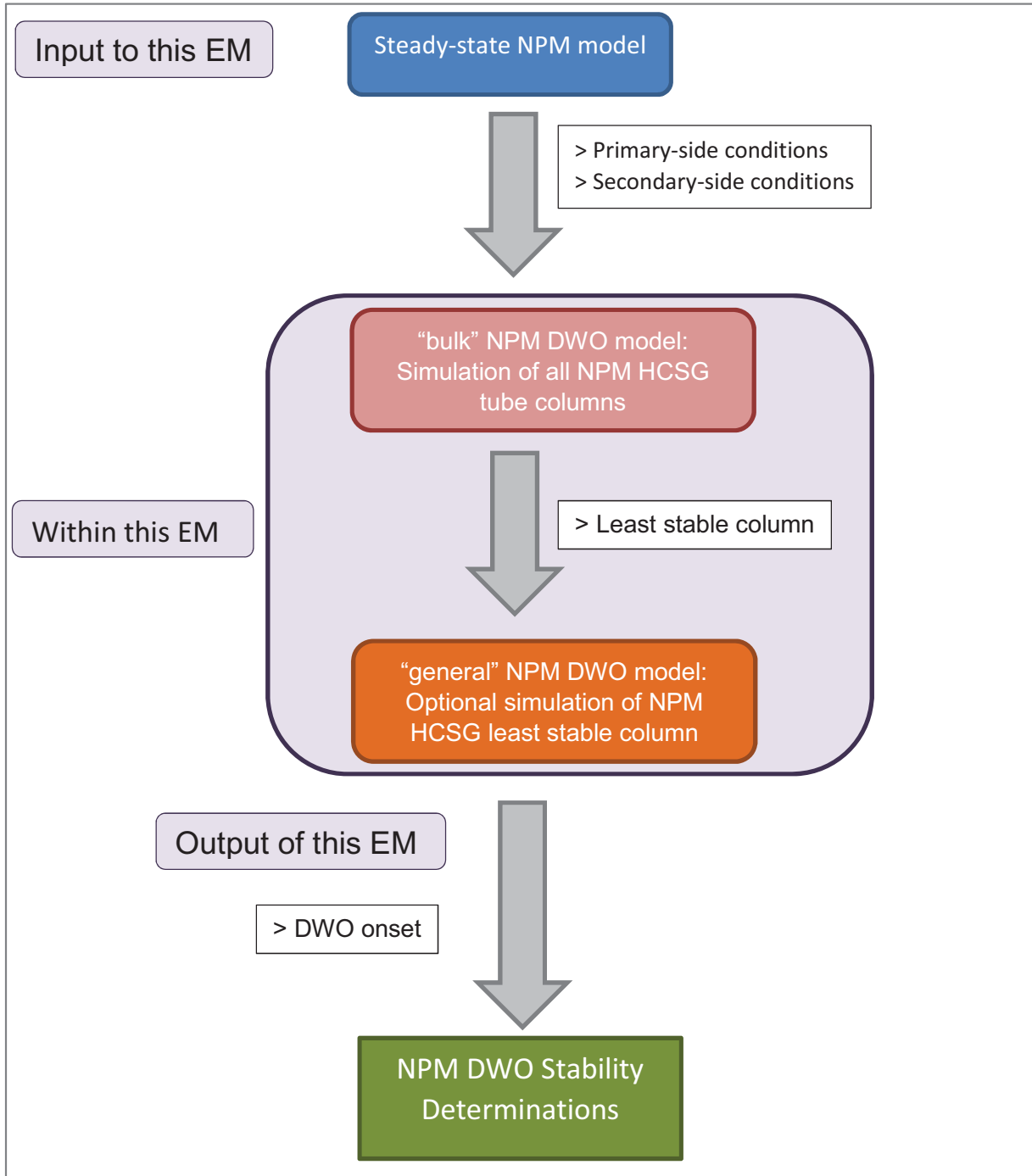


Table 7-1 Density Wave Oscillation Stability Phenomena Identification and Ranking Table Versus NuScale Power Module Density Wave Oscillation Model Incorporation

}}

}}2(a),(c)

Table 7-1 Density Wave Oscillation Stability Phenomena Identification and Ranking Table Versus NuScale Power Module Density Wave Oscillation Model Incorporation (Continued)

}}

}}2(a),(c)

7.2 Overview of Density Wave Oscillation Simulation

7.2.1 Overview of Boundary Condition Methods to Induce Density Wave Oscillation Onset

The methods described herein rely on a quasi-steady-state analysis of NPM-20 steam generator stability relative to DWO. Section 7.4 provides the determination of DWO characteristics.

Historically, the stability of a system over different operating conditions is typically examined by introducing a user-defined perturbation at steady-state, such as a pulse. The perturbation causes flow oscillations, which either grow if the system is unstable or decay to the pre-perturbation state if the system is stable. Often decay ratios or other quantifications are used as stability parameters.

However, due to non-linear effects, fully-developed DWO has large-amplitude oscillations with a decay ratio of 1.0, sometimes referred to as limit-cycle oscillations if they do not grow further. Therefore, while decay ratio can be used to quantify how quickly oscillations grow from initially stable conditions, in simulations, DWO development time is not considered as important as the DWO flow behavior itself (e.g., the flow amplitude and flow period). The DWO flow behavior informs the impact of DWO on a system (e.g., potential stresses), which are not further discussed herein.

To determine whether a system is stable at given conditions, a simulation is run at specific conditions. For an unstable system, a very small perturbation can trigger DWO onset by allowing the system response to occur at the resonant DWO frequency; this is often characterized via period for convenience. Within SGs, a method of BC changes can be applied to perform a quasi-steady state analysis wherein very small perturbations are constantly being introduced. For example, the slow ramping of a BC from a higher value to a lower value is called down ramping (e.g., decreasing FW flow rate).

When sufficient BC changes are applied to an initially stable condition, the system transitions from stable conditions to large-amplitude DWO via DWO onset. This method allows for the analysis of a stability boundary where the system transitioned between stable and unstable states. Comparison of stability boundaries allows for a determination of the distance that any stable condition has to potential instability, which is the margin in that BC to the stability boundary.

While BC step changes can be used to determine stability boundaries, the introduction of larger perturbations generally reduces the resolution of the determined stability boundary. Therefore, BC step changes are not discussed herein.

From a given set of initial conditions, DWO onset can be induced by ramping different BCs. For this EM, the selected methods focus on the ramping of the FW flow rate. The FW flow rate is used because it can both change the overall system conditions (e.g., the total primary-to-secondary heat transfer) and the local HCSG tube

conditions (e.g., the void fraction, pressure drop) within a specific HCSG tube volume. This approach allows for sufficient perturbations to allow for stability boundary investigation.

7.2.2 Overview of Parameters Impactful on Density Wave Oscillation Characteristics

The dynamic behavior of boiling systems depends on their geometry and operating conditions. This section discusses effects of different parameters on stability relative to DWO for the NPM-20 helical coil SG tubes.

Total power and its effects on stability are easier to interpret for boiling channels with two-phase exit conditions. Increases in power result in increased exit quality and increased average tube quality, which are generally destabilizing. {{

}}^{2(a),(c)}

The FW flow is an important parameter to stability. Increased FW flow results in a larger length of single-phase liquid within boiling channels and thus lower average tube quality, which tends to generally decrease the relative weight of two-phase and single-phase gas pressure drop. In addition, both the boiling channel inlet pressure drop due to K_{inlet} and the wall friction pressure drop are dependent on the inlet mass flow rate. Increasing FW flow generally leads to more stable conditions.

The FW temperature can have different effects on stability. For subcooled inlet conditions, increased subcooling is generally stabilizing because it lowers the average tube quality.

Boiling channel pressure, most commonly referred to via steam pressure, affects pressure drop and density. Increasing pressure decreases the density ratio between the liquid and gas phases, which helps to weaken disturbances in two-phase conditions. Furthermore, increasing pressure decreases the relative dependence of two-phase pressure drop on local quality. Therefore, increasing system pressure generally leads to more stable conditions.

The boiling channel pressure drop profile (i.e., the pressure drop as a function of channel length) plays an important role in determining the stability of the system. A large concentrated pressure drop at the channel inlet (e.g., K_{inlet}) enables the system to compensate for fluctuations in total channel pressure drop due to small perturbations and thus leads to stability. Thus, a higher K_{inlet} generally leads to more stable conditions. Conversely, increasing the exit loss coefficient is equivalent to increasing the pressure drop of the two-phase and/or single-phase gas regions of the boiling channel and generally makes the system less stable.

7.3 Steady-State NuScale Power Module Model for Input to NuScale Power Module Density Wave Oscillation Analysis

7.3.1 Boundary Conditions for NuScale Power Module Density Wave Oscillation Analysis

Table 7-2 details the BCs needed to perform the NPM-20 DWO analysis. The details regarding the NRELAP5 Location column are provided.

To determine values for Table 7-2, simulations of realistic operating conditions (i.e., primary-side and secondary-side steady-state parameters) are needed. For example, a simulation performed at 30 percent power conditions runs to convergence. Section 7.3.2 provides more details on high-level requirements for such models. Section 1.2 states that this EM is applied to NPM-20 conditions between 20 percent and 100 percent nominal power.

The FW temperature entry in Table 7-2 is applied just before the HCSG tube inlet and accounts for any heat transfer in the FW line to or from the containment vessel. If this heat transfer results in a temperature change smaller than 5 degrees C, it is considered negligible.

The FW pressure entry in Table 7-2 is applied just before the HCSG tube inlet and accounts for any pressure drop along the FW line.

The entries in Table 7-2 are at the following NPM-20 nominal operating conditions.

- 100 percent, 90 percent, 80 percent, 70 percent, 60 percent, 50 percent, 40 percent, 30 percent, and 20 percent power.
 - These conditions reflect TF-2 DWO test conditions per Section 8.2.
 - Additional operating conditions in this range may be evaluated.
- For any condition above 5 percent power where nominal operating conditions may include one or two active SGs, simulations are needed for both configurations.
- For any condition above 5 percent power that includes step-changes as a function of power (e.g., rapid FW changes as a result of disabling/enabling pre-heaters), simulations are needed before and after the step change.

Table 7-2 NuScale Power Module Steady-State Operating Parameters for Density Wave Oscillation Analysis

System	Parameter	NRELAP5 Location
Primary side	RCS hot temperature	Primary-side inlet
	RCS mass flow rate	Primary-side inlet
	Upper downcomer exit pressure	Primary-side exit
Secondary side	Main steam pressure	steam exit
	FW temperature	FW inlet
	FW mass flow rate	FW inlet

7.3.2 Steady-State NuScale Power Module Model

This section defines the models that provide inputs to NPM-20 DWO analysis per Table 7-2.

The three regions modeled are the primary side, the secondary side, and the containment vessel.

7.3.2.1 Primary-Side Models

The primary side modeling provides an accurate simulation of the natural circulation flow within the RPV.

The natural circulation flow is driven by heat transfer from the core paired with heat removal from the SG. Therefore, requisite steady-state models include sufficient detail to capture significant contributors to primary-side energy balance and primary-side pressure drop. For example, a detailed primary-side circulation loop with hydrodynamic volumes and heat structures for the core, riser, upper plenum, pressurizer, upper downcomer, downcomer, and lower plenum must be determined. Note that per Section 7.6 this level of detail is not required for DWO analysis models.

Because bulk conditions are needed per Table 7-2, it is considered acceptable to use one-dimensional (1-D) components to model primary-side hydrodynamic volumes even though numerical study places emphasis upon liquid outside the HCSG tube flow distribution and temperature distribution. Section 9.2.2.7 details how TF-2 DWO test data illustrates the appropriateness of a 1-D primary-side component.

As steady-state operating conditions are modeled, the simulation of systems like the emergency core cooling system are not needed as long as they do not have a significant impact on the steady-state operating conditions.

7.3.2.2 Secondary-Side Models

The secondary side provides an accurate simulation of the forced flow and total heat transfer between the inlet to the FW plenums and the exit of the steam plenums.

Models include sufficient detail to capture significant contributors to secondary-side energy balance and secondary-side pressure drop. A detailed once-through system with hydrodynamic volumes and heat structures for the FW line, FW plenum, HCSG tubes, steam plenum, and steam lines must be determined.

As steady-state operating conditions are modeled, the simulation of systems like the decay heat removal system are not needed as long as they do not have a significant impact on the steady-state operating conditions.

7.3.2.3 Containment Vessel Models

The containment vessel provides an accurate simulation of any significant heat transfer to or from the primary side and secondary side.

Models include sufficient detail to capture significant contributors to primary-side energy balance and secondary-side energy balance. For example, a detailed system with hydrodynamic volumes and heat structures for the containment vessel components and a representation of the ultimate heat sink is included.

7.4 Specific Methods for Density Wave Oscillation Simulation

7.4.1 Specific Methods to Induce Density Wave Oscillation Onset

Although other methods can be used to induce DWO onset, this EM focuses on the general FW flow-controlled BC method and the bulk FW flow-controlled BC method. The latter is used to determine the relative stability between NPM-20 helical coil SG tube columns. The former is used with that information to analyze DWO stability with a less-detailed model.

Section 7.4.2 contains the analysis of stability boundaries.

For either method, a FW flow-controlled BC method relies on directly ramping the simulated FW mass flow rate. Figure 7-3 and Figure 7-4 provide graphical representations of the ramping, and Section 7.8 provides more information regarding HCSG tube nodalization. Flow ramping steps are:

- {{

}}2(a),(c)

Figure 7-3 General Feedwater Flow-Controlled Boundary Condition Method, Example Illustration

{{

}}2(a),(c)

Figure 7-4 Bulk Feedwater Flow-Controlled Boundary Condition Method, Example Illustration

{{

}}^{2(a),(c)}

7.4.2 Determination of Density Wave Oscillation Stability Boundaries

For the BC methods discussed in Section 7.4.1, the stability boundary encountered is DWO onset during FW flow ramp down. The determination of the points associated with these stability boundaries is described below. Section 7.4.3 explains the determination of the DWO flow period.

{{

}}^{2(a),(c)}

The following method of DWO onset determination is applied.

- {{

}}2(a),(c)

Figure 7-5 provides an example of this method applied to a set of TF-2 DWO test data. The blue line shows tube inlet mass flow rate (Row 3, Tube 11). The red line shows the relative error. The green line denotes the DWO onset time.

Figure 7-5 {{

}}2(a),(c)

{{

}}2(a),(c)

7.4.3 Determination of Density Wave Oscillation Flow Period

An effective and consistent method for determining DWO period is needed.

This method is illustrated in Figure 7-6. Each cycle is defined by a return to the minimum value, and the calculated DWO flow period is an average of the flow period for each cycle within the time window selected for analysis. {{

}}2(a),(c)

Figure 7-6 Example Illustrating Density Wave Oscillation Flow Period Behavior Summary

{{

}}^{2(a),(c)}

7.4.4 Application of Specific Methods to Induce Density Wave Oscillation Onset

The NPM-20 DWO analysis simulations are performed at the conditions for which BCs are sourced per Section 7.3.1. Each condition is first assessed via the {{

}}^{2(a),(c)} Section 7.8 contains HCSG tube nodalization details. Ramping is applied per Section 7.4.1 and then DWO stability boundaries for different columns are determined per Section 7.4.2.

{{

}}^{2(a),(c)}

{{

}}^{2(a),(c)}

7.4.5 Steam Generator Separation

Section 7.6, Section 7.7, and Section 7.8 detail methods for modeling any number of HCSG tubes, which includes anything between one HCSG tube and 1380 HCSG tubes.

{{

}}^{2(a),(c)} within Section 7.6, Section 7.7, and Section 7.8.

7.5 NuScale Power Module Density Wave Oscillation Analysis Model Requirements

In NRELAP5 methodologies, various assumptions and approximations are made to represent a physical configuration via a numerical model. This section discusses the general assumptions and approximations made in the NPM-20 DWO analysis model.

Note that NRELAP5 models used to produce steady-state NPM-20 operating conditions per Section 7.3.2 do not need to follow these requirements.

7.5.1 Hydrodynamic Volume and Junction Options

This section discusses the general assumptions and approximations made relative to hydrodynamic components.

Specific discussion is provided for flags related to hydrodynamic volume velocity (i.e., the homogeneous flag) and to the hydrodynamic volume temperature (i.e., the equilibrium flag). Other flags are discussed more succinctly.

7.5.1.1 Non-Homogeneous Flag

{{

}}^{2(a),(c)}

7.5.1.2 Non-Equilibrium Flag

{{

}}^{2(a),(c)}

{{

}}^{2(a),(c)}

7.5.1.3 Other Hydrodynamic Volume Flags

The following hydrodynamic volume control flags are applied within the NPM-20 DWO model:

- {{

}}^{2(a),(c)}

7.5.1.4 Other Hydrodynamic Junction Options

The following hydrodynamic junction control flags are applied within the NPM-20 DWO model:

- {{

}}^{2(a),(c)}

7.5.2 Heat Structure Options

This section discusses the general assumptions and approximations made relative to heat structures. Section 5.3 provides more details on the specifics of the NRELAP5 heat transfer numerics and correlations.

In the NPM-20 DWO analysis model, the primary use of heat structures is to facilitate primary-to-secondary heat transfer. Other heat structure applications (e.g., approximating primary-side or secondary-side heat losses) are significantly less

important. Because no core heat structures are included, many models are not needed.

{{

}}^{2(a),(c)}

For general applications, the heat transfer type 101 boundary condition are used.

{{

}}^{2(a),(c)}

7.5.3 Time Step and System Options

The semi-implicit time scheme is applied for hydrodynamic components. Section 5.6 contains more details on the specifics of NRELAP5 time step numerics.

Starting from user inputs for minimum and maximum time step sizes, NRELAP5 determines the appropriate global time step such that:

- {{

}}^{2(a),(c)} The heat structure time scheme is implicitly coupled to the hydrodynamic solution.

Besides preventing significant mass error accumulation, concerns regarding time step size focus on reducing numerical instabilities in the model (e.g., artificial perturbations introduced by flow regime or heat transfer flip-flopping) and reducing numerical diffusion in the HCSG tubes (i.e., artificial damping of perturbations). Because the BC methods discussed in Section 7.4.1 rely on the introduction of perturbations to the HCSG tubes, it is important that HCSG tube models not include egregious amounts of numerical diffusion.

 {{

}}2(a),(c)

Because both the primary side and secondary side operate in a once-through configuration (Section 7.6 and Section 7.7), the system-wide mass error checks may be disabled. Disabling mass error checks only prevents code termination based on cumulative mass error buildup (i.e., at 1 percent of total system mass); it does not prevent time-step controls based on mass error accumulation during the current time step.

7.5.4 Initial Conditions

For the NPM-20 DWO analysis model, ICs are set to values that allow for simulation convergence within a reasonable period of time (e.g., ~2,000 seconds) before ramping begins per Section 7.4. Herein, simulation convergence refers to behavior wherein BCs are fixed and wherein conditions within individual components (e.g., HCSG tubes, upper downcomer, etc.) are not noticeably changing as a function of time.

Generally, poorly tailored ICs only lead to the need for extended convergence times. However, very poor ICs can lead to initial instability. In these cases, it can take some time for convergence to occur. Therefore suggestions for IC tailoring is provided for each relevant component in Section 7.6 through Section 7.8.

7.6 Model Nodalization - Steam Generator Primary Side

The required components for the SG primary side are the primary-side inlet, the upper downcomer (i.e., the upper section containing the HCSG tubes), and the primary-side exit.

The optional components for the SG primary side are the riser, the riser holes, and the upper plenum.

7.6.1 Steam Generator Primary Side: Inlet

{{

}}2(a),(c)

{{

}}^{2(a),(c)}

7.6.1.1 Steam Generator Primary Side: Inlet Boundary Conditions

{{

}}^{2(a),(c)}

Section 7.3.1 provides more information on BCs.

7.6.2 Steam Generator Primary Side: Upper Downcomer

{{

}}^{2(a),(c)}

{{

}}^{2(a),(c)}

7.6.2.1 Steam Generator Primary Side: Upper Downcomer Heat Structures

{{

}}^{2(a),(c)}

7.6.2.2 Steam Generator Primary Side: Upper Downcomer Initial Conditions

{{

}}^{2(a),(c)}

7.6.3 Steam Generator Primary Side: Exit

{{

}}^{2(a),(c)}

7.6.3.1 Steam Generator Primary Side: Exit Boundary Conditions

{{

}}^{2(a),(c)}

7.6.4 Steam Generator Primary Side: Riser

This component is not required.

{{

}}^{2(a),(c)}

7.6.4.1 Steam Generator Primary Side: Riser Heat Structures

These heat structures are not required.

{{

}}^{2(a),(c)}

7.6.4.2 Steam Generator Primary Side: Riser Initial Conditions

Pressure is set to values similar to initial BCs per Section 7.6.3.1. Temperature is set to initial BCs per Section 7.6.1.1. Mass flow rate is set to initial BCs per Section 7.6.1.1.

7.6.5 Steam Generator Primary Side: Riser Holes

This component is not required.

{{

}}^{2(a),(c)}

If included, the riser holes must include realistic and accurate flow area, hydraulic diameter, and loss coefficient inputs.

7.6.5.1 Steam Generator Primary Side: Riser Holes Initial Conditions

{{

}}^{2(a),(c)}

7.6.6 Steam Generator Primary Side: Upper Plenum

This component is not required.

{{

}}^{2(a),(c)}

7.6.6.1 **Steam Generator Primary Side: Upper Plenum Heat Structures**

Any HCSG tubes in the upper plenum require heat structures. Other heat structures are not required for this component.

7.6.6.2 **Steam Generator Primary Side: Upper Plenum Initial Conditions**

Pressures are set to values similar to initial BCs per Section 7.6.3.1. Temperatures are set to initial BCs per Section 7.6.1.1. Mass flow rates are set to initial BCs per Section 7.6.1.1.

7.7 **Model Nodalization - Feedwater and Steam Plenums**

{{

}}^{2(a),(c)}

7.7.1 **Feedwater Source**

{{

}}^{2(a),(c)}

7.7.1.1 Feedwater Source: Inlet Boundary Conditions

{{

}}^{2(a),(c)}

Section 7.3.1 provides more information on BCs.

7.7.2 Feedwater Plenum

{{

}}^{2(a),(c)}

7.7.2.1 Feedwater Plenum: Heat Structures

{{

}}^{2(a),(c)}

7.7.2.2 Feedwater Plenum: Initial Conditions

Pressure is set to values slightly higher than initial steam pressure BCs per Section 7.7.3. Temperature is set to initial FW temperature BCs per Section 7.7.1.1.

7.7.3 Steam Plenum

{{

}}^{2(a),(c)}

7.7.3.1 Steam Plenum: Heat Structures

{{

}}^{2(a),(c)}

7.7.3.2 Steam Plenum: Initial Conditions

Pressure is set to the initial values per Section 7.7.3. Temperature is set to T_{hot} initial values per Section 7.6.1.1.

7.7.4 Steam Exit

{{

}}^{2(a),(c)}

7.7.4.1 Steam Exit: Exit Boundary Conditions

{{

}}^{2(a),(c)}

Section 7.3.1 provides more information on BCs.

7.8 Model Nodalization - Helical Coil Steam Generator Tubes

The HCSG tubes are composed of the tube inlet(s), the tubes, and the tube exit(s).

7.8.1 Helical Coil Steam Generator Tube Inlets

{{

}}^{2(a),(c)}

{{

}}^{2(a),(c)}

7.8.1.1 Helical Coil Steam Generator Tube Inlets: Initial Conditions

{{

}}^{2(a),(c)}

7.8.2 Helical Coil Steam Generator Tubes

{{

}}^{2(a),(c)}

7.8.2.1 Helical Coil Steam Generator Tubes: Columns

{{

}}^{2(a),(c)}

7.8.2.1.1

{{

}}2(a),(c)

{{

}}2(a),(c)

7.8.2.1.2

{{

}}^{2(a),(c)}

{{

}}^{2(a),(c)}

7.8.2.2

Helical Coil Steam Generator Tubes: Sections

{{

}}^{2(a),(c)}

{{

}}2(a),(c)

7.8.2.3 HCSG Helical Coil Steam Generator Tubes: Main Section General Nodalization

{{

}}2(a),(c)

{{

}}^{2(a),(c)}

7.8.2.4 Helical Coil Steam Generator Tubes: Heat Structures

{{

}}^{2(a),(c)}

7.8.2.5 Helical Coil Steam Generator Tubes: Initial Conditions

{{

}}^{2(a),(c)}

Mass flow rates are set consistent with Section 7.8.1.1.

7.8.3 Helical Coil Steam Generator Tube Exits

{{

}}^{2(a),(c)}

7.8.3.1 Helical Coil Steam Generator Tube Inlets: Initial Conditions

{{

}}^{2(a),(c)}

8.0 NRELAP5 Assessments

The following section provides a summary of SET and IET assessment that have been completed for NRELAP5 application to DWO. The results of these assessments support Section 9.0 to justify the adequacy of NRELAP5 for modeling high-ranked phenomena identified in the SG stability PIRT described in Section 4.0.

Three experimental programs used in the assessment of NRELAP5 are summarized below.

- SIET TF-1: Electrically heated test facility with three full-length HCSG tubes. The testing was performed to characterize pressure drop, heat transfer coefficients, and DWO in parallel-coiled tubes.
- SIET TF-2: Primary fluid-heated test facility with 252 HCSG tubes in five rows, which includes the effect of primary-to-secondary heat transfer through the tube walls. Testing included a large-scale facility, near-prototypic HCSG tube geometry, and NPM-20-based operating conditions.
- Polytechnic Institute of Milan (POLIMI): Electrically-heated test facility with two HCSG tubes in parallel fed by a single FW line. Both tubes are connected to a shared FW header and steam header.

For each assessment, the following information is summarized in Section 8.1, Section 8.2, and Section 8.3:

- brief description and purpose of the experimental facility
- summary of the phenomena addressed
- experimental procedure
- important NRELAP5 modeling techniques
- comparison of NRELAP5 calculations against data

Table 8-1 provides a comparison of geometrical parameters for the NPM-20 and the three assessments. A graph showing the HCSG tube diameter ratio (SG tube inner diameter over helical coil inner diameter or d_i/D_{coil}) for the NPM-20 and the three experimental programs is shown in Figure 8-1. TF-1 covers the full NPM-20 range of SG tube diameters. TF-2 models the five innermost tube rows of the NPM-20 helical coil SG and covers the upper range of d_i/D_{coil} . The POLIMI tests have a larger diameter ratio, representing larger centrifugal forces than those that would exist in the NPM-20.

The NPM-20 operating conditions from 5 percent to 100 percent power are shown Table 8-2 along with T-H parameter ranges from the three test programs. Figure 8-2 plots (as a horizontal bar) secondary-side parameter ranges for steam pressure, FW temperature and flow per tube for NPM-20 and the three tests. The plot includes both DWO and non-DWO conditions. For the three parameters, TF-2 fully covers the NPM-20 range.

Table 8-1 Comparison of Geometrical Parameters for NuScale Power Module and Assessment Tests

Parameter	NPM-20	TF-1	TF-2	POLIMI
Tube material	Alloy 690	AISI 304L	AISI 304L	SS AISI 316
Number of tubes	1380 tubes in 21 columns	3 tubes (2 for DWO)	252 tubes in 5 rows	2 tubes
Tube outside diameter (mm)	15.88	15.88	16.07	17.15
Tube inside diameter (mm)	13.34	13.086	13.17	12.53
Tube length (active, m)	22.4 - 25.9	26.82	25.01 - 26.42	32
Tube thickness (mm)	1.27	1.397	1.45	2.31
Tube inclination (degrees)	12.8 to 15.1 (13.69 for C3)	C1(1) 10.0 C2 14.0 C3 14.0	13.6 to 14.5	14.3
Helical coil radius (m)	{{ }} ^{2(a),(c),ECI}	{{ }} ^{2(a),(c)}	{{ }} ^{2(a),(c),ECI}	0.5
Tube inner diameter to Coil diameter ratio (d_i/D_{coil})	{{ }} ^{2(a),(c),ECI}	{{ }} ^{2(a),(c)}	{{ }} ^{2(a),(c),ECI}	0.0125
Tube length to tube inner diameter ratio (L_{tube}/d_i)	1679 to 1942	2052	1899 to 2006	2554
Test section height or NPM-20 SG height (m)	5.87	6.49	6.44 to 6.61	8.0

Note (1): For TF-1 entries, C1 means Coil 1, C2 means Coil 2, and C3 means Coil 3.

Figure 8-1 Tube-to-Coil Diameter Ratio for NuScale Power Module and Assessment Test Programs

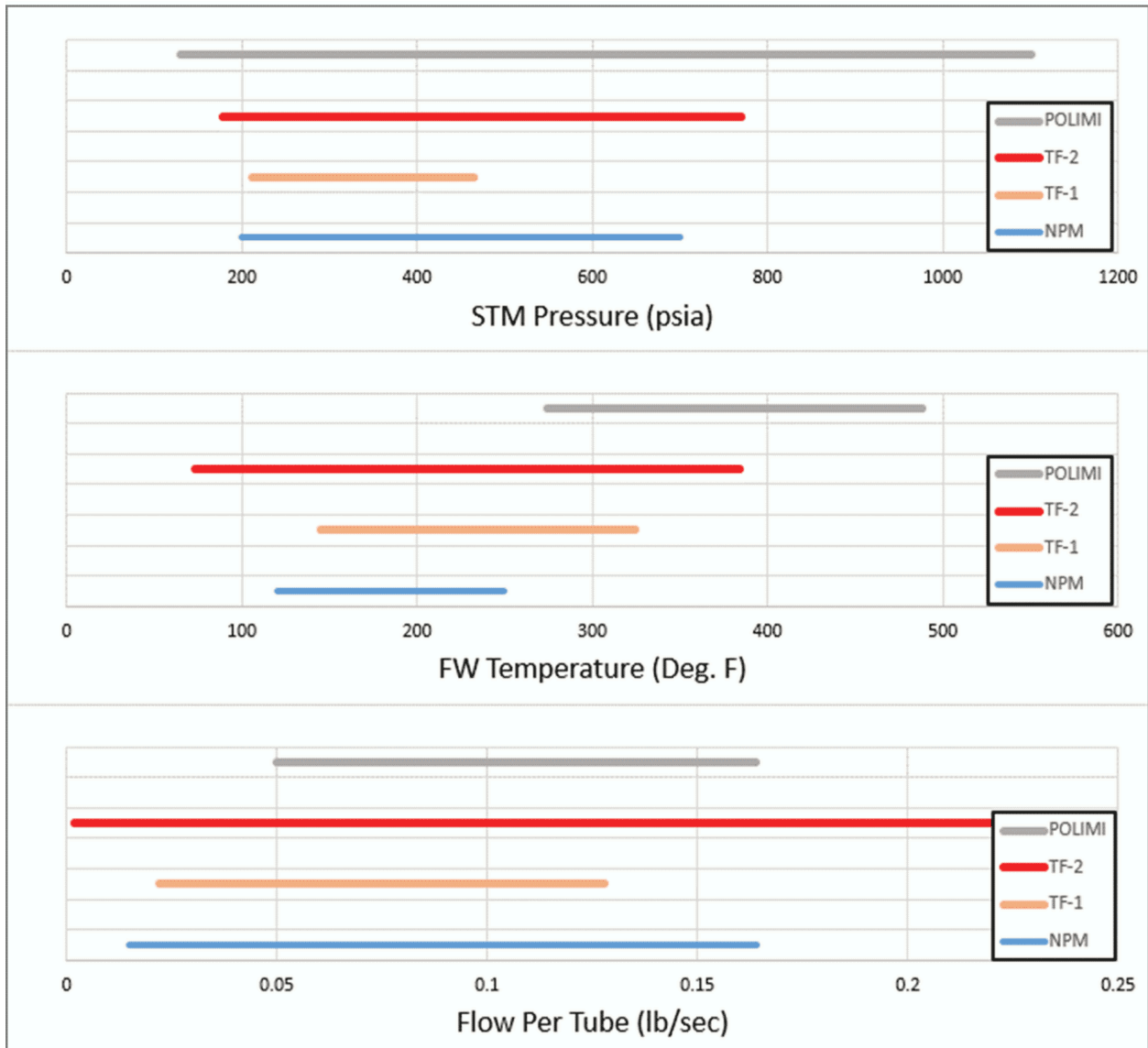
{{

}}^{2(a),(c)}

Table 8-2 NuScale Power Module Thermal-Hydraulic Conditions Compared to Assessment Test Program Conditions

Parameter	Units	NPM-20	TF-1 (non-DWO/SET)	TF-1 (DWO)	TF-2 (non-DWO/SET)	TF-2 (DWO)	POLIMI (DWO)
Secondary-side exit pressure	Psi MPa	200 - 700 1.38 - 4.83	217.5 - 464 1.50 - 3.20	211 - 233 1.46 - 1.61	450 3.10	178-769 1.23 - 5.30	130 - 1,100 0.90 - 7.58
FW temperature	degrees F degrees C	120 - 250 48.9 - 121.1	149 - 417 65 - 214	145 - 324 62.8 - 162.2	300 148.9	73 - 384 22.8 - 195.6	274 - 488 134.4 - 253.3
Total flow rate/tube (average)	lb/sec kg/sec	0.015 - 0.164 0.007- 0.074	0.023 - 0.124 0.01 - 0.056	0.022 - 0.128 0.01 - 0.058	0.002 - 0.115 0.001 - 0.052	0.037 - 0.22 0.017 - 0.10	0.05 - 0.164 0.023 - 0.074
Power/tube (average)	kW	15.6 - 158	23 - 131	20 - 120	20 - 110	18.3 - 151.2	7 - 97
Tube exit steam superheat	degrees F degrees C	20- 94 11 - 52	0 - ~200 0 - ~111	~0 (usually)	0 - ~120 0 - ~67	0 - 104 0 - 58	~0
Primary-side T _{hot}	degrees F degrees C	409 - 598 209 - 314	n/a	n/a	533.9 - 588.4 279 - 309	481 - 582 249 - 306	n/a
Primary-side T _{cold}	degrees F degrees C	387 - 482 197 - 250	n/a	n/a	524.2 - 560.0 273 - 293	440 - 540 227 - 282	n/a
Primary-side flow	lb/sec kg/sec	510 - 1,611 231 - 731	n/a	n/a	22.5 - 333.6 10.2 - 151.	50.7 - 134.9 23.0 - 61.2	n/a

Figure 8-2 Secondary Side Parameter Ranges for NuScale Power Module and Assessment Tests



8.1 Assessment of TF-1 Data

8.1.1 Test Description and Experimental Procedure

The TF-1 test facility at SIET was operated to perform a series of testing in 2016. The main components and loops of the SIET TF-1 facility in the NPM-20 helical coil SG test configuration are described here and shown in Figure 8-3.

A pump system drives water from a water storage tank to the pre-heating zone where it is brought to the specified operating conditions and sent to a FW header. The FW header provides inlet flow to the three HCSG tubes of the test section (Coil 1, Coil 2, and Coil 3) that can be activated by valves singularly or two in parallel.

Superheated steam exits the test section toward a header connected to the separation and discharge system. Steam enters a water-steam separator that allows the two phases to be discharged separately. Electric power is provided to the pre-heaters and to the desired test section coils by a direct current generator. For the adiabatic tests, no electric power is provided to the test section coils. For the diabatic tests and the DWO tests, the power generator connections to the coils are suitable to deliver heat to the sub-cooled, saturated and superheated zones, which can be controlled independently.

The TF-1 tube geometry and coil geometry details are provided in Table 8-1. The instrumentation details are shown in Figure 8-3. The run number prefixes appearing on some of the plots mean: for adiabatic testing, TD for diabatic testing, and TO for DWO testing.

}}2(a),(c)

Figure 8-3 TF-1 Test Section and Instrumentation Configuration

}}

The relative heat flux profile along the tube for the three zones is shown in Figure 8-4. The three zones are intended to approximately simulate differing heat inputs in the single-phase, boiling two-phase, and superheated steam regions of the SG.

Figure 8-4 Relative Heat Flux Versus Position Along the Tube

{{

}}2(a),(c)

8.1.2 Phenomena Addressed

Phenomena addressed by TF-1 data include single-phase and two-phase pressure drop, single-phase and two-phase heat transfer, void fraction, and interfacial drag. Several of the high ranked phenomena are addressed by TF-1 (Section 9.0). The facility lacks primary-side fluid, so primary-side heat transfer effects are not addressed as in TF-2 testing (Section 8.2).

8.1.3 NRELAP5 TF-1 Model

For SET simulation, the NRELAP5 input model of the TF-1 test facility is depicted in Figure 8-5.

Figure 8-5 NRELAP5 Model of TF-1

{{

}}^{2(a),(c)}

 {{

}}2(a),(c)

8.1.4 Performance against TF-1 Single Effects Test Data

TF-1 SETs include analyses of pressure drop, as described in Section 8.1.4.1, and heat transfer via wall and fluid temperatures, as described in Section 8.1.4.2.

8.1.4.1 Pressure Drop Comparison

This section presents an assessment of NRELAP5 with respect to single-phase and two-phase pressure drop in the HCSG tubes using TF-1 data. The TF-1 experiments included both adiabatic and diabatic test configurations. TF-1 non-DWO testing consisted of 77 adiabatic (unheated) test runs (TA-0001 to TA-0077) and 84 diabatic (heated) test runs (TD-0001 to TD-0084). The TF-1 DWO (integral effects) testing consisted of 22 runs. For the adiabatic tests, liquid and vapor flow was injected through the FW line, and pressure drop was measured across the channels at different locations as indicated in Figure 8-3.

The TF-1 tube geometries are comparable with the NPM-20 (Table 8-1 and Figure 8-1). It is apparent from Table 8-2 and Figure 8-2 that the TF-1 adiabatic tests cover a significant range of NPM-20 operation. The assessment of different tubes at TF-1 for pressure drop comparison demonstrates the NRELAP5 capability to predict the pressure drop for NPM-20.

NRELAP5 Code Assessment

For TF-1 SET code-to-data comparisons, agreement herein is determined as follows:

- within ± 10 percent: excellent
- within ± 20 percent: reasonable
- within ± 40 percent: minimal
- greater than 40 percent: insufficient

In the following figures, the purple lines provide boundaries within 15 percent of the data value.

NRELAP5 was assessed against the TF-1 adiabatic tests to establish its capability to predict the two-phase pressure drop. Figure 8-6, Figure 8-7, and Figure 8-8 show the pressure drop comparison from adiabatic tests for Coil 1, Coil 2, and Coil 3. The majority of points are within 15 percent, though some are outside 15 percent.

NRELAP5 was assessed against the TF-1 diabatic tests to establish its capability to predict pressure drop and fluid and wall temperatures along the HCSG tubes at several locations. Figure 8-9, Figure 8-10, and Figure 8-11 show the pressure drop comparison from adiabatic and diabatic tests for Coil 1, Coil 2, and Coil 3. Most points are within 15 percent of the data value.

Overall, the calculated two-phase pressure drops along the coil are in reasonable-to-excellent agreement with the adiabatic and diabatic test data.

Figure 8-6 TF-1 Differential Pressure for Coil 1 Adiabatic Tests

{{

}}2(a),(c)

Figure 8-7 TF-1 Differential Pressure for Coil 2 Adiabatic Tests

{{

}}2(a),(c)

Figure 8-8 TF-1 Differential Pressure for Coil 3 Adiabatic Tests

{{

}}2(a),(c)

Figure 8-9 TF-1 Differential Pressure for Coil 1 Diabatic Tests

{{

}}2(a),(c)

Figure 8-10 TF-1 Differential Pressure for Coil 2 Diabatic Tests

{{

}}2(a),(c)

Figure 8-11 TF-1 Differential Pressure for Coil 3 Diabatic Tests

}}

}}2(a),(c)

8.1.4.2 Fluid and Wall Temperature Comparison

TF-1 diabatic cases (TD cases) are used to assess two-phase heat transfer. The incoming FW is heated and eventually becomes a two-phase mixture. Diabatic tests measure pressure drop, fluid temperature, and wall temperature along the HCSG tubes at several locations. The accuracy of wall temperature and fluid temperature comparison between NRELAP5 and test data directly depends on the heat transfer coefficient prediction.

Figure 8-2 lists the TF-1 diabatic test condition range and comparison with NPM-20 operating conditions. Overall, diabatic test conditions cover the NPM-20 operation range. Although the power per tube in TF-1 is lower than NPM-20, TF-1 tubes undergo a wide quality range and therefore show the effect of quality on two-phase heat transfer.

Fluid temperature code-to-data comparisons with NRELAP5 are shown in Figure 8-12, Figure 8-13, and Figure 8-14 for the three coils. Values are within 15 percent of the data value. Excellent predictions of fluid temperatures by NRELAP5 indicate the heat input to the fluid is correctly modeled.

Predicted versus measured wall temperatures are plotted in Figure 8-15, Figure 8-16, and Figure 8-17 for the three coils. Most values are within 15 percent of the data value. Reasonable agreement of wall temperature predictions indicates the accuracy of the heat transfer coefficient model in NRELAP5. Some over-prediction of wall temperature is observed, which is believed to be due to NRELAP5 predicting tube dryout upstream of where it is observed in the test. For TF-1, if the NRELAP5 dryout location is only slightly (e.g., 10 cm) off near the step change in heat flux (Figure 8-4), a large temperature error occurs. This heat flux step change due to the application of electrical heating is not typical of the NPM-20 or TF-2 HCSG tubes.

Figure 8-12 TF-1 Fluid Temperature Comparison for Coil 1

{{

}}2(a),(c)

Figure 8-13 Fluid Temperature Comparison for Coil 2

{{

}}2(a),(c)

Figure 8-14 Fluid Temperature Comparison for Coil 3

{{

}}2(a),(c)

Figure 8-15 Wall Temperature Comparison for Coil 1

{{

}}2(a),(c)

Figure 8-16 Wall Temperature Comparison for Coil 2

{{

}}2(a),(c)

Figure 8-17 Wall Temperature Comparison for Coil 3

{{

}}2(a),(c)

8.1.5 Performance against TF-1 Density Wave Oscillation Data

{{

}}2(a),(c),ECI

Previous analysis demonstrated alternative TF-1 NRELAP5 modeling methods that could be used to produce excellent code-to-data agreement for DWO flow period and reasonable-to-excellent agreement for DWO flow amplitude. These are not presented here because the focus of the TF-1 assessment is DWO onset prediction with the more optimized model.

Figure 8-18 TF-1 Density Wave Oscillation Code-to-Data Comparison, Density Wave Oscillation Onset Power

{{

}}^{2(a),(c)}

8.1.6 Summary and Conclusions from TF-1 Density Wave Oscillation Code-to-Data Comparisons

Prediction of pressure drop, fluid temperature, and wall temperature are generally within ± 15 percent, which is reasonable-to-excellent agreement.

Prediction of power at DWO onset are generally within ± 15 percent, which is reasonable-to-excellent. The seven case that are outside ± 15 percent are on the conservative side from a code prediction perspective and are acceptable. In other words, NRELAP5 predicts DWO onset before it occurs in the experiment.

8.2 Assessment of TF-2 Data

8.2.1 TF-2 Test Description and Experimental Procedure

The TF-2 test facility at SIET was operated to perform one series of testing in 2015 and another in 2022.

TF-2 is a fluid-heated test facility where the secondary-side fluid is heated by the primary-side fluid. Boundary conditions (e.g., primary-side and secondary-side flow, temperature, and pressure) are varied during testing for DWO investigation.

The objective of TF-2 testing was to obtain quality HCSG data with fluid-heated HCSG tubes. Testing was performed to characterize primary-side characteristics (e.g., pressure drop and heat transfer), and secondary-side DWO characteristics (e.g., DWO onset, DWO flow amplitude, and DWO flow period). To accomplish these objectives, the TF-2 test program was divided into two-phases.

During the first phase, testing was conducted to simulate the T-H behavior of the primary side and secondary side of the NPM-20 helical coil SG. A small set of initial DWO runs were tested and analyzed with NRELAP5.

During the second phase, testing was focused on obtaining HCSG tube data for DWO characteristics during simulated NPM-20 conditions. Lessons learned from the first set of DWO testing were implemented. The DWO tests were performed by varying boundary conditions (e.g., FW flow) until DWO onset occurred, after which testing continued if possible. For many tests, measurement of DWO behavior continued while boundary conditions were ramped towards stability (e.g., increased FW flow) until DWO cessation. Sets of facility characterization data were also collected.

The TF-2 facility test section consists of a bundle of 252 HCSG tubes split between five rows as shown in Figure 8-19. The five tube rows are placed in an annulus formed by two cylindrical barrels installed axially within the pressure vessel. Each row of HCSG tubes (i.e., groups of 48 or 52 tubes) is fed by a row-specific FW header, which is mounted inside the vessel and distributes water to each tube inlet as shown in Figure 8-20. Steam exiting the tubes is collected on a per-row basis by a steam header and driven out through the top nozzle. The five rows of the SG can either operate together or individually (i.e., FW flow is delivered on a per-row basis).

The TF-2 testing was conducted in both single-row and multi-row configurations. TF-2 adiabatic and diabatic tests involve a series of single-row and multi-row tests with conditions designed to analyze primary-side flow behavior. The TF-2 DWO tests involve a series of single-row and multi-row tests with scaled NPM-20 operating

conditions and sensitivity parameter variations. Row 3 is the most highly-instrumented for HCSG tube inlet differential pressure, which is used to calculate SG tube inlet flow.

Geometric information for TF-2 HCSG tubes is provided in Table 8-1. The TF-2 HCSG tubes represent geometries that are similar to the five innermost columns of the NPM-20 helical coil SG at the time the facility was first commissioned in terms of diameter, length, and helical coil characteristics. Compared to the latest version of the NPM-20 design, the TF-2 HCSG tubes have a very similar inside diameter, a slightly longer tube length, a helical radius within the NPM-20 range, and a tube inclination angle within the NPM-20 range. Therefore, TF-2 provides a valuable assessment base for analyzing DWO in the NPM-20.

TF-2 test condition ranges are provided in Table 8-2.

The overall goal of each test in this experiment is to induce DWO onset. The method to induce DWO was varied along with the operating parameters. The test conditions for each test are shown in Table 8-4. The main conditions varied during testing were:

- {{

}}2(a),(c)

}}2(a),(c),ECI

Table 8-5 {{

{{

}}2(a),(c),ECI

}}2(a),(c),ECI (Continued)

{{

Table 8-5 {{

}}2(a),(c),ECI

Figure 8-19 TF-2 Secondary-side Tube Bundle Configuration in the Primary-Side Flow Annulus

{{

}}2(a),(c)

Figure 8-20 TF-2 Configuration Piping and Instrumentation Diagram

{{

}}2(a),(c),ECI

8.2.2 Phenomena Addressed

The TF-2 tests were run to assess primary-side behavior (i.e., adiabatic and diabatic tests) and DWO behavior (i.e., DWO tests).

Phenomena covered by TF-2 testing are pressure drop (single-phase and two-phase), heat transfer (single-phase and two-phase), and primary-to-secondary heat transfer. Due to the presence of boiling channels and primary-to-secondary heat transfer, TF-2 tests cover a wide range of applicable phenomena.

The TF-2 DWO tests are used to assess the FoMs of DWO onset, DWO flow period, and DWO flow amplitude.

8.2.3 Important NRELAP5 Modeling Techniques

The TF-2 adiabatic and diabatic tests involve SG operation with primary-to-secondary heat transfer. {{

}}2(a),(c)

Figure 8-21 TF-2 NRELAP5 Adiabatic and Diabatic Test Nodalization Diagram

{{

}}2(a),(c)

{{

}}2(a),(c)

}}2(a),(c)

Figure 8-22 TF-2 Density Wave Oscillation Test NRELAP5 Model Nodalization Diagram - Only Row 3 Active

}}

{{

}}^{2(a),(c)}

8.2.4 Performance against TF-2 Single Effects Test Data

The TF-2 facility is equipped with thermocouples and pressure drop sensors across the primary side of the test section. The TF-2 adiabatic and diabatic tests evaluate primary-side pressure drop and heat transfer. Primary-side pressure drop is dominated by cross-flow over tubes. Primary-side temperature conditions are dominated by primary-to-secondary heat transfer.

Adiabatic tests were run without primary-side heating and without secondary-side flow. Diabatic tests were performed to evaluate primary-side pressure drop and heat transfer. These tests characterized the thermal performance of the HCSG tubes for a range of primary-side and secondary-side flows and temperatures.

For TF-2 SET code-to-data comparisons, agreement herein is determined as follows:

- within ± 10 percent: excellent
- within ± 20 percent: reasonable
- within ± 40 percent: minimal
- greater than 40 percent: insufficient

In the following figures, the purple lines provide boundaries within 15 percent of the data value.

Adiabatic experimental data are used to assess modeling of primary-side friction and form losses in NRELAP5. Figure 8-23 shows a comparison of predicted and measured primary-side pressure drop with instrument uncertainty for adiabatic tests. NRELAP5 values provide excellent code-to-data agreement.

Figure 8-23 TF-2 Adiabatic Tests, Primary-side Differential Pressure Comparison

{{

}}2(a),(c)

Figure 8-24 shows a comparison of predicted and measured primary-side pressure drop with uncertainty for diabatic tests. Code-to-data agreement is reasonable-to-excellent.

Figure 8-25 shows the primary-side temperature prediction by NRELAP5 for diabatic tests. For most of the test conditions, NRELAP5 closely predicted the change in the primary side temperature. Code-to-data agreement is reasonable-to-excellent.

For TF-2 diabatic tests, NRELAP5 validation shows reasonable-to-excellent agreement with test data for primary-side pressure drop, primary-side fluid temperatures, HCSG tube wall temperatures, HCSG tube dryout locations, and HCSG tube fluid temperatures. Based on the primary-side and secondary-side fluid temperatures and tube wall temperatures predicted by NRELAP5, the heat transfer coefficients of both the primary side and secondary side are well-predicted by NRELAP5.

Figure 8-24 TF-2 Diabatic Tests, Primary-Side Differential Pressure Comparison

{{

}}2(a),(c)

Figure 8-25 TF-2 Diabatic Tests, Primary-Side Temperature Comparison

{{

}}^{2(a),(c)}

8.2.4.1 TF-2 Tube-Side Data

{{

}}^{2(a),(c)}

{{

}}2(a),(c)

Figure 8-26 {{

}}2(a),(c),ECI

{{

}}2(a),(c),ECI

{{

}}2(a),(c),ECI

Figure 8-27 {{

}}2(a),(c),ECI

{{

}}2(a),(c),ECI

Figure 8-28 {{

}}2(a),(c),ECI

{{

}}2(a),(c),ECI

Figure 8-29 {{

}}2(a),(c),ECI

{{

}}2(a),(c),ECI

{{

}}2(a),(c),ECI

Figure 8-30 {{

}}2(a),(c),ECI

{{

}}2(a),(c),ECI

Figure 8-31 {{

}}2(a),(c),ECI

{{

}}2(a),(c),ECI

Figure 8-32 {{

}}2(a),(c),ECI

{{

}}2(a),(c),ECI

{{

}}2(a),(c),ECI

Figure 8-33 {{

}}2(a),(c),ECI

{{

}}2(a),(c),ECI

Figure 8-34 {{

}}2(a),(c),ECI

{{

}}2(a),(c),ECI

Figure 8-35 {{

}}2(a),(c),ECI

{{

}}2(a),(c),ECI

{{

}}2(a),(c),ECI

{{

}}2(a),(c),ECI

Figure 8-36 {{

}}2(a),(c),ECI

{{

}}2(a),(c),ECI

{{

}}2(a),(c),ECI

Figure 8-37 {{

}}2(a),(c),ECI

{{

}}2(a),(c),ECI

{{

}}2(a),(c),ECI

Figure 8-38 {{

}}2(a),(c),ECI

{{

}}2(a),(c),ECI

Figure 8-39 {{

}}2(a),(c),ECI

{{

}}2(a),(c),ECI

{{

}}2(a),(c),ECI

Figure 8-40 {{

}}2(a),(c),ECI

{{

}}2(a),(c),ECI

Figure 8-41 {{

}}2(a),(c),ECI

{{

}}2(a),(c),ECI

8.2.5 Performance against TF-2 Density Wave Oscillation Integral Effects Test Data

For TF-2 DWO test simulation, both base and biased NRELAP5 cases were run to quantify uncertainty for DWO onset. The biased cases include conservative values for input parameters with potentially large impacts: higher HCSG tube K_{inlet} , colder FW temperature, and higher total FW flow. The magnitudes of these biases were determined per uncertainty estimates.

Table 8-6 provides a summary for the base and biased results. An NRELAP5 case showing DWO onset at a higher FW flowrate is considered conservative. A positive error denotes a conservative prediction, while a negative error denotes a non-conservative prediction. For NRELAP5 code-to-data comparisons of DWO onset, relative error is calculated separately for Row 3 and also for all rows.

For the uncertainty analysis, Row 1 and Row 5 results are included along with Row 3 results. While Row 3 is the most highly instrumented and thus provides the highest level of resolution, Row 1 and Row 5 also are instrumented and therefore provide useful information. Besides just providing additional tube measurements, Row 1 and Row 5 have slightly different geometries.

The NRELAP5 base cases are conservative for DWO onset; NRELAP5 predicts DWO onset at a higher FW flow compared to the test data. When a 95 percent confidence uncertainty is applied, NRELAP5 base cases become slightly non-conservative.

The NRELAP5 biased cases are non-conservative for DWO onset; NRELAP5 predicts DWO onset at a lower FW flow compared to the test data. When a 95 percent confidence uncertainty is applied, NRELAP5 biased cases become more non-conservative.

To account for the uncertainty of NRELAP5 in predicting DWO onset, the one-sided uncertainty results are defined as the overall NRELAP5 uncertainty. For NRELAP5 downstream usage for predicting DWO onset, a one-sided bias uncertainty of $\pm 2(a),(c)$ with a 95 percent confidence interval is recommended.

Table 8-6 TF-2 Density Wave Oscillation Test NRELAP5 Simulation, Density Wave Oscillation Onset Total Error Summary Results

Table with 3 columns and 10 rows. The table is mostly empty, with a few faint markings. A $\pm 2(a),(c)$ symbol is located at the bottom right of the table area.

Figure 8-42, Figure 8-43, and Figure 8-44 show code-to-data comparisons for DWO onset, DWO flow period, and DWO flow amplitude for the least-stable tube. The NRELAP5 values are from the base cases.

For code-to-data comparisons of these FoM, the following criteria were applied to determine code-to-data agreement:

- less than -40 percent: minimal
- between -40 percent and -10 percent: reasonable
- between -10 percent and 10 percent: excellent

- between 10 percent and 20 percent: reasonable
- between 20 percent and 40 percent: minimal
- greater than 40 percent: insufficient

For DWO onset, a negative value means that NRELAP5 DWO onset occurs at a lower FW flow rate.

For DWO flow period, a negative value means that NRELAP5 has a smaller period.

For DWO flow amplitude, a negative value means that NRELAP5 has a smaller amplitude.

For DWO onset, NRELAP5 base cases show reasonable-to-excellent agreement. The vast majority of cases were within 15 percent agreement, and most cases outside of 15 percent agreement were conservative.

For DWO flow period, NRELAP5 base cases show generally reasonable agreement. Some outliers are outside of 15 percent agreement.

For DWO flow amplitude, NRELAP5 base cases show generally reasonable agreement. While many cases were outside of 15 percent agreement, overall agreement is deemed reasonable because minimal or insufficient agreement for the majority of cases is due to NRELAP5 over-predictions, which are considered conservative and acceptable; this is consistent with the EM requirements in Section 3.2.

It is important to note an important difference between characterizing DWO onset versus characterizing DWO flow amplitude and DWO flow period. Within most tests, values tend to change based on the tube; they are not constant between the tubes within a row. Also, within most tests, values tend to change based on time; they are not constant throughout the test. Therefore, the values presented herein are largely simplified to give a high-level overview of DWO flow behavior.

Figure 8-42 Predicted Versus Measured Feedwater Flowrate at Density Wave Oscillation Onset for the Least-Stable Tube

{{

}}2(a),(c)

**Figure 8-43 Predicted Versus Measured Average Density Wave Oscillation Flow Period
for the Least-Stable Tube**

{{

}}2(a),(c)

Figure 8-44 Predicted Versus Measured Average Density Wave Oscillation Amplitude for the Least-Stable Tube

{{

}}^{2(a),(c)}

8.2.6 Summary and Conclusions from TF-2 Code-to-Data Comparisons

NRELAP5 simulations of TF-2 adiabatic and diabatic data show reasonable-to-excellent code-to-data agreement for primary-side pressure drop and heat transfer.

NRELAP5 simulations of TF-2 DWO data allow for assessment for DWO behavior. The primary FoM is the ability of NRELAP5 to predict DWO onset.

For DWO onset:

- The base model results predict Row 3 DWO onset with reasonable-to-excellent agreement.
- The base model results are generally slightly conservative, but were slightly non-conservative at the 95 percent confidence level.
- The biased model results determine a {{

}}^{2(a),(c)}

For DWO flow period and DWO flow amplitude:

- The base model results for DWO flow period show reasonable agreement.
- The base model results for DWO flow amplitude show minimal agreement overall, but are mostly conservative and considered acceptable per Section 3.2 EM requirements.

8.3 Assessment of POLIMI Data

This section provides a summary of the testing activities and subsequent code-to-data comparisons for the POLIMI data.

The test data presented in this section is from the POLIMI parallel HCSG tests. Because POLIMI data was not developed under NQA-1 2008/2009a, the data was qualified for use in this EM following the NuScale Procedure for the Qualification of Existing Data.

8.3.1 Test Description and Experimental Procedure

The POLIMI Parallel HCSG configuration included two electrically-heated HCSG tubes in parallel fed by a single FW line, as shown in Figure 8-45. Both coils were connected to a shared FW header and steam header.

{{

}}2(a),(c),ECI

Figure 8-45 Overview of POLIMI Parallel Helical Coil Steam Generator Configuration

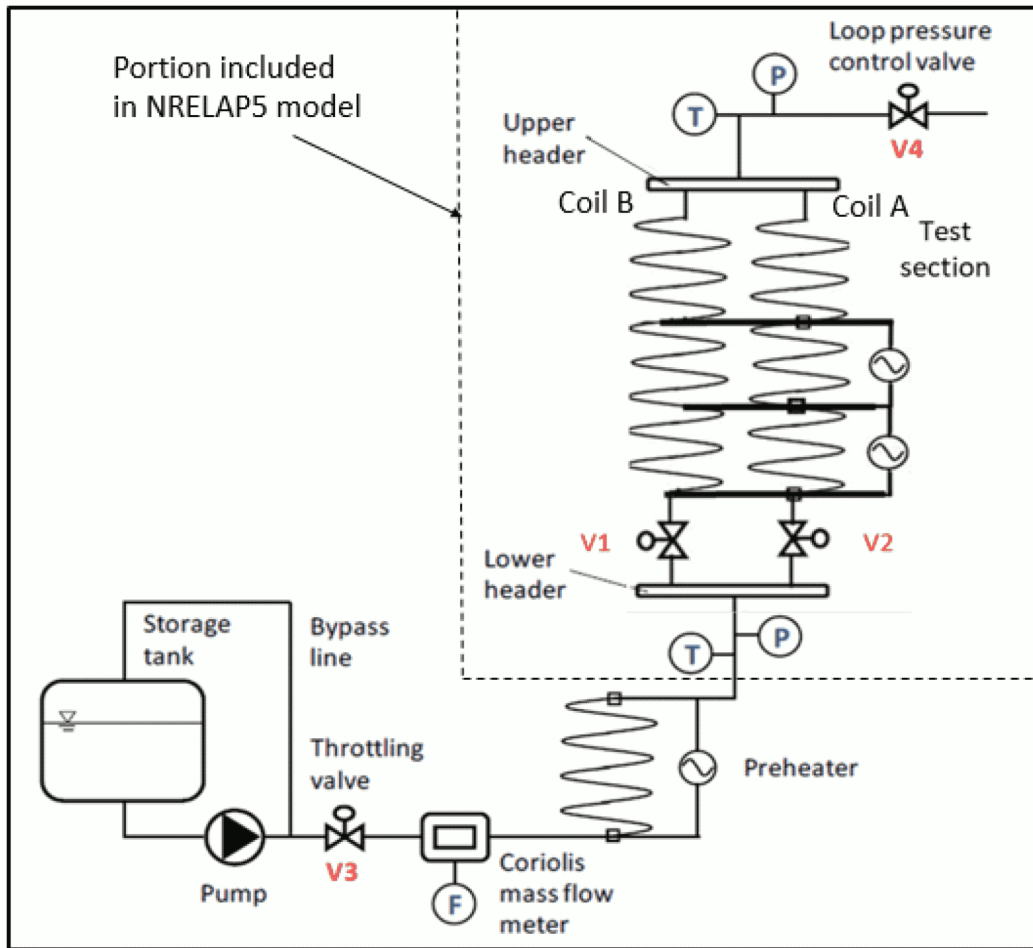
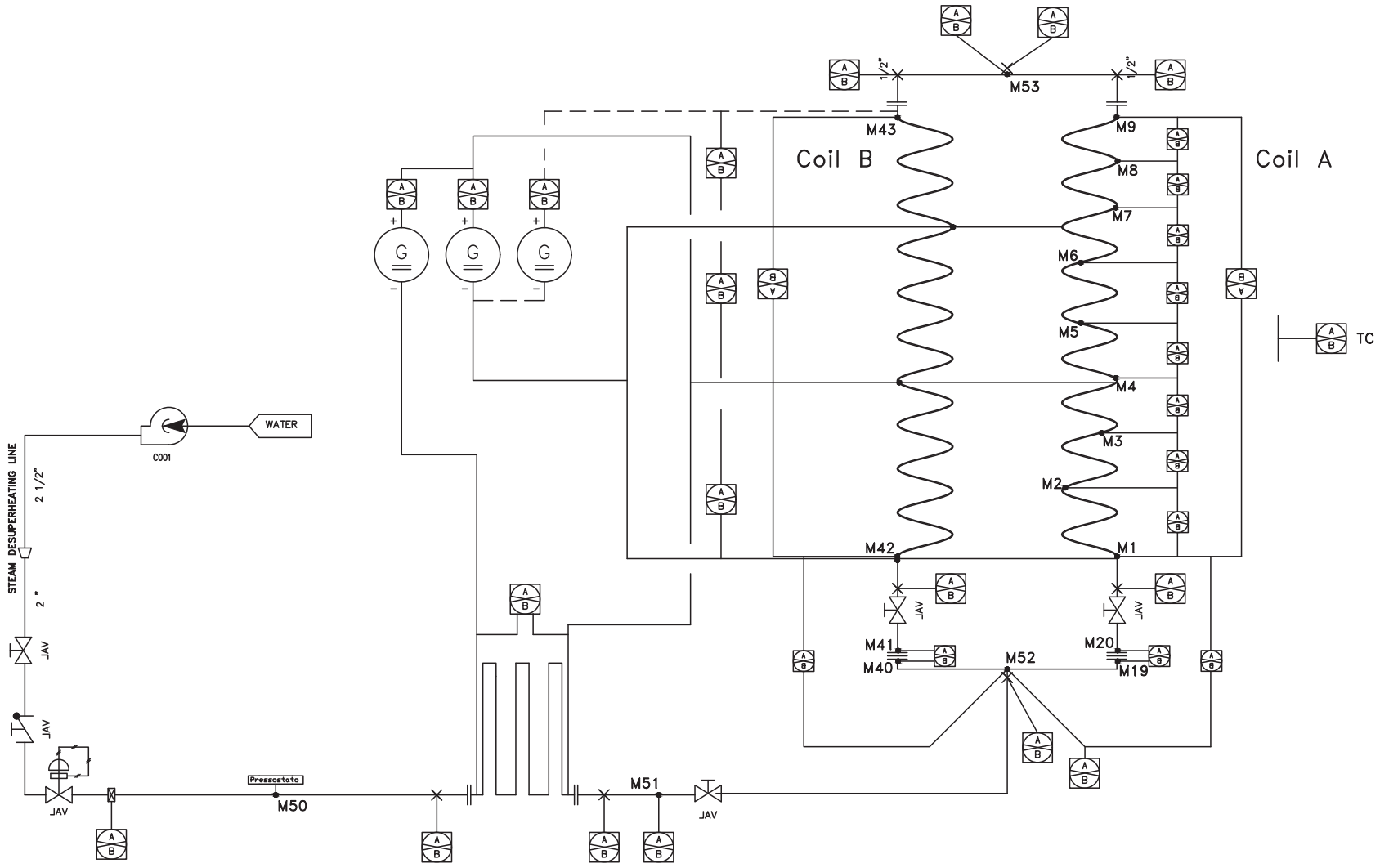


Figure 8-46 Schematic of POLIMI Test with Instrumentation Locations



8.3.2 Phenomena Addressed

Phenomena addressed by the POLIMI tests include single-phase and two-phase pressure drop, wall-to-secondary heat transfer (wall temperatures), and DWO onset.

8.3.3 NRELAP5 Modeling Techniques

Figure 8-47 shows the nodalization diagram for the NRELAP5 model. Connections are axial, and arrows entering/exiting from the sides of the box indicate a horizontal component, not use of crossflow.

{{

}}^{2(a),(c)}

Figure 8-47 POLIMI Parallel Helical Coil Steam Generator Facility NRELAP5 Model Nodalization Diagram

{{

}}2(a),(c)

8.3.4 POLIMI Code-to-Data Comparisons

The POLIMI testing was published in several PhD theses, along with some unpublished data, at the University of Milan. Therefore, the POLIMI DWO test conditions and HCSG tube geometry are not as close to NPM-20 values as TF-1 and TF-2, as illustrated in Figure 8-1 and tabulated in Table 8-1.

{{

}}2(a),(c)

From a total of 126 test runs, a set of 45 cases were selected for code-to-data comparison because they were deemed to be the most applicable to NPM-20 conditions.

8.3.5 POLIMI Base Model versus Cases Run with TF-1 Characteristics

The POLIMI test series evaluated herein has similarities to the TF-1 TO test series in both facility geometry (two parallel HCSG tubes) and in the test procedure (gradual power increases until DWO onset occurs). However, as discussed previously, the geometry of the POLIMI HCSG tubes are more tightly wound than those used in TF-1 testing, as shown by the d_i/D_{coil} ratio plotted in Figure 8-1. Tightly wound tubes result in greater centrifugal forces on the fluid, which may exceed the range of parameters upon which the two-phase pressure drop model was developed.

{{

}}2(a),(c)

Figure 8-48 plots the POLIMI Test 46 code-to-data comparison for differential pressure along the instrumented HCSG tube (Tube A). The first differential pressure, low in the tube where single-phase liquid is present, shows excellent agreement; however, higher up the tube in the two-phase region, a significant over-prediction of pressure drop by NRELAP5 is observed. This trend was observed for the vast majority of POLIMI NRELAP5 code-to-data comparisons. The NRELAP5 over-prediction of two-phase pressure drop is considered conservative for DWO onset predictions because a higher two-phase pressure drop is destabilizing for DWO onset.

Figure 8-48 POLIMI Test 46 Code to Data Differential Pressure Along the Tube Compared to NRELAP5

{{

}}^{2(a),(c)}

To study HCSG tube geometry impacts on NRELAP5 pressure drop predictions, POLIMI NRELAP5 cases were also run with TF-1 HCSG tube characteristics. NRELAP5 was run as a sensitivity using the TF-1 HCSG tube d_i and d_i/D_{coil} ratio, with results discussed below. These sensitivity cases were called TF-1 characteristics cases. Note that these changes also have an effect on heat transfer terms. The full set of POLIMI cases were run in NRELAP5 both with and without TF-1 HCSG tube characteristics.

Figure 8-49 shows the HCSG tube pressure drop ratio compared to HCSG tube pressure. The pressure drop ratio is the NRELAP5 total HCSG differential pressure divided by the data total HCSG differential pressure. A value greater than 1 is an under-prediction of pressure drop. For the base model, every test except one shows an under-prediction. For the model with TF-1 HCSG tube characteristics, the prediction is significantly improved with the mean differential pressure ratio decreasing from 1.44 to 1.09. The trend lines indicate increasing over-prediction with decreasing pressure, and the model with TF-1 coil characteristics matches the differential pressure data reasonably well for pressures greater than 3.0 MPa, with the trend line passing through 1.0 at 4 MPa.

Figure 8-49 POLIMI NRELAP5 Helical Coil Steam Generator Tube Pressure Drop Ratio Versus Pressure (Base Model and Model with TF-1 Characteristics)

{{

}}2(a),(c)

Figure 8-50 presents the HCSG tube DWO onset power ratio. The DWO onset power ratio is the NRELAP5 power at DWO onset divided by the data power at DWO onset. Therefore, values less than one mean that NRELAP5 predicted DWO onset at a lower power than the data, which is conservative. Both the base cases and TF-1 characteristics cases have power ratios less than 1 for most tests.

Figure 8-50 POLIMI NRELAP5 Density Wave Oscillation Onset Power Ratio Versus Pressure (Base Model and Model with TF-1 Coil Characteristics)

{{

}}2(a),(c)

Figure 8-51 and Figure 8-52 show the previously discussed pressure drop ratio and power ratio, but compared to the Tube A test-specific HCSG tube K_{inlet} values. Both ratios improve (move toward one) as K_{inlet} increases. This observation is noteworthy because the higher POLIMI K_{inlet} values are closer to TF-2 values and also to the expected NPM-20 K_{inlet} values (i.e., in the range at or above a K_{inlet} of {{ }}2(a),(c)).

**Figure 8-51 POLIMI NRELAP5 Helical Coil Steam Generator Tube Pressure Drop Ratio
Versus Tube A Inlet Loss Coefficient**

{{

}}2(a),(c)

Figure 8-52 POLIMI NRELAP5 Density Wave Oscillation Onset Power Ratio Versus Tube A Inlet Loss Coefficient

{{

}}^{2(a),(c)}

Taken together, these plots show that both pressure and K_{inlet} are significant parameters for ratios with higher pressures and K_{inlet} values greater than 100 giving improved code-to-data agreement. The trends show that for values that move towards the range of NPM-20 conditions (e.g., higher K_{inlet} and higher exit quality), improved code-to-data agreement occurs.

Tube inside wall temperature measurements are compared to calculations in Figure 8-53. Code-to-data comparisons are made at the five axial locations shown in the legend in meters along the tube from the tube inlet. Code-to-data agreement is reasonable-to-excellent, with most of the data predicted to within +/-10K. High code-to-data agreement indicates that wall heat transfer to the fluid is accurately modeled by NRELAP5.

Figure 8-53 POLIMI NRELAP5 Code-to-Data Comparison, Tube A Axial Wall Temperature

{{

}}^{2(a),(c)}**8.3.6 Summary and Conclusions from POLIMI Data to Code Comparisons**

For the POLIMI DWO tests and NRELAP5 predictions, agreement rankings of excellent, reasonable, minimal, and insufficient agreement are assigned. The different agreement levels for POLIMI are stated below. Note that the definition of excellent agreement herein is restructured compared to previous sections, and that these definitions are not necessarily applicable to code-to-data comparisons in other situations.

- excellent agreement: ratio within +/-5 percent
- reasonable agreement: ratio within +/-15 percent
- minimal agreement: ratio within +/-30 percent
- insufficient agreement: ratio greater than +/-30 percent

Each test run was assigned one of the above rankings. Overall, the agreement is described as follows.

- {{

}}2(a),(c)

The overall conclusions from the POLIMI DWO NRELAP5 simulations are:

- NRELAP5 substantially over-predicts pressure drop and under-predicts the power needed for DWO onset. NRELAP5 conservatively predicts DWO onset.
- Based on the runs of POLIMI with TF-1 helical coil characteristics, the NRELAP5 differential pressure over-prediction may be due to coil geometry being out of range of the specific correlations implemented in the HLCOIL logic of NRELAP5.
- Because the NRELAP5 predictions of DWO onset are generally conservative and are often very conservative when {{ }}2(a),(c), NRELAP5 may be used to conservatively determine the DWO stability boundary for HCSG tube systems.
- Prediction of wall temperatures is reasonable-to-excellent, indicating the wall to fluid heat transfer modeling is satisfactory.
- For parameters that move toward the range of NPM-20 conditions (e.g., higher K_{inlet} and higher exit quality), NRELAP5 shows better predictions, while poorer NRELAP5 predictions with considerable conservatism are associated with conditions that are quite different from NPM-20 conditions.

9.0 Assessment of Evaluation Model Adequacy

The adequacy of the NRELAP5 code for analysis of DWO in the NPM-20 is demonstrated by closure model and correlations reviews and assessments against relevant SET and IET experimental data.

9.1 Adequacy Demonstration Overview

The EM adequacy for DWO analysis of the NPM-20 is demonstrated with bottom-up and top-down evaluations performed with NRELAP5 for high ranked PIRT phenomena and NRELAP5 validation against relevant test data.

The adequacy of the DWO evaluation model is demonstrated through the following steps.

- Section 9.2 documents the bottom-up assessment of the NRELAP5 models and correlations to determine their adequacy to predict the high ranked phenomena. The code models used to represent each high ranked phenomena are identified with emphasis on the phenomena with low knowledge level. These assessments address the fidelity of the models and correlations to the appropriate fundamental or SET data. Fidelity of the assessments is evaluated using the criteria of excellent, reasonable, minimal, and insufficient. These criteria are defined in Table 1-2. The comparisons to SET data identify modeling deficiencies that could impose limitations on the application of the NRELAP5-based DWO evaluation model.
- Section 9.3 covers the top-down assessment of the EM, including a review of EM governing equations and numerical solution scheme to determine their applicability to NPM-20 DWO analysis and evaluation of the integral code performance based on the assessments of the EM against relevant IET data.

9.2 Evaluation Models and Correlations (Bottom-Up Assessment)

The adequacy of the models and correlations in NRELAP5 for modeling the high ranked phenomena per Section 4.2 are examined by considering their pedigree, applicability, and fidelity to appropriate fundamental or SET data (established by assessment of the EM against legacy and NPM-20-specific SET data), and scalability to the NPM-20 DWO scenario.

During the PIRT process there were no high ranked phenomena identified with knowledge level 1 (the lowest knowledge level).

 {{

}}2(a),(c)

The pedigree of the identified closure relations and correlations is based on their historical development and subsequent assessment in the literature. Section 8.0 describes comparisons of NRELAP5 to the three assessment tests (TF-1, TF-2, and POLIMI), which included both SETs for evaluation of the fundamental models (bottom-up evaluation), and IETs to validate the integral performance of the models working together to predict DWO onset and DWO flow behavior (top-down evaluation)

Assessment cases were identified to demonstrate the capability of NRELAP5 to predict the experimental data. The applicability of NRELAP5 to model the subject phenomena is established by demonstrating that the assessment cases cover the range of parameters that approximate the NPM-20 operating range and by evaluating how NRELAP5 compares with test data.

9.2.1 Evaluation of Models and Correlations (Bottom-Up Assessment)

Table 9-1 identifies the dominant code models or correlations for the PIRT high ranked phenomena. Key parameters that are influenced by the dominant models and correlations are listed, along with phenomenological and SETs that are used to assess the model or correlation capabilities. The absence of data for a phenomena

Table 9-1 NRELAP5 Models and Correlations Associated with High Ranked Phenomena Along with Relevant Assessment Test Data (Continued)

{{

}}^{2(a),(c)}

Table 8-2 provides a summary of the estimated range of key parameters that each test program covered and a comparison with NPM-20 operating conditions. Parameter ranges identify the minimum range that should be covered; the applicability of models and correlations are not restricted to these ranges. Ranges are provided for NPM-20 beginning of life conditions (best estimate).

9.2.2 Applicability Evaluation

To determine the adequacy of the models and correlations used to simulate the high-ranked phenomena, the results of assessments against phenomenological and SETs are discussed. The assessments results are drawn from the NRELAP5 assessment report for each experimental program.

9.2.2.1 Overview

A graded approach is used to address the bottom-up evaluation method. More emphasis is given to high ranked phenomena with a low knowledge level. Less emphasis is placed on phenomena that are well-understood with a high knowledge level, including well-accepted or engineering handbook models.

Each of the following four areas is evaluated to the extent that they are relevant for each high ranked phenomenon.

- **Background** of the model development is described, including pedigree and experimental data used in development of the model or correlation. Assumptions and limitations attributed to the model are identified.
- **Applicability Range** identifies the range covered by the model(s) and correlation(s) based on the initial development and subsequent assessments. The model's range is compared to the range of the NPM-20 application. The manner of addressing the limitations for the NPM-20 application is discussed.
- **Validation** of the model(s) and correlation(s) evaluates the fidelity of the models and correlations to appropriate fundamental or SET data. Results of the comparison to experimental data are summarized.
- **Scalability** evaluates whether there are scaling effects resulting from the development of the model, which would impose a limitation on the application of the model to full-plant geometries and operation conditions. The scalability evaluation is limited to whether the specific model or correlation is appropriate for application to the configuration and conditions of the plant and transient under evaluation.

9.2.2.2 High Ranked Phenomena

The PIRT identified some phenomena within specified components as high ranked phenomena. These high ranked phenomena are given the highest focus in the development of the DWO evaluation model.

The high ranked, low knowledge phenomena are addressed first, followed by the other high ranked phenomena listed in Table 9-1.

9.2.2.3 {{ }}^{2(a),(c)}

9.2.2.3.1 **Background**

{{

}}^{2(a),(c)}

9.2.2.4.2 Technical Evaluation

{{

}}2(a),(c)

Figure 9-1 {{

}}2(a),(c)

}}2(a),(c)

Figure 9-2 {{

}}2(a),(c)

}}2(a),(c)

Figure 9-3 {{

}}^{2(a),(c)}

{{

}}^{2(a),(c)}

Figure 9-4 {{

}}^{2(a),(c)}

{{

}}^{2(a),(c)}

Figure 9-5 {{ }}^{2(a),(c)}
{{

Figure 9-6 {{ }}^{2(a),(c)}
{{

}}^{2(a),(c)}

Figure 9-7 {{ }}^{2(a),(c)}
{{

Figure 9-8 {{ }}^{2(a),(c)}
{{

}}^{2(a),(c)}

Figure 9-9 {{

}}^{2(a),(c)}

{{

}}^{2(a),(c)}

Figure 9-10 {{

}}^{2(a),(c)}

{{

}}^{2(a),(c)}

Figure 9-11 {{ }}^{2(a),(c)}
{{

Figure 9-12 {{ }}^{2(a),(c)}
{{

Figure 9-13 {{

}}^{2(a),(c)}

{{

}}^{2(a),(c)}

Figure 9-14 {{

}}^{2(a),(c)}

{{

}}^{2(a),(c)}

Figure 9-15 {{ }}^{2(a),(c)}

{{

}}^{2(a),(c)}

These code-to-data comparisons conclude that:

- {{

}}^{2(a),(c)}

9.2.2.5 {{ }}^{2(a),(c)}

9.2.2.5.1 **Background**

{{

}}^{2(a),(c)}

{{

}}2(a),(c)

9.2.2.5.2 Technical Evaluation

{{

}}2(a),(c)

9.2.2.6 {{ }}2(a),(c)

9.2.2.6.1 **Background**

{{

}}2(a),(c)

9.2.2.6.2 **Technical Evaluation**

{{

}}2(a),(c)

Table 9-2 TF-1 Void Fraction Comparison

{{

}}2(a),(c)

Table 9-3 TF-2 Cases Used in Primary-Side Temperature Distribution Assessment

{{

}}^{2(a),(c)}

{{

}}^{2(a),(c)}

{{

}}2(a),(c)

}}2(a),(c)

}}2(a),(c)

Figure 9-16 {{

{{

{{

}}2(a),(c)

}}2(a),(c)

}}2(a),(c)

Figure 9-17 {{

{{

{{

}}2(a),(c)

}}2(a),(c)

}}2(a),(c)

Figure 9-18 {{

{{

Figure 9-19 {{
{{

}}2(a),(c)

{{

}}2(a),(c)

}}2(a),(c)

Table 9-4 Numerical Evaluation of the Transverse Temperature Profiles

}}

}}2(a),(c)

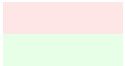


Figure 9-20 {{

}}^{2(a),(c)}

{{

}}^{2(a),(c)}

{{

}}^{2(a),(c)}

Figure 9-21 {{

}}^{2(a),(c)}

{{

}}^{2(a),(c)}

Figure 9-22 {{

}}^{2(a),(c)}

{{

}}^{2(a),(c)}

Figure 9-23 {{
{{

}}2(a),(c)

}}2(a),(c)

Figure 9-24 {{
{{

}}2(a),(c)

}}2(a),(c)

Figure 9-25 {{
{{

}}2(a),(c)

}}2(a),(c)

Figure 9-26 {{

}}2(a),(c)

{{

}}2(a),(c)

Figure 9-27 {{
{{

}}2(a),(c)

}}2(a),(c)

Figure 9-28 {{

}}2(a),(c)

{{

}}2(a),(c)

Figure 9-29 {{

}}2(a),(c)

{{

}}2(a),(c)

Figure 9-30 {{
}}2(a),(c)
{{

9.2.2.9 {{
}}2(a),(c)
9.2.2.9.1 **Background**
{{

}}2(a),(c)

9.2.2.9.2 Technical Evaluation

{{

}}2(a),(c)

9.2.2.10 {{

}}2(a),(c)

9.2.2.10.1 Background

{{

}}2(a),(c)

9.2.2.10.2 Technical Evaluation

{{

}}2(a),(c)

**Figure 9-31 Numerical Diffusion Evaluation in Helical Coil Steam Generator Tube
Single-Phase Liquid Region**

{{

}}2(a),(c)

{{

}}^{2(a),(c)}

Figure 9-32 Single-Phase Liquid Temperature Oscillation Numerical Damping Evaluation

{{

}}^{2(a),(c)}

{{

}}2(a),(c)

Figure 9-33 Single-Phase Liquid Temperature Oscillation Numerical Damping Evaluation

{{

}}2(a),(c)

Figure 9-34 Two-Phase Void Fraction Oscillation Numerical Damping Evaluation

{{

9.2.2.12 {{ }}^{2(a),(c)}

9.2.2.12.1 Background

{{

}}^{2(a),(c)}

}}^{2(a),(c)}

9.2.2.12.2 Technical Evaluation

{{

}}^{2(a),(c)}

9.2.2.13 {{

}}^{2(a),(c)}

9.2.2.13.1 Background

{{

}}^{2(a),(c)}

{{

}}^{2(a),(c)}

9.2.2.13.2 Technical Evaluation

{{

}}^{2(a),(c)}

Figure 9-35 NuScale Power Module Feedwater Plenum (Top) and Steam Plenum (Bottom)

{{

}}2(a),(c),ECI

9.2.2.15 {{

}}2(a),(c)

9.2.2.15.1 **Background**

{{

}}2(a),(c)

9.2.2.15.2 Technical Evaluation

{{

}}2(a),(c)

9.2.2.16 {{

}}2(a),(c)

9.2.2.16.1 Background

{{

}}2(a),(c)

9.2.2.16.2 Technical Evaluation

{{

}}2(a),(c)

Table 9-5 Summary of Bottom-Up Evaluation of NRELAP5 Models and Correlations

}}

}}2(a),(c)

Table 9-5 Summary of Bottom-Up Evaluation of NRELAP5 Models and Correlations (Continued)

}}

}}2(a),(c)

Table 9-5 Summary of Bottom-Up Evaluation of NRELAP5 Models and Correlations (Continued)

}}

}}2(a),(c)

Table 9-6 Applicability Summary for High Ranked Phenomena with Original Knowledge Level 2

}}

}}2(a),(c)

Table 9-6 Applicability Summary for High Ranked Phenomena with Original Knowledge Level 2 (Continued)

{{

}}2(a),(c)

9.3 Evaluation of Integral Performance (Top Down Evaluation Summary)

Integral or top-down performance is assessed by evaluating mathematical models for mass, momentum, and energy conservation; numerical solution techniques employed; and IET test predictions where integral system response is present.

- The code governing equations and numerical solutions are reviewed for their underlying assumptions and whether those assumptions are appropriate for the NPM-20 DWO analysis. The governing equations are appropriate to model DWO phenomena. The NRELAP5 numerical solution tends to be diffusive. However, appropriate nodalization and time-step control is shown to mitigate numerical diffusivity (Section 9.2.2 - {{ }}^{2(a),(c)}
- The integrated performance of NRELAP5 is assessed against IETs conducted at different test facilities. Three test programs provide data to evaluate NRELAP5 for NPM-20 DWO. The TF-1 and POLIMI are SETs that cover the range of high ranked phenomena, but they also provide integral response to a limited extent. TF-2 is an IET, which models the underlying high ranked phenomena, but due to the complex configuration and by design TF-2 cannot realistically include instrumentation for detailed measurements at all locations.
- A scaling analysis was performed to demonstrate the sufficiency of the TF-2 facility to represent the phenomena and processes that are important to DWO. Calculations are performed in the scaling analysis to evaluate differences and distortions between the TF-2 facility and the NPM-20 design and to establish the capability of NRELAP5 to scale-up the phenomena and processes to the full scale NPM-20.
- For the top-down evaluation of NRELAP5 for DWO, integral effects of the high ranked phenomena are evaluated based on the NRELAP5 applicability in predicting FoMs in the TF-2 facility such as DWO onset, DWO flow period, and DWO flow amplitude. Results of the adequacy evaluation based on the IETs are summarized in Table 9-9.

To ensure maximum fidelity of the assessments, the NRELAP5 DWO analysis models were developed using consistent nodalization and option selection.

Table 9-1 provides an overview of the phenomena present in the DWO tests discussed herein compared to the high ranked PIRT phenomena in Section 4.0.

Table 9-7 Assessment Test Data and Associated High-Ranked PIRT Phenomena

{{

}}^{2(a),(c)}

9.3.1 Review of Code Governing Equations and Numerics

The field equations solved by NRELAP5 are discussed in Section 2.1 of Reference 12.8. Herein, the applicability of the field equations to represent the processes and phenomena that can occur in the NPM-20 is evaluated, along with an assessment of the ability of the NRELAP5 numerical solution to approximate the set

of governing field equations. This evaluation addresses the mathematical models implemented in NRELAP5 for the NPM-20 DWO analysis and considers the applicability of the assumptions and processes involved in developing the NRELAP5 system of governing equations and related physical, thermodynamic, and transport property representations.

9.3.1.1 Conservation of Mass, Momentum, and Energy

The 1D equations and numerical solution scheme have been used in various versions of the RELAP5 codes for many years; their pedigree is well established by code assessments and applications. The semi-implicit solution technique used by NRELAP5 has been in the RELAP5 code as the primary solution technique for the governing conservation equations since the code's initial development. The solution technique continues to be used in NRELAP5 as discussed in Section 2.1.3 of the Reference 12.8.

The basic governing equations for mass, momentum, and energy conservation utilize a lumped parameter approach with two fields: a vapor field and a liquid field. Mass, momentum, and energy conservation equations are written for each phase, resulting in what is referred to as a six-equation model. A single pressure is assumed for both phases. Mass, energy, and momentum transfer between the two fields is modeled by various closure relations and correlations that depend on the physical and thermodynamic state of the phases. The interaction of each phase with the flow boundaries also depends on the physical and thermodynamic state of each phase and also on the relative amount of each phase described by the vapor (or void) fraction. The closure relations are defined for various flow regimes that are based on the flow structure. The flow regimes determine the appropriate closure relationships used to model heat transfer, interfacial drag, and flow losses.

The numeric solution evaluation considers conservation of physical properties, convergence, and stability of code calculations performed to solve the set of governing equations for an NRELAP5 NPM-20 model. The objective of this evaluation is to summarize information regarding the domain of applicability of the numerical techniques and user options that may impact the accuracy, stability, and convergence of NRELAP5 calculations. User guidelines for model development and execution were developed based on lessons learned during the code reviews and assessments. The guidelines include requirements for assuring convergence of solutions, accounting for uncertainty in results, and monitoring code function to assure that the basic conservation equations are being solved correctly.

As part of the CGD of RELAP5-3D[®] to serve as the development platform for NRELAP5, NuScale performed acceptance testing and receipt inspection as documented in a CGD dedication report. The testing and inspection verified that RELAP5-3D[®] has the necessary critical characteristics to be used as the code development platform for NRELAP5. The critical characteristics include the suitability of the basic governing equations described above for the NuScale

application. The review identified 12 limitations of RELAP5-3D[®] as the code development platform for NRELAP5 (Table 9-8). Limitations 2 and 10 are related to DWO and are discussed in Section 9.3.1.3. Some of the limitations derive from the numerical solution techniques used to discretize and solve the governing equations. These are discussed in Section 9.3.1.2.

9.3.1.2 Numerical Solution Techniques

The governing equations are discretized in time and space. The lumped parameter approach consists of dividing the T-H domain into a number of control volumes (also called mesh cells or nodes) that include the entire fluid domain of interest. The control volumes are connected by flow junctions.

The difference equations implement mass and energy conservation by equating accumulation to the rate of mass or energy inflow and outflow through the cell boundaries, minus the rate of mass or energy out through the cell boundaries, plus source terms such as heat input. This approach necessitates defining mass and energy volume average properties and requiring knowledge of velocities at the volume boundaries. The velocities at the cell edges are defined through the use of momentum control volumes centered on the mass and energy cell boundaries. This approach results in a numerical scheme having a staggered spatial mesh with the momentum control volumes extending from the mass and energy cell centers to the neighboring mass and energy cell centers. The scalar properties of the flow (pressure, specific internal energies, and void fraction) are defined at mass and energy cell boundaries.

The governing equations for the system model are solved numerically using a semi-implicit finite-difference technique. A nearly-implicit finite-difference technique, which allows violation of the material Courant limit, is also available. However, the DWO evaluation model and the supporting assessment calculations use only the semi-implicit numerical scheme. The semi-implicit numerical solution scheme is based on replacing the system of differential equations with a system of finite difference equations partially implicit in time.

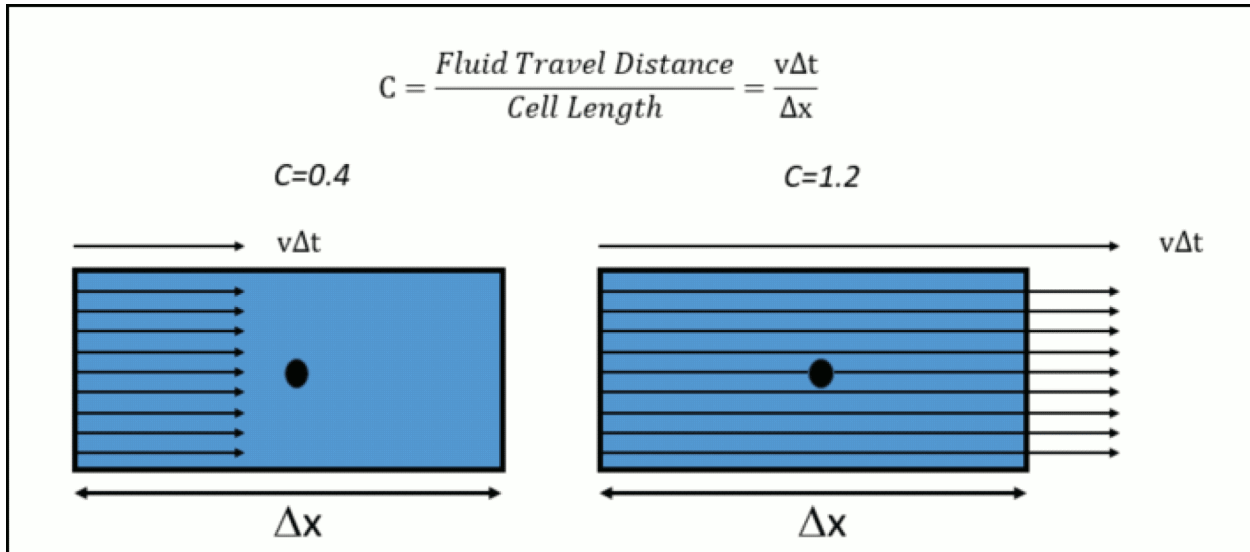
For HCSG tube propagation, the NRELAP5 semi-implicit solution scheme behaves like a classic explicit scheme and introduces numerical diffusion, which acts to damp inlet perturbations. The amount of numerical diffusion can vary considerably because it is dependent on the number of nodes used and the Courant number (C), which is the time-step size normalized to the transport time through a volume per Equation 9-1:

$$C = v\Delta t / \Delta x \quad \text{Equation 9-1}$$

Variable v is the velocity (m/s), Δt is the time step (s), and Δx is the node length (m). The physical meaning of C , illustrated in Figure 9-36, is the distance a fluid particle travels in a time step ($v\Delta t$), divided by the node length (Δx). It is desirable to keep the distance traveled less than the node length ($C=0.4$, as seen

on the left). If the distance traveled exceeds the node length ($C=1.2$, as seen on the right), information may not be correctly propagated from node to node.

Figure 9-36 Physical Meaning of the Courant Number



For the NRELAP5 semi-implicit scheme, the range of allowable values is $0 < C < 1$. In an NRELAP5 simulation, if the liquid velocity or gas velocity in a node causes C to be greater than one, the time-step is automatically reduced such that C is less than one. Note that in NRELAP5, the nodes use the same time-step. Often, NRELAP5 models with uniform nodalization have their time step controlled by the node with the highest velocity, so more coarse nodalization in high velocity regions is sometimes used to keep the time step from becoming very small, which has the effect of impacting the overall solution time.

When generating a solution of finite difference equations, there is a possibility that the solution may not converge. Lack of convergence could be the result of an ill-posed problem, inappropriate time-step size selection, inadequate spatial nodalization, or an instability. Sensitivity studies have proven useful to assure convergence and stability of the NRELAP5 solutions.

Adherence to the known modeling limitations and requirements of NRELAP5, discussed in the next section, assist in assuring that the governing equations are well-posed. Solutions are examined to identify unstable or unphysical behavior.

}}2(a),(c)

9.3.1.3 Limitations on Applicability for Density Wave Oscillation

Limitations of RELAP5-3D[®] for the NuScale loss of coolant accident applications were identified during the CGD and acceptance testing of RELAP5-3D[®] and in subsequent NRELAP5 code assessments. This report documents three limitations that impact DWO analysis, which are provided in Table 9-8.

Table 9-8 NRELAP5 Limitations and Improvement Needs Related to Density Wave Oscillation

Limitation or Needed Improvement	How Limitation Is Addressed	Baseline Acceptance Testing Section
Improve modeling of heat transfer in the HCSG tubes	Steady-state NPM-20 model TF-1	4.3 4.11
Improve CHF correlation to accurately simulate fluid and wall temperatures in the upper third of the steam generator coils	TF-1 Note (1)	4.11
Improve the two-phase pressure drop correlation needed to accurately simulate DWO in the HCSG	Literature data Note (2)	4.11

{{

}}^{2(a),(c)}

9.3.2 Evaluations of Density Wave Oscillation Tests

TF-1, TF-2, and POLIMI assessments for DWO characteristics are presented in Section 8.0. These assessments provide a comparison of geometrical parameters and conditions between the NPM-20 and different test programs. Geometrical distortions or deviations are also explained. Variations in test conditions and their impact on DWO behavior is evaluated.

Results from the adequacy evaluation based on TF-1, TF-2, and POLIMI are summarized in Table 9-9. Additional details are provided below for each assessment.

POLIMI

The purpose of the POLIMI code-to-data comparisons are to provide sufficient assurance that the NRELAP5 model is robust for DWO analysis that NRELAP5 can be used for other helical coil configurations than TF-1 or TF-2.

The POLIMI test data was primarily used to predict DWO onset. Data-wide comparisons to DWO flow period and DWO flow amplitude were not made because they were not the focus of the analysis. NRELAP5 is conservative in predicting DWO onset for POLIMI, indicating the code performed adequately for a non-NPM-20 HCSG system.

TF-1

NRELAP5 is conservative in predicting DWO onset for TF-1 with reasonable-to-excellent agreement.

NRELAP5 comparisons to DWO flow period and DWO flow amplitude are more varied, with the latter being most often conservative, which still meets the EM requirements for minimal agreement. TF-1 is an electrically-heated system and therefore DWO flow period and DWO flow amplitude are affected because energy addition is unbounded by the secondary-side conditions. This configuration makes predictions sensitive. For these parameters, code-to-data comparisons to systems with primary-to-secondary fluid heating like TF-2 are considered more applicable. Separate NRELAP5 models were developed for improved DWO flow period and DWO flow amplitude predictions and are not presented in this report.

TF-2

NRELAP5 provides reasonable-to-excellent agreement for DWO onset compared to TF-2 data. When conservative biases are applied, the NRELAP5 results are slightly non-conservative for DWO onset.

NRELAP5 provides reasonable agreement for DWO flow period and DWO flow amplitude compared to TF-2 data. NRELAP5 predictions of DWO flow amplitude are conservative (larger) and exceed the requirement of minimal agreement. It is noted that both DWO flow period and DWO flow amplitude are complex, and TF-2 data are not easily simplified to a single value. TF-2 tests continued varying ramped parameters like FW flow beyond DWO onset, which induces multiple frequencies and amplitudes. A different modeling scheme is required to better predict the range of DWO frequencies and amplitudes observed during each DWO test and is not presented in this report.

Table 9-9 Top-Down Assessment Summary for Integral Effects Test

Test Facility	Integral Effects Tests		
	DWO Onset	DWO Flow Period	DWO Flow Amplitude
POLIMI (DWO)	Conservatively predicted by NRELAP5; DWO onset predicted by NRELAP5 at lower power compared to data	Not compared	Not compared
TF-1 (DWO)	Reasonable-to-excellent agreement, conservative overall	Minimal-to-reasonable agreement	Minimal-to-reasonable agreement (mostly conservative)
TF-2 (DWO)	Reasonable-to-excellent agreement	Reasonable agreement	Reasonable agreement (conservative)

10.0 Uncertainty Evaluation and Margin for the NuScale Power Module with Respect to Density Wave Oscillation

This section describes the methodology for uncertainty quantification and margin evaluation applied to the NRELAP5 calculation of DWO onset for the NPM-20. The uncertainty methodology takes into account code input uncertainties stemming from a variety of sources (e.g., initial and boundary conditions, models and correlations), as well as output uncertainty associated with the code calculations. Code predictions of both SETs and IETs assess how well important phenomena and processes are predicted, and a global sensitivity analysis distills the important geometric and operating conditions to be modeled. Margin to DWO onset is calculated for the NPM-20 by evaluating DWO onset with biased inputs at varying nominal power levels.

For the NPM-20, a deterministic methodology is applied using a combination of conservative and realistic input data and boundary and initial conditions. Uncertainty is assessed using the methodology described as follows.

10.1 Sensitivity Analysis Methodology Development

{{

}}2(a),(c),ECI

{{

}}2(a),(c),ECI

Table 10-1 {{

}}2(a),(c),ECI

{{

}}2(a),(c),ECI

**Table 10-1 {{
}}^{2(a),(c),ECI} (Continued)**

{{

^{2(a),(c),ECI}

10.2 NRELAP5 Code Uncertainty

{{

}}^{2(a),(c)}

{{

}}2(a),(c)

$$\{$$

Equation 10-1

Equation 10-2

Equation 10-3

Equation 10-4

$\}^{2(a),(c)}$

{

Equation 10-5

Equation 10-6

}}^{2(a),(c)}

{

Equation 10-7

Equation 10-8

Equation 10-9

}}^{2(a),(c)}

4. {{

Equation 10-10

}}2(a),(c)

{{

}}2(a),(c)

Table 10-2 {{

}}2(a),(c)

{{

}}2(a),(c)

Table 10-2 {{

}}^{2(a),(c)} (Continued)

{{

}}^{2(a),(c)}

Table 10-2 {{

}}^{2(a),(c)} (Continued)

{{

}}^{2(a),(c)}

{{

}}^{2(a),(c)}

The error in NRELAP5 DWO onset prediction is calculated using Equation 10-11.

$$\varepsilon = \frac{NRELAP5 - Data}{Data} \quad \text{Equation 10-11}$$

Variable *NRELAP5* is the FW flow rate as predicted by NRELAP5 at DWO onset, and *Data* is the FW flow rate as measured by test facility at DWO onset.

Using the statistical methods described in previous key steps, NRELAP5 average error \bar{x} and standard deviation of mean \bar{u} are calculated. Assuming t-distribution and a 95 percent one-sided distribution and degrees of freedom of 35, the coverage factor is 1.69. The one-sided confidence interval value is calculated using Equation 10-12.

$$95\% \text{ CI}_t = \bar{x} - 1.69 \times \bar{u} \quad \text{Equation 10-12}$$

A 95 percent confidence interval method is used for evaluating the NRELAP5 DWO onset prediction uncertainty. A 95 percent confidence interval error estimate (Equation 10-12) indicates that there is a 95 percent probability that the NRELAP5 error in predicting the DWO onset phenomena is within the error span.

5. Overall NRELAP5 Density Wave Oscillation Prediction Uncertainty

{{

}}2(a),(c),ECI

{{

}}^{2(a),(c),ECI}

{{

}}^{2(a),(c)}

10.3 Other High Ranked Phenomena Identification and Ranking Table Phenomena Not Considered in the Uncertainty Evaluation

10.3.1 {{ }}^{2(a),(c)}

{{

}}^{2(a),(c)}

10.3.2 {{ }}^{2(a),(c),ECI}

{{

}}^{2(a),(c),ECI}

{{

}}2(a),(c),ECI

Table 10-3 {{

}}2(a),(c),ECI

{{

}}2(a),(c),ECI

{{

}}2(a),(c),ECI

10.3.3

{{

}}2(a),(c),ECI

{{

}}2(a),(c),ECI

Figure 10-1 {{

}}2(a),(c),ECI

{{

}}2(a),(c),ECI

{{

}}2(a),(c),ECI

Figure 10-2 {{

}}2(a),(c),ECI

{{

}}2(a),(c),ECI

{{

}}2(a),(c),ECI

{{

}}2(a),(c)

10.3.4 {{ }}^{2(a),(c)}

{{

}}^{2(a),(c)}

Figure 10-3 {{

}}^{2(a),(c),ECI}

{{

}}^{2(a),(c)}

{{

}}2(a),(c)

10.3.5

{{

}}2(a),(c)

{{

}}2(a),(c),ECI

10.3.6

{{

}}2(a),(c),ECI

{{

}}2(a),(c),ECI

{{

}}2(a),(c),ECI

Table 10-4 {{

}}2(a),(c),ECI

{{

}}2(a),(c),ECI

{{

}}2(a),(c),ECI

}}2(a),(c),ECI

}}2(a),(c),ECI

Figure 10-4 {{

{{

{{

}}2(a),(c),ECI

}}2(a),(c),ECI

}}2(a),(c),ECI

}}2(a),(c),ECI

}}

Figure 10-5 {{

}}

}}2(a),(c),ECI

}}2(a),(c),ECI

Figure 10-6 {{

{{

Figure 10-7 {{

}}2(a),(c),ECI

{{

}}2(a),(c),ECI

{{

}}2(a),(c),ECI

Figure 10-8 {{

}}2(a),(c),ECI

{{

}}2(a),(c),ECI

Figure 10-9 {{

}}2(a),(c),ECI

{{

}}2(a),(c),ECI

{{

}}2(a),(c),ECI

10.3.7 {{}}2(a),(c),ECI

{{

}}2(a),(c),ECI

10.3.8 {{}}2(a),(c),ECI

{{

}}2(a),(c),ECI

10.3.9 {{}}2(a),(c)

{{

}}2(a),(c)

10.4 Methodology for Density Wave Oscillation Analysis

{{

}}^{2(a),(c)}

Table 10-6 {{

}}^{2(a),(c)} **(Continued)**

{{

}}^{2(a),(c)}

10.4.1 {{

}}^{2(a),(c)}

{{

}}^{2(a),(c)}

{

Equation 10-13

Equation 10-14

}}^{2(a),(c)}

}}2(a),(c)

}}2(a),(c)

Figure 10-10 {{

{{

11.0 Results/Conclusions

This topical report presents the EM used to evaluate DWO in the NPM-20 during nominal and off-nominal operating conditions. Although not required, this DWO evaluation model is consistent with guidance provided in the EMDAP of “Transient and Accident Analysis Methods,” Regulatory Guide 1.203.

The DWO evaluation model uses the proprietary NRELAP5 code as the computational tool. NRELAP5 includes the necessary models for the characterization of the NPM-20 hydrodynamics, heat transfer between structures and fluids, modeling of fuel, reactor kinetics models, and control systems. Additional models and correlations are added to model the NPM-20 helical coil SG configuration.

Validation and verification of the EM and NRELAP5 code are conducted using a well-established process. A PIRT, which identifies the important phenomena and processes for HCSG stability, is developed. A total of 17 phenomena are identified as high ranked and thus important to capture in the DWO evaluation model.

Extensive NRELAP5 code validation is performed to ensure that the EM is applicable for the important phenomena and processes over the range encountered in NPM-20 operation. The validation suite includes SETs and IETs developed and run specifically for the NPM-20 SG application. The FoM for the DWO evaluation model is DWO onset.

The SETs were performed at the TF-1 facility. TF-1 provided data on pressure drop and heat transfer for the secondary side. TF-1 also provided DWO test data with DWO onset, DWO flow period, and DWO flow amplitude. Both SETs and IETs were performed at the TF-2 facility. TF-2 SETs provided data on primary-side heat transfer and pressure drop. TF-2 also provided DWO test data with DWO onset, DWO flow period, and DWO flow amplitude. Additional validation of NRELAP5 is carried out with an external DWO database obtained from POLIMI. The POLIMI DWO test data validation shows that NRELAP5 is conservative in predicting DWO onset for a non-prototypical HCSGs with longer tubes and a tighter helix.

The NRELAP5-based DWO evaluation model is evaluated for applicability to analyze DWO in the NPM-20. The applicability of NRELAP5 for high ranked phenomena is demonstrated by comparing NRELAP5 predictions to data from SETs and IETs. Reasonable-to-excellent agreement obtained via comparison establishes the applicability of NRELAP5 to accurately predict DWO onset phenomena at both the SETs and IETs.

Uncertainty analysis is carried out based on TF-1 SET data and on TF-2 DWO integral effects test data. Using a 95 percent confidence interval, the {{

}}^{2(a),(c)}, respectively. When highly conservative biasing parameter uncertainty is applied to TF-2 DWO NRELAP5 models, the NRELAP5 uncertainty for predicting DWO onset is {{

}}^{2(a),(c)}

This report also contains the methodology for evaluating margin to DWO onset in the NPM-20 at normal and off-normal operating conditions and is applied for NPM-20 nominal reactor power levels between 20 percent and 100 percent. The sample calculations in Appendix B demonstrate application of the DWO evaluation model in an NPM-20 NRELAP5 model configured to predict DWO onset following the DWO evaluation model. The sample results show that DWO onset does not occur in the NPM-20 helical coil SG at the nominal or off-nominal, steady-state 100 percent power level if the minimum IFR K_{inlet} value is $\{ \{ \} \}^{2(a),(c)}$. Results are conservatively biased for code uncertainty. Margin to DWO onset is demonstrated at nominal and off-nominal 100 percent power conditions.

The EM developed herein has an established pedigree and is determined to be adequate for downstream NPM-20 analysis for DWO onset.

12.0 References

- 12.1 U.S. Nuclear Regulatory Commission, "Transient and Accident Analysis Methods," Regulatory Guide 1.203, December 2005.
- 12.2 Boyack, B.E. and G.E. Wilson, "Lessons Learned in Obtaining Efficient and Sufficient Applications of the PIRT Process," Best Estimates 2004, Washington DC, November 14-18, 2004.
- 12.3 Convective Boiling and Condensation, 3rd Edition, JG Collier and J.R. Thome, Clarendon Press - Oxford, 1994.
- 12.4 U.S. Nuclear Regulatory Commission, "An Integrated Structure and Scaling Methodology for Severe Accident Technical Issue Resolution," Draft Report for Comment. Appendix D, NUREG/CR-5809, November 1991.
- 12.5 Zuber, N., The effects of complexity, of simplicity, and of scaling in thermal-hydraulics," *Nuclear Engineering and Design*, 204 (1-3), Number 1: pp. 1-27, 2001.
- 12.6 Zuber, N., U.S. Rohatgi, W. Wulff, and I. Catton, Application of fractional scaling analysis (FSA) to loss of coolant accidents (LOCA) Methodology development," *Nuclear Engineering and Design*, 237:1593-1607, 2007.
- 12.7 Catton, I., W. Wulff, N. Zuber, and U. Rohatgi, "Application of Fractional Scaling Analysis to Loss of Coolant Accidents: Component Level Scaling for Peak Clad Temperature," *ASME Journal of Fluids Engineering*, 131 (12) pp. 1-8, 2009.
- 12.8 SwUM-0304-17023, Rev. 10, NRELAP5 Version 1.6 Theory Manual.
- 12.9 MN-122626, Rev. 0, NuScale Topical Report: Quality Assurance Program Description for the NuScale Power Plant.
- 12.10 U.S. Code of Federal Regulations, "Domestic Licensing of Production and Utilization Facilities," Part 50, Title 10, Appendix B, "Quality Assurance Criteria for Nuclear Power Plants and Fuel Reprocessing Plants", (10 CFR 50 Appendix B).
- 12.11 American Society of Mechanical Engineers, *Quality Assurance Program Requirements*
- 12.12 Y. Taitel and A. E. Dukler, "A Model of Predicting Flow Regime Transitions in Horizontal and Near Horizontal Gas-Liquid Flow", *AIChE Journal*, 22, 1976, pp. 47-55
- 12.13 Y. Taitel, D. Bornea, and A. E. Dukler, "Modeling Flow Pattern Transitions for Steady Upward Gas-Liquid Flow in Vertical Tubes", *AIChE Journal*, 26, 1980, pp. 345-354

-
- 12.14 M. Ishii and G. De Jarlais, "Inverted Annular Flow Modeling", Advanced Code Review Group Meeting, Idaho Falls, ID, July 27, 1982
- 12.15 M. Ishii and T. C. Chawla, "Local Drag Laws in Dispersed Two-Phase Flow", NUREG/CR-1230, ANL-79-105, Argonne National Laboratory, December 1979
- 12.16 M. Ishii and K. Mishima, "Study of Two-Fluid Model and Interfacial Area", NUREG/CR-1873, ANL-80-111, Argonne National Laboratory, December 1980
- 12.17 T. N. Tandon, H. K. Varma, and C. P. Gupta, "A New Flow Regime Map for Condensation Inside Horizontal Tubes", Journal of Heat Transfer, 104, November 1982, pp. 763-768.
- 12.18 R. W. Lockhart and R. C. Martinelli, "Proposed Correlations of Data for Isothermal Two-Phase, Two-Component Flow in Pipes", Chemical Engineering Progress, 45, 1, 1949, pp. 39-48
- 12.19 D. J. Zigrang and N. D. Sylvester, "A Review of Explicit Friction Factor Equations", Transactions of the ASME, Journal of Energy Resources Technology, 107, 1985, pp. 280-283
- 12.20 C. F. Colebrook, "Turbulent Flow in Pipes with Particular Reference to the Transition Region between Smooth and Rough Pipe Laws", Journal of Institute of Civil Engineers, 11, 1939, pp. 133-156
- 12.21 Chen, J.C., "A Correlation for Boiling Heat Transfer to Saturated Fluids in Convective Flow," Process Design and Development, (1966), 5:322-327.
- 12.22 Crank, J., and P. Nicolson, "A Practical Method for Numerical Evaluation of Solutions of Partial Differential Equations of the Heat Conduction Type," Proceedings of the Cambridge Philosophical Society, (1947): 43:50-67.
- 12.23 J. K. Vennard, "One-Dimensional Flow", in: V. L. Streeter (ed.), Handbook of Fluid Dynamics, 1st Edition, New York: McGraw Hill, 1961
- 12.24 Ito, H., "Friction factors for turbulent flow in curved pipes," Transactions of the ASME, Journal of Basic Engineering, (1959): 81:123-124.
- 12.25 Sreenivasan K.R., and P.J. Strykowski, "Stabilization Effects in Flow Through Helically Coiled Pipes," Experiments in Fluids 1, 1983, pp. 31-36.
- 12.26 Prasad, B.V.S.S.S, D.H. Das, and A.K. Prabhakar, "Pressure drop, heat transfer and performance of a helically coiled tubular exchanger," Heat Recovery Systems and CHP, (1989), 9: 249-256.
- 12.27 Dittus, F.W., and L.M.K. Boelter, "Heat transfer in automobile radiators of the tubular type," International Communications in Heat and Mass Transfer, (1985),

- Vol 12, Issue 1, pp. 3-22. Originally published in University of California Publications in Engineering, Vol. 2, No. 13, October 13, 1930, pp. 443-46.
- 12.28 Green, D.W. and Perry, R.H., *Perry's Chemical Engineers' Handbook*, 8th Edition, McGraw-Hill, New York, NY, 2008.
- 12.29 J. C. Chen, "A Correlation for Boiling Heat Transfer to Saturated Fluids in Convective Flow", *Process Design and Development*, 5, 1966, pp. 322-327
- 12.30 Seban, R.A., and E.F. McLaughlin, "Heat transfer in tube coils with laminar and turbulent flow," *International Journal of Heat and Mass Transfer*, (1963): 6:387-395.
- 12.31 Donaldson, A.J., "Once-through steam generator heat transfer models for SIR," *Dynamics and control in nuclear power stations*, Thomas Telford, London, (1991).
- 12.32 Yang, S.H., et al., "Experimental validation of the helical steam generator model in the TASS/SMR code," *Annals of Nuclear Energy*, Volume 35, Issue 1, pp. 49-59, (2008).
- 12.33 Saha, P. and Zuber, N. (1974). Point of net vapor generation and vapor void fraction in subcooled boiling, *Proceedings of the 5th international heat transfer conference*, Tokyo, Paper B4.7.
- 12.34 The RELAP5-3D[®] Code Development Team, "RELAP5-3D[®] Code Manual, Volume IV: Models and Correlations, INEEL-EXT-98-00834, Revision 4.1, September 2013.
- 12.35 R. T. Lahey, "A Mechanistic Subcooled Boiling Model," *Proceedings of the 6th International Heat Transfer Conference*, Toronto, Canada, August 7-11, 1978, Volume 1, pp. 293-297
- 12.36 Levy, S. (1967). "Forced convection subcooled boiling prediction of vapor volumetric fraction". *Int. J. Heat Mass Transfer*, 10, pp 951-965.
- 12.37 Neil Todreas and Mujid Kazimi, *Nuclear Systems Volume 1*, 3rd edition, CRC Press (2021).
- 12.38 Lee, S. C., Dorra, H., and Bankoff, S. G. (1992). 'A critical review of predictive models for the onset of significant void in forced convection subcooled boiling'. Presented in *Fundamentals of Subcooled Flow Boiling HTD-Vol. 2* 17, pp. 33-39. Paper presented at ASME Winter Ann. Mtg, Anaheim, CA.
- 12.39 Ishii, M., "Thermally Induced Flow Instabilities in Two-Phase Mixtures in Thermal Equilibrium", Georgia Institute of Technology 1971.

-
- 12.40 The RELAP5-3D[®] Code Development Team, “RELAP5-3D[®] Code Manual, Volume I: Code Structure, System Models and Solution Methods”, INEEL-EXT-98-00834, Revision 4.1, September 2013.
 - 12.41 Handbook of Hydraulic Resistance, 3rd Edition, I.E. Idelchik, 1994.
 - 12.42 Szilard, R.H., et. al., “Industrial Application Emergency Core Cooling System Cladding Acceptance Criteria Problem Statement”, INL/EXT-35073.
 - 12.43 M. Colombo, A. Cammi, D. Papini, and M. E. Ricotti, “RELAP5/MOD3.3 study on density wave instabilities in single channel and two parallel channels,” Progress in Nuclear Energy, vol. 56, pp. 15-23, 2012.
 - 12.44 Colombo, M., “Experimental Investigation and Numerical Simulation of the Two-Phase Flow in the Helical Coil Steam Generator,” Ph.D. thesis, Doctoral program in “Energy and Nuclear Science and Technology”, Politecnico di Milano, (2013).
 - 12.45 Santini, L., et al., “Two-phase pressure drops in a helically coiled steam generator,” International Journal of Heat and Mass Transfer 51, pp. 4926-4939, (2008).
 - 12.46 Zhao, L., et al., “Convective boiling heat transfer and two-phase flow characteristics inside a small horizontal helically coiled tubing once-through steam generator” International Journal of Heat and Mass Transfer, Vol. 46, Issue 25, pp. 4779-4788.
 - 12.47 Taylor B.N. and Kuyatt, C.E., “Guidelines for Evaluating and Expressing the Uncertainty of NIST Measurement Results”, NIST Technical Note 1297 1994 Edition.
 - 12.48 Mann P. S. and Lacke, C.J., Introductory Statistics”, 7th Edition, John Wiley and Sons, 2010.

Appendix A Evaluation Model Development and Assessment Process and Roadmap to the Density Wave Oscillation Evaluation Model

The RG 1.203 defines four elements for the EMDAP process (Reference 12.1). These elements are divided into 20 different steps used to create an EM. Figure A-1 shows various elements of the EMDAP as defined in RG 1.203. Table A-1 provides a roadmap that relates the sections of this report to the elements of the EMDAP. The EMDAP described by RG 1.203 provides a structured approach, which is widely used in the industry, that guides the development of this EM.

Figure A-1 Evaluation Model Development and Assessment Process

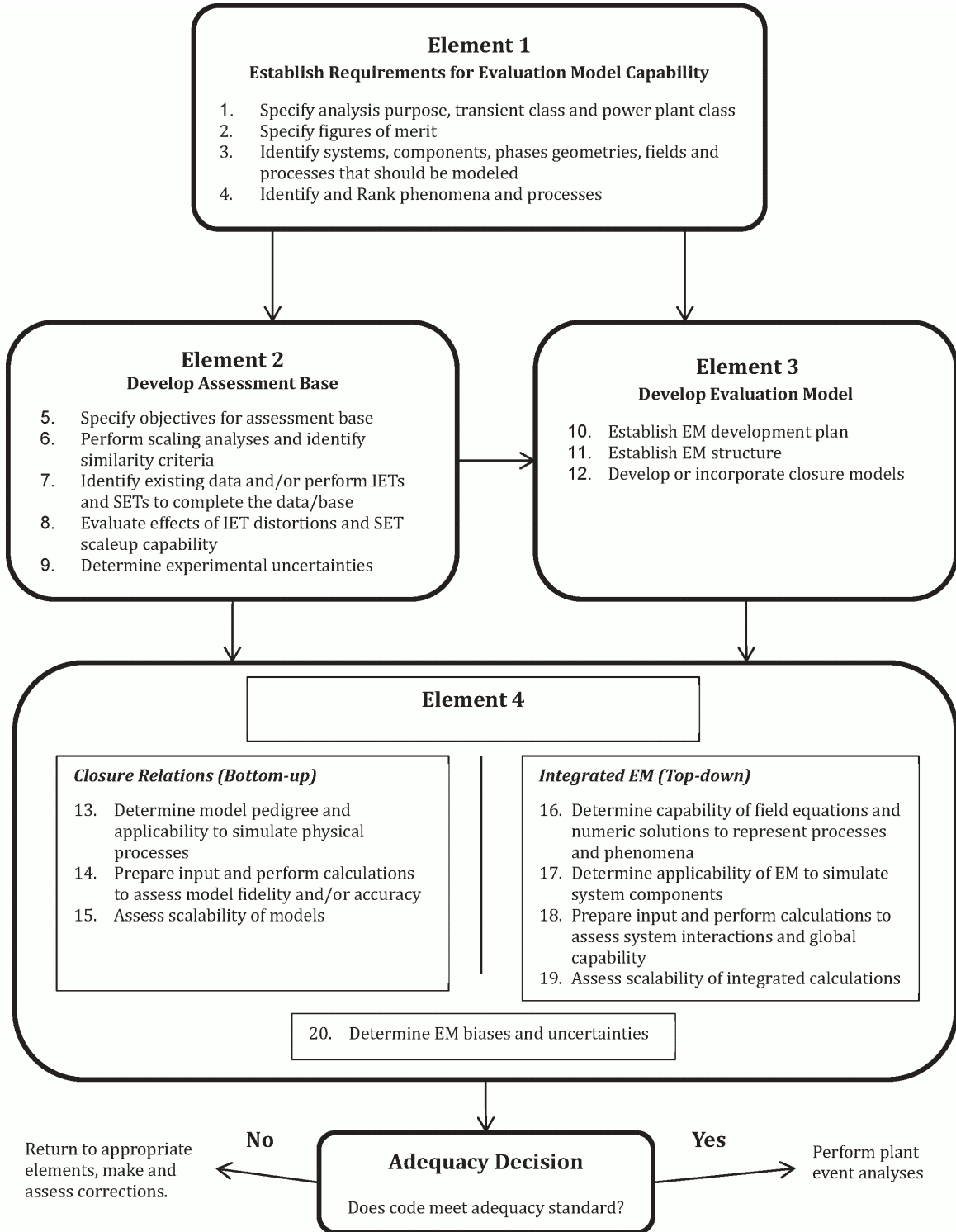


Table A-1 Evaluation Model Development and Assessment Process Steps and Associated Document Sections

EMDAP Element	Description	Section
Element 1	Establish requirements for EM Capability	1.2 and 3.2
Element 2	Develop assessment base	4.0 and 8.0
Element 3	Develop EM	7.0
Element 4A	Assess EM adequacy closure relations (bottom-up)	9.2
Element 4B	Assess EM adequacy integrated EM (top-down)	9.3

Appendix B Sample Calculation for NuScale Power Module

B.1 NuScale Power Module Density Wave Oscillation Onset Calculations

The sample calculations of the implemented EM are provided for illustrative purposes to:

- demonstrate that the NPM-20 DWO model, created in accordance with EM specifications, models DWO onset consistently in multiple configurations,
- show that the NPM-20 DWO model, coupled with an IFR K_{inlet} designed to prevent DWO, predicts stability at 100 percent nominal power conditions and calculates the margin to expected setpoints when accounting for code uncertainty,
- illustrate that the NPM-20 DWO model is not subject to DWO at off-nominal 100 percent power conditions, with margin to expected setpoints when accounting for uncertainty and operational deviations.

B.2 Density Wave Oscillation Model Nodalization and Development

A bulk FW flow-controlled boundary condition NRELAP5 model similar to Figure 7-4 is created to match the NPM-20 helical coil SG geometry and characteristics.

B.2.1 Percent Nominal Power Equilibrium Profile

Equilibrium quality (X_{eq}) profiles from SG-averaged and column-averaged steady-state models are extracted and evaluated to determine the DWO model nodalization required to evaluate stability at 100 percent nominal power. The model nodalization is fixed during the DWO onset evaluation, yet the optimum nodalization sizing is related to the quality profile as discussed in Section 7.8.2.3. Quality profiles are evaluated against HCSG tube length.

First, the equilibrium profiles for all column-averaged and total SG-averaged tubes are plotted versus tube length along the helical axis. Figure B-1 shows an overall plot of equilibrium quality and tube length, and Figure B-2 shows a detailed view of the 55 feet to 70 feet in length. {{

}}^{2(a),(c)}

Generally, as power decreases, changes in NPM-20 conditions (e.g., pressures, temperatures, flow) cause the length of the subcooled liquid and two-phase regions to decrease while the single-phase steam region of the HCSG tube increases.

Comparing the nature of these shifts, a model is developed that provides a similar width of variation in the two-phase region. The model encompasses the equilibrium quality profiles between 70 percent and 100 percent nominal power, while other models with other nodalizations are developed to evaluate other powers. {{

}}^{2(a),(c)}

{{

}}^{2(a),(c)}

Figure B-1 100 Percent Nominal Power, Equilibrium Quality Versus Helical Coil Steam Generator Tube Length

{{

}}^{2(a),(c)}

**Figure B-2 100 Percent Nominal Power, Equilibrium Quality Versus Helical Coil Steam
Generator Tube Length, Detailed View**

{{

}}^{2(a),(c)}

**Figure B-3 Density Wave Oscillation Model 1, For Evaluations from 70 Percent to 100
Percent Nominal Power**

{{

}}^{2(a),(c)}

B.2.2 NRELAP5 Model Development

The development of the NRELAP5 DWO model is performed in conjunction with the methodology presented in Section 7.0. The DWO model features {{

}}^{2(a),(c)}

Figure B-4 shows a representation of the primary fluid in the NRELAP5 DWO model. Figure B-5 shows a representation of the secondary-side fluid portion. A brief description illustrates the numbering scheme of the hydraulic components and heat structures:

{{

}}^{2(a),(c)}

{{

}}^{2(a),(c)}

{{

}}^{2(a),(c)}

Figure B-4 Representation of the Primary Side of the NRELAP5 Density Wave Oscillation Model

{{

}}^{2(a),(c)}

Figure B-5 Representation of the Secondary Side of the NRELAP5 Density Wave Oscillation Model

{{

}}^{2(a),(c)}

B.4 Inlet Flow Restrictor Loss Coefficient Selection

The IFR is a restricting orifice designed to induce a large pressure drop as the subcooled fluid enters the HCSG tube from the FW plenum. If the IFR pressure drop is sufficiently sized, DWO is prevented and secondary-side stability is maintained. The K_{inlet} of the IFR is a crucial component of secondary-side stability.

The NPM-20 IFR is a thick orifice, with a {{

}}^{2(a),(c),ECI}

Figure B-6 {{

}}^{2(a),(c)}

{{

}}^{2(a),(c)}

Figure B-7 {{

}}^{2(a),(c)}

{{

}}^{2(a),(c)}

B.5 Density Wave Oscillation Number of Channels Comparison

The NRELAP5 DWO model is developed according to the EM features of {{

}}^{2(a),(c)}

{{

}}^{2(a),(c)}

Figure B-8 {{

}}^{2(a),(c)}

{{

}}^{2(a),(c)}

Figure B-9 {{

}}^{2(a),(c)}

{{

}}^{2(a),(c)}

 {{

 }}^{2(a),(c)}

Margin is calculated using Equation B-1.

$$\text{Margin} = 1 - \frac{\dot{m}_{onset}}{m_{action}} \quad \text{Equation B-1}$$

The variable \dot{m}_{onset} (lb_m/s) is the FW mass flow rate at the time of DWO onset, accounting for code uncertainty.

The variable m_{action} (lb_m/s) is the FW mass flow rate at the time of operator action or nominal trip setpoint.

B.7 Stability Evaluations at 100 Percent Nominal Power Conditions

The following calculation demonstrates the stability of the NPM-20 helical coil SG to DWO at nominal conditions for 100 percent nominal power. The evaluations initiate from BCs correlated to the nominal, best-estimate, beginning-of-life steady-state conditions. The IFR K_{inlet} corresponds to the minimum K_{inlet} discussed in Section B.4. {{

 }}^{2(a),(c)}

Density wave oscillation onset in single average-tube channels is identified using the methodology presented in Section 7.4.2. Least-stable columns and significant margin to DWO are defined according to Section 7.4.4. Code uncertainty is accounted for as an adjustment of the FW mass flow rate corresponding to DWO onset, as described in Section 10.2. Margin to DWO onset is defined through comparison of the FW mass flow rates corresponding to DWO onset including code uncertainty, and FW mass flow rates that are expected to form conservative bounds for NPM-20 operation.

The NPM-20 DWO model is used to evaluate the 100 percent nominal power condition by applying the BCs described in Section B.3. {{

}}^{2(a),(c)}

Geometrical differences between the 21 column-averaged tubes in the NPM-20 DWO model result in small differences in mass flow rates per column at all steady-state flow conditions. Total FW flow ramping results in symmetrical changes to columnar mass flows that are proportional to the original mass flow distribution.

{{

}}^{2(a),(c)} The DWO onset times for the SG tubes at the 100 percent nominal power condition are shown in Table B-3.

The earliest DWO onset occurs at {{

}}^{2(a),(c)} Figure B-10 illustrates a zoomed-in view of DWO onset, as determined per Section 7.4.2. The red line in the figure, which represents the relative error of a 100-second moving average, exceeds 20 percent at the vertical green line, indicating DWO onset. The first ten peaks of DWO following onset are shown in Figure B-11.

Figure B-12 shows several differential pressure calculations for Tube one. These include the total pressure drop from the center of the FW plenum to the center of the first tube cell (representing the IFR pressure drop, friction head, and static head between the two cells), the pressure drop through the single-phase liquid region (fixed by the model nodalization), and the differential pressure of the two-phase region (fixed by the model nodalization). Because the single-phase liquid and two-phase region entries are fixed by the model nodalization to define the initial region lengths, they may include other regions as FW flow is ramped (i.e., single-phase steam as the two-phase region moves lower in the tube), but they remain representative of proportional tube pressure drop terms.

Accounting for the NRELAP5 code uncertainty as described in Section 10.2, {{
}}^{2(a),(c)}

Figure B-13 shows two equilibrium quality profiles: one at the initial nominal FW flow rate for the 100 percent nominal power condition, and the second 2000 seconds before the code-calculated DWO onset. The difference between these quality profiles reflects the approximate change in tube conditions prior to DWO onset.

{{

}}^{2(a),(c)}

Figure B-10 {{

}}^{2(a),(c)}

{{

}}^{2(a),(c)}

Figure B-11 {{

}}^{2(a),(c)}

{{

}}^{2(a),(c)}

Figure B-12 {{

}}^{2(a),(c)}

{{

}}^{2(a),(c)}

Figure B-13 {{

}}^{2(a),(c)}

{{

}}^{2(a),(c)}

{{

}}^{2(a),(c)}

{{

}}^{2(a),(c)}

Table B-6 details the DWO onset times and margins for the SG tubes for Case 11. Accounting for the NRELAP5 code uncertainty as described in Section B.6, {{

}}^{2(a),(c)}

Table B-4 NuScale Power Module 100 Percent Nominal Power Off-Nominal Assumed Control Action and Trip Times

{{

}}^{2(a),(c)}

Table B-6 {{

}}^{2(a),(c)}

{{

}}^{2(a),(c)}

B.9 Results and Conclusions

The NPM-20 helical coil SG is stable with respect to secondary-side instabilities at the nominal, steady-state 100 percent power level if the minimum IFR K_{loss} value is

{{ }}^{2(a),(c)} Results are conservatively biased by including a one-side bias code uncertainty value of {{ }}^{2(a),(c)}

Margin to DWO onset is demonstrated at all nominal power levels and at off-nominal 100 percent power conditions that are reasonably expected to be bounded by the final control system design and nominal trip setpoints. Minimum margins at nominal and off-nominal conditions are summarized in Table B-7.

Table B-7 Summary of Margin to Density Wave Oscillation Onset

{{

}}^{2(a),(c)}

Enclosure 3:

Affidavit of Mark W. Shaver. AF-142066

NuScale Power, LLC

AFFIDAVIT of Mark W. Shaver

I, Mark W. Shaver, state as follows:

- (1) I am the Director of Regulatory Affairs of NuScale Power, LLC (NuScale), and as such, I have been specifically delegated the function of reviewing the information described in this Affidavit that NuScale seeks to have withheld from public disclosure, and am authorized to apply for its withholding on behalf of NuScale
- (2) I am knowledgeable of the criteria and procedures used by NuScale in designating information as a trade secret, privileged, or as confidential commercial or financial information. This request to withhold information from public disclosure is driven by one or more of the following:
 - (a) The information requested to be withheld reveals distinguishing aspects of a process (or component, structure, tool, method, etc.) whose use by NuScale competitors, without a license from NuScale, would constitute a competitive economic disadvantage to NuScale.
 - (b) The information requested to be withheld consists of supporting data, including test data, relative to a process (or component, structure, tool, method, etc.), and the application of the data secures a competitive economic advantage, as described more fully in paragraph 3 of this Affidavit.
 - (c) Use by a competitor of the information requested to be withheld would reduce the competitor's expenditure of resources, or improve its competitive position, in the design, manufacture, shipment, installation, assurance of quality, or licensing of a similar product.
 - (d) The information requested to be withheld reveals cost or price information, production capabilities, budget levels, or commercial strategies of NuScale.
 - (e) The information requested to be withheld consists of patentable ideas.
- (3) Public disclosure of the information sought to be withheld is likely to cause substantial harm to NuScale's competitive position and foreclose or reduce the availability of profit-making opportunities. The accompanying report reveals distinguishing aspects about the method by which NuScale develops its evaluation methodology for the determination of the onset of density wave oscillations.

NuScale has performed significant research and evaluation to develop a basis for this method and has invested significant resources, including the expenditure of a considerable sum of money.

The precise financial value of the information is difficult to quantify, but it is a key element of the design basis for a NuScale plant and, therefore, has substantial value to NuScale.

If the information were disclosed to the public, NuScale's competitors would have access to the information without purchasing the right to use it or having been required to undertake a similar expenditure of resources. Such disclosure would constitute a misappropriation of NuScale's intellectual property, and would deprive NuScale of the opportunity to exercise its competitive advantage to seek an adequate return on its investment.

- (4) The information sought to be withheld is in the enclosed report entitled Methodology for the Determination of the Onset of Density Wave Oscillations (DWO). The enclosure contains the designation "Proprietary" at the top of each page containing proprietary information. The information considered by NuScale to be proprietary is identified within double braces, "{{ }}" in the document.

- (5) The basis for proposing that the information be withheld is that NuScale treats the information as a trade secret, privileged, or as confidential commercial or financial information. NuScale relies upon the exemption from disclosure set forth in the Freedom of Information Act ("FOIA"), 5 USC § 552(b)(4), as well as exemptions applicable to the NRC under 10 CFR §§ 2.390(a)(4) and 9.17(a)(4).
- (6) Pursuant to the provisions set forth in 10 CFR § 2.390(b)(4), the following is provided for consideration by the Commission in determining whether the information sought to be withheld from public disclosure should be withheld:
- (a) The information sought to be withheld is owned and has been held in confidence by NuScale.
 - (b) The information is of a sort customarily held in confidence by NuScale and, to the best of my knowledge and belief, consistently has been held in confidence by NuScale. The procedure for approval of external release of such information typically requires review by the staff manager, project manager, chief technology officer or other equivalent authority, or the manager of the cognizant marketing function (or his delegate), for technical content, competitive effect, and determination of the accuracy of the proprietary designation. Disclosures outside NuScale are limited to regulatory bodies, customers and potential customers and their agents, suppliers, licensees, and others with a legitimate need for the information, and then only in accordance with appropriate regulatory provisions or contractual agreements to maintain confidentiality.
 - (c) The information is being transmitted to and received by the NRC in confidence.
 - (d) No public disclosure of the information has been made, and it is not available in public sources. All disclosures to third parties, including any required transmittals to NRC, have been made, or must be made, pursuant to regulatory provisions or contractual agreements that provide for maintenance of the information in confidence.
 - (e) Public disclosure of the information is likely to cause substantial harm to the competitive position of NuScale, taking into account the value of the information to NuScale, the amount of effort and money expended by NuScale in developing the information, and the difficulty others would have in acquiring or duplicating the information. The information sought to be withheld is part of NuScale's technology that provides NuScale with a competitive advantage over other firms in the industry. NuScale has invested significant human and financial capital in developing this technology and NuScale believes it would be difficult for others to duplicate the technology without access to the information sought to be withheld.

/I declare under penalty of perjury that the foregoing is true and correct. Executed on 7/17/2023.



Mark W. Shaver